TU/e EINDHOVEN UNIVERSITY OF TECHNOLOGY

Scanning force microscopy of organic thin films

Citation for published version (APA):
Feldman, K. (2000). *Scanning force microscopy of organic thin films*. [Phd Thesis 2 (Research NOT TU/e / Graduation TU/e), Chemical Engineering and Chemistry]. Technische Universiteit Eindhoven. https://doi.org/10.6100/IR542440

DOI:
10.6100/IR542440

Document status and date:
Published: 01/01/2000

Document Version:
Publisher's PDF, also known as Version of Record (includes final page, issue and volume numbers)

Please check the document version of this publication:

• A submitted manuscript is the version of the article upon submission and before peer-review. There can be important differences between the submitted version and the official published version of record. People interested in the research are advised to contact the author for the final version of the publication, or visit the DOI to the publisher's website.
• The final author version and the galley proof are versions of the publication after peer review.
• The final published version features the final layout of the paper including the volume, issue and page numbers.

Link to publication

General rights
Copyright and moral rights for the publications made accessible in the public portal are retained by the authors and/or other copyright owners and it is a condition of accessing publications that users recognise and abide by the legal requirements associated with these rights.

• Users may download and print one copy of any publication from the public portal for the purpose of private study or research.
• You may not further distribute the material or use it for any profit-making activity or commercial gain
• You may freely distribute the URL identifying the publication in the public portal.

If the publication is distributed under the terms of Article 25fa of the Dutch Copyright Act, indicated by the "Taverne" license above, please follow below link for the End User Agreement:

www.tue.nl/taverne

Take down policy
If you believe that this document breaches copyright please contact us at:

openaccess@tue.nl

providing details and we will investigate your claim.

Download date: 16. Nov. 2023

Scanning Force Microscopy of Organic Thin Films

Druk: Universiteitsdrukkerij TU Eindhoven
Omslag: Ben Mobach

Scanning Force Microscopy of Organic Thin Films

PROEFSCHRIFT

ter verkrijging van de graad van doctor aan de
Technische Universiteit Eindhoven, op gezag van de
Rector Magnificus, prof.dr. M. Rem, voor een
commissie aangewezen door het College voor
Promoties in het openbaar te verdedigen
op donderdag 14 december 2000 om 16.00 uur

door

Kirill Feldman

geboren te Moskou

Dit proefschrift is goedgekeurd door de promotoren:

prof.dr. P.J. Lemstra
prof.dr. N.D. Spencer

Contents

Summary vii

1 Introduction
1.1 General Introduction 1
1.2 Scope of the Thesis 3
1.3 Survey of the Thesis 4
References 5

2 Scanning Force Microscopy
2.1 Principles and Modes of Operation 7
2.2 Contact Mechanics and Adhesion 17
References 20

3 Morphological Characterisation of Organic Thin Films
3.1 Introduction 23
3.2 Preparation and Imaging of Thin and Ultrathin Spin- Cast Polymer Films 24
3.3 Thin Polymer Films By Means of Friction Deposition 35
3.4 Self-Assembled Monolayers of Alkanethiols 38
3.5 Conclusions 42
References 43

4 Force Spectroscopy of Polymer Surfaces
4.1 Introduction 47
4.2 Van der Waals Interaction 48
4.3 Effects of Polymer Molecular Weight 50
4.4 Choice of Medium for the SFM Measurements 51
4.5 Force Measurements 53
4.6 Probes for Force Spectroscopy 54
4.7 Non-Polar Polymer Series 55
4.8 Polar Polymer Series 60
4.9 Frictional Measurements 67
4.10 Conclusions 69
References 69

5 Force Spectroscopy of Oligo- and Poly(ethylene Glycol) Self-Assembled Monolayers
5.1 Introduction 73
5.2 Protein Resistance of OEG- and PEG-Grafted Surfaces 73
5.3 Methoxytri(etheylene Glycol) Thiolates: Conformational Effects 74
5.4 Experimental 77
5.4.1 Materials 77
5.4.2 SAM Preparation 77
5.4.3 SFM Measurements 78
5.5 SFM Imaging of EG3-OMe SAMs on Gold and Silver 79
5.6 SFM Measurements With Fibrinogen-Modified Probes 81
5.7 SFM Measurements with Hydrophilic Probes 86
5.8 SFM Measurements With Hydrophobic Probes 89
5.9 Electrostatic Versus Hydrophobic Interaction 92
5.10 SFM Measurements of PEG-thiolates 102
5.11 Conclusions 105
5.12 Post Scriptum: Frictional Properties of Grafted PEGs 106
References 108

6 Conclusions and Outlook.....113
References.....116

Samenvatting.....117

List of Publications.....121

Acknowledgements.....123

Curriculum Vitae 125

Summary

Although mechanical applications of polymers generally take advantage of their bulk properties, there are numerous technologies in which ultrathin and thin polymer films are used. For example, they are applied as resists and interlayer dielectrics in microelectronic fabrication, as alignment layers in liquid-crystal displays, and as lubricants in magnetic information storage devices. Additionally they are incorporated into light-emitting diodes, non-linear optical devices, and biosensors. Polymer films have become building blocks in functional structures on rapidly decreasing length scales. Nanometre-sized molecular devices, particulate films, and patterned surfaces are of increasing importance in the development of microelectromechanical systems (MEMS), microelectronics, sensor technology, and biotechnology. Nanometre-scale, chemically specific information on polymeric surfaces presents a substantial analytical challenge, however. Rapid developments in scanning probe microscopy (SPM) techniques over the last 10 years have provided scientists with invaluable tools for the study of surface physical and chemical properties with sub-nanometre spatial resolution, and have found wide-spread use in polymer science. Scanning probe microscopy with chemical sensitivity has been successfully applied mainly to the study of self-assembled molecular systems. The application of this technique to polymer films, however, is rather difficult since many physical parameters, rather than the surface chemical composition alone, influence the contrast mechanisms.

The main objective of this thesis is to explore the capabilities of SPM for the morphological, surface-chemical, and surface-force characterisation of polymer thin films. By means of scanning force microscopy (SFM), polymer systems have been investigated with regard to their morphology and chemical structure. The adhesional forces between a series of polymer film surfaces and chemically well-defined scanning probe microscopy tips have been measured and found to depend strongly on the chemical nature of both probe and sample surfaces. For a given series of polymers, the

ranking in adhesion strength was markedly different for polar and non-polar probes. In the case of non-polar polymers, a correlation of adhesion force with calculations based on the Lifshitz theory of Van der Waals interactions was observed. The adhesional differences determined for a series of polymer films of increasing surface functionality with different probe tips translated into reversals of contrast in high-spatial-resolution lateral force images of blends prepared from these polymers. The reversal of contrast due to differences in chemical composition demonstrated the potential of this approach for the nanometre-scale, friction-mediated surface-chemical imaging of polymers. However, the contrast mechanism in SFM strongly depends on the mechanical properties of the polymeric constituents in phase-separated systems, such as polymer blends. Therefore, specifically chemically sensitive contrast could be obtained only for those blends, for which the mechanical properties were very similar. This can be viewed as both a shortcoming and an advantage, since chemical sensitivity provides a contrast mechanism in situations where mechanical contrast is absent. Central to these experiments has been the use of perfluorodecalin as a medium for measuring interactions. Employment of this liquid greatly facilitated measurement of the forces between probe tip and polymer surface.

The scanning force microscopy methodology developed during the study of polymer films was applied to the problem of protein-adhesion resistance. While the resistance to protein adsorption of poly(ethylene glycol)-modified (PEG) surfaces is well described by the steric repulsion theory and is employed in many biomedical applications, the physical nature of the protein-resistant behaviour of short oligo(ethylene glycol)-terminated (OEG) monolayers remains unclear. Functionalised scanning force microscope probes were used to investigate and to mimic the interaction between a plasma protein, fibrinogen, and self-assembled monolayers (SAMs) of methoxytri(ethylene glycol) undecanethiolate (EG3-OMe) on gold and silver surfaces. The EG3-OMe SAMs on gold were resistant to protein adsorption, whereas the films on silver adsorbed variable amounts of fibrinogen. Experiments were performed with both charged and hydrophobic tips as models for local protein structures, in order to determine the influence of these parameters on the interaction with the SAMs. A long-range repulsive interaction that scaled with the ionic strength of aqueous solutions was observed for the SAM on gold, and long-range attractive interaction that was weakly dependent on the ionic strength was observed for the EG3-OMe monolayer on silver,

when measured with hydrophobic probe. This study showed that the conformational differences between the two molecular layers (helical for the EG3-OMe SAM on gold and "all trans" for that on silver) dictated the distinct type of physical forces observed–electrostatic for EG3-OMe on gold and hydrophobic for that on silver. A rare type of electrostatic behaviour that is induced by the dipole field of the soft permeable interface of the oligoethylene glycol tails of EG3-OMe on gold was discovered. Polymer brushes of poly(ethylene glycol) thiolates were also investigated. The extent of the repulsive interactions detected with SFM probes depended on the layer thickness and was found to be in good agreement with the steric repulsion calculations.

While ordered monolayers of short organic molecules, such as self-assembled thiolates, are not necessarily representative models for polymeric thin films, this class of surfaces has proved to be extremely useful in understanding many important surface phenomena, such as adhesion, friction, wettability, lubrication, biological activity, and resistance to protein adsorption. It is vital, however, that SFM experiments on actual polymer surfaces themselves are also carried out, in order to evaluate the relevance of the SAM model in any particular case.

Chapter 1

Introduction

1.1 General Introduction

Thin polymer films represent a distinctive field of academic research with substantial relevance to a wide range of technological applications.[1] Polymers have become building blocks in functional structures on rapidly decreasing length scales.[2,3] Nanometre-size molecular devices, particulate films, and patterned surfaces are of increasing importance in the development of microelectromechanical systems (MEMS), microelectronics, catalysts, sensor technology, and biotechnology.[4-8] Progress in nanotechnology crucially relies on the developments of analytical tools that can resolve, study and test sub-micron and nanometre-sized features. Spatially resolved information on a sub-micron scale can be obtained with spectroscopic tools, such as small-area x-ray photoelectron spectroscopy[9] (XPS) or time-of-flight secondary-ion mass spectroscopy[10] (ToF-SIMS) with a resolution of several hundred nanometres. Limitations of these techniques include the ultra-high vacuum conditions of analysis and possible beam damage. Similar problems with beam damage often hinder the applicability of scanning and transmission electron microscopy (SEM and TEM) to the study of organic materials.

A breakthrough in lateral resolution was made by the invention of the scanning tunneling microscope[11] (STM) in 1981, when, for the first time, atomic resolution images were reported under ambient conditions. The STM became the first member of a new class of scanning probe microscopes (SPM), which are based on a different principle than the optical and electron microscopy. The principle of the SPM techniques

is very similar to profilometry, a sharp miniature-size probe scans across the surface to sense different types of interactions in the near-field region or in contact with the surface. The limitation of the STM in imaging predominantly conducting materials was soon overcome by the development of the atomic force microscope[12] (AFM) in 1986. The AFM technique allowed the probing of non-conductive materials, which immediately opened the door to the study of polymeric surfaces. Since its invention, the AFM has been applied to the characterisation of many polymeric materials. The first images of polymeric materials published in 1988-1991 ignited a great interest in the polymer community[13-15] and attracted widespread attention to this new experimental technique. Materials for which invaluable information has been obtained range from rigid polymers to soft biological macromolecules, from polymer single crystals to amorphous materials, from liquid-crystalline polymers to viscoelastic materials, and from molecular monolayers to fibrillar structures.[16] The important advantages of the SPM techniques include high lateral resolution (down to 0.1Å), three dimensional imaging of the surface topography, ease of sample preparation, the capability of imaging under diverse environmental conditions, ranging from vacuum to a liquid environment and diverse contrast mechanisms.

Within the last 10 years new operational modes, such as frictional, intermittent contact, dynamic (non-contact), electrostatic, magnetic, thermal and others have been introduced, and the family of the SPM techniques is growing rapidly. SPM can also probe a number of material properties, such as elastic modulus, viscosity, friction, work of adhesion and surface energy, by sensing different forces exerted on a probe;[17] these local mechanical properties are of great importance in the field of micro and nanotechnology.

Another important development in the field of scanning probe microscopy was the introduction of chemically-modified probes that, in combination with frictional and normal force measurements, provide contrast mechanisms with chemical sensitivity on a nanometre scale. This type of SFM measurements was termed “chemical force microscopy”[18] (CFM). The latter method involves chemical functionalisation of the SPM probes with self-assembled monolayers[19] of mainly ω-functionalised thiols on gold and trichlorosilanes on hydroxylated silicon oxide. The technique has been principally used to measure differences in the chemical composition of the patterned

surfaces–self-assembled monolayers (SAMs). While much effort has been expended on the study of chemically distinct areas of self-assembled monolayers, very little research has been carried out on applying the CFM to chemically distinguish between components (or phases) in polymer films. This is due to the fact that the contrast mechanism in, for example, frictional measurements is not directly related to the extent of the tip-sample interaction (the work of adhesion for given chemical groups), but is greatly influenced by the mechanical properties of a given phase and the energy dissipative processes that occur in the contact area. So, while it is relatively easy to obtain image contrast in frictional force microscopy or other SPM modes for polymer blends, block-copolymers and other phase-separated polymer systems, chemical *identification* of the components in a polymer system with the CFM remains extremely difficult. It is, therefore, of great interest to conduct a systematic application of chemically sensitive SPM to the imaging of phase-separated polymer films. Our efforts to obtain chemical sensitivity with scanning force microscopy (SFM) for surfaces of thin polymer films is presented as part of this dissertation.

While self-assembled monolayers of short molecules cannot be employed as models for the behaviour of the polymeric thin films, self-assembled monolayer (SAM) systems are of great importance in developing fundamental understanding of phenomena in adhesion, lubrication, wetting, friction, biocompatibility, protein adhesion and other processes. SAMs also provide chemically well-defined, structured, robust model surfaces for which important physical parameters such as a surface free energy, functional group density, conformational order, and orientation can be varied and tested. The contrast between SAM and polymer-surface behaviour can be both dramatic and highly informative, however. A detailed SFM study of ultrathin films of both oligo and poly(ethylene glycol)-terminated SAMs relevant to understanding their resistance to protein adsorption and their frictional properties is also presented in this work.

1.2 Scope of the Thesis

The main objective of this thesis is to explore the capabilities of scanning probe microscopy for the morphological, surface-chemical, and surface-force characterisation of polymer thin films. These three aspects are of importance, not only for a better

understanding of polymer thin films in general, but also in the context of, for example, electronic and biomedical applications of these materials.

SPM shows distinct advantages over more widely used surface-morphological characterisation approaches, such as TEM, due to its ability to operate under ambient and even liquid conditions and its inherently high resolution. In this thesis, SPM was applied on the μm scale to the study of solvent effects on spin-casting, and, on the nanometre scale, to molecular orientation induced by friction-deposited PTFE.

By manipulating surface forces by means of a low-dielectric-constant medium, SPM was used to chemically distinguish between different polymer surfaces, based on force and adhesion measurements between tip and surface. The approach was also be used to chemically image a polymer blend on a nanometre scale.

Much of this work concerns measurements on self-assembled monolayers, which might, superficially, be thought to function as models for polymer surfaces. It is clear from the results in this dissertation (particularly those concerned with tip-surface interactions and protein adsorption) that polymer brush and low-molecular-weight SAM surfaces, even those of similar surface chemical composition, can display vastly different behaviour, and that mechanical, chemical, and structural properties are all intimately connected in defining the interaction of a polymer surface with its surroundings.

1.3 Survey of the Thesis

The use of scanning force microscopy (SFM) is central to the investigations of organic thin films presented in this thesis. The principles, modes of operations, advantages and drawbacks of SFM for polymeric surfaces, as well as contact mechanics theories and adhesion, are presented in **Chapter 2**.

The attainment of chemically specific and surface-force information for polymer and self-assembled monolayer thin films forms the scope of the studies presented in this work. An important component of such studies is the preparation of thin and ultrathin organic films for subsequent SFM measurements. These films should be smooth and chemically well defined. Different methods of preparing thin polymeric films, such as

spin-casting and friction deposition, are described in **Chapter 3**. This chapter also includes numerous examples of morphological characterisation of semicrystalline and amorphous films prepared by means of spin-casting, the imaging of adsorbed alkanes on oriented PTFE, and the description of the self-assembly process for the alkanethiolates.

Chapter 4 is devoted to force spectroscopy with chemical sensitivity of polymeric thin films. This chapter includes adhesional and frictional measurements of two series of polymer films: a) non-polar and b) of increasing surface polarity. In this chapter, it is demonstrated that chemically sensitive imaging with high-spatial-resolution is achievable for thin films of polymer blends if the mechanical properties of the components are similar and steps are taken to enhance the signal-to-noise ratio of the measured forces.

SFM methodology developed in the previous chapter was employed to study the behaviour of oligo- and poly(ethylene glycol)-terminated SAMs relevant to protein adsorption. In **Chapter 5** it is shown that, unlike the steric repulsion behaviour of poly(ethylene glycol) brushes, the conformational state of the oligoethylene glycol tails dictates a distinct nature of interaction with the proteins. A rare type of electrostatic behaviour that is induced by the dipole field of the soft, permeable interface of the oligoethylene glycol tails is discovered and described.

Finally, conclusions of this work and some recommendations are presented in **Chapter 6**.

References

1. *Organic Thin Films: Structure and Applications*; Frank, C. W., Ed.; ACS Symposium Series 695; American Chemical Society: Washington, D. C., 1998.
2. Böltau, M.; Walheim, S.; Mlynek, J.; Krausch, G.; Steiner, U. *Nature* **1998**, *391*, 877.
3. Ulrich, R.; Chesne, A. D.; Templin, M.; Wiesner, U. *Adv. Mater*. **1999**, *11*, 141.
4. Bhushan, B. *Tribology Issues and Opportunities in MEMS*; Kluwer Academic: Dordrecht, 1998.

5. Mann, S. *Biomimetic Materials Chemistry*; VCH: Weinheim, 1996.
6. Ball, P. *Made to Measure. New Materials for 21st century*; Princeton University Press: Princeton, 1997.
7. Fendler, J. H. *Nanoparticles and Nanostructured Films: Preparation, Characterisation, and Applications*; Wiley-VCH: Weinheim, 1998.
8. *Micro- and Nanopatterning Polymers*; Ito, H., Reichmanis, E., Nalamasu, O., Ueno, T., Eds.; ACS Symposium Series 706; American Chemical Society: Wasington, D. C., 1998.
9. Chan, C.-M. *Polymer Surface Modification and Characterizaion*; Hanser Publishers: Munich, 1994.
10. *Practical Surface Analysis*; Briggs, D., Seah, M. P., Eds.; Wiley: Chichester, Vol. 2, 2nd ed., 1992.
11. Binnig, G.; Rohrer, H.; Gerber, Ch.; Weibel, E. *Phys. Rev. Lett*. **1982**, *49*, 57.
12. Binnig, G.; Quate, C. F.; Gerber, Ch. *Phys. Rev. Lett*. **1986**, *56*, 930.
13. Drake, B.; Prater, C. B.; Weisenhorn, A. L.; Gould, S. A.; Albrecht, T. R.; Quate, C. M.; Cannell, D. S.; Hansma, H. G.; Hansma, P. K. *Science* **1988**, *243*, 1586.
14. Stocker, W.; Bar. G.; Kunz, M.; Möller, M.; Magonov, S. N.; Cantow, H. J. *Polym. Bull*. **1991**, *26*, 215.
15. Sarid, D. *Scanning Force Microscopy*; Oxford University Press: New York, 1991.
16. *Scanning Probe Microscopy of Polymers*; Ratner, B. D., Tsukruk, V. V., Eds.; ACS Symposium Series 694; American Chemical Society: Wasington, D. C., 1998.
17. *Procedures in Scanning Probe Microscopies*; Colton, R. J., Engel, A., Frommer, J. E., Gaub, H. E., Gewirth, A. A., Guckenberger, R., Rabe, J., Heckl, W. M., Parkinson, B., Eds.; Willey: New York, 1998.
18. Noy, A.; Vezenov, D. V.; Lieber, C. M. *Annu. Rev. Mater. Sci*. **1997**, *27*, 381.
19. Ulman, A. *Introduction to Ultrathin Organic Films*; Academic Press: San Diego, 1991.

Chapter 2

Scanning Force Microscopy

2.1 Principles and Modes of Operation

The use of a scanning force microscope (SFM) as a high-resolution tool for surface phenomena investigations of organic thin films has been central to the work presented in this dissertation and, therefore, requires a more detailed look at its operating principles, advantages and limitations.

The scanning force microscope was invented by Binnig, Quate, and Gerber[1] in an effort to overcome the limitations of a scanning tunneling microscope[2] (STM), which could image predominantly conductive materials. Since that time, the development of the force microscopy techniques and their applications in surface science has experienced an exponential growth with more than 2000 journal publications in 1999 alone.

As it is clear from its name, the scanning force microscope consists of a scanning component and a force sensing tool, and it enables one to obtain microscopic information on a surface under investigation. In fact, the principle of this instrument is genuinely simple: a sharp probe attached to a mechanical beam is rastered in the proximity of, or in contact with, a surface, measuring local physical properties. As a result, one obtains a digital "image" of an interaction force over the scanned area.

Scanning is performed by piezoelectric translators, which actuate either a probe or a sample surface. An electric field applied across a piezoelectric material causes the unit cells to deform in a defined way; depending on the sign of the applied field the material will either expand or contract (transverse piezoelectric effect). Piezoelectric materials

commonly used are ceramic hollow tubes based on lead zirconate titanates (PZT) with the electrodes segmented into four equal sectors of 90°. A voltage gradient of the same magnitude, but opposite sign, is applied to the two opposite sectors, causing one to contract and the other to expand, generating a bowing movement in one direction. The same can be done to the other two opposite sectors, and as a result the x-y scanning movement is achieved. A separate piezoactuator is built into the scanning assembly to generate movements in the z-direction. Piezoactuators yield high lateral resolution (<0.01Å), although, such effects as non-linearity (voltage-versus-displacement hysteresis), creep, and thermal drift may reduce resolution significantly.[3,4] In order to minimise the effects of non-linearity, "memory" and creep, a non-linear voltage function is usually applied to the pair of opposite electrodes; calculation of the second-order parameters in the voltage function requires careful calibration by means of scanning over well-defined calibration gratings.

A key element of a scanning force microscope is a force sensor–a probe with a sharp tip integrated close to the free end of a mechanical beam, a so-called "cantilever". This definition implies that a cantilever-probe assembly is a spring–a mechanical resonator which can be excited by thermal noise, an oscillating driver, or an oscillating surface, when the probe is in contact with it. The eigen-frequency, f, of a cantilever depends on the spring stiffness, k, and an effective mass m_{eff}, and is given by

$$f = \frac{1}{2\pi}\sqrt{\frac{k}{m_{eff}}}. \qquad (2.1)$$

The spring stiffness, or the spring constant, k, depends on the material properties and geometrical parameters of a cantilever. For a cantilever with a rectangular cross-section it is given by

$$k = \frac{Ebh^3}{4l^3} \qquad \text{(N/m)} \qquad (2.2)$$

where E is the Young's modulus of the cantilever material, b and h are the width and height of a cross-section, respectively, and l is a length of the cantilever. During an SFM experiment, a vertical deflection, Δz, of a cantilever is monitored and measured. To obtain force information Hook's law is applied

$$F=-k\Delta z. \qquad (2.3)$$

Therefore, a more accurate estimation of a cantilever spring constant significantly reduces experimental errors. One way of measuring cantilever's spring constant

involves attaching a bead of known mass to the end of a cantilever and measuring the resonant frequency before and after the attachment,[5] a cantilever spring constant can then be readily calculated from the set of two equations (Eq. 2.1) with two unknowns, k and m_{eff}. However, this method is experimentally challenging and incorporates the error in the estimation of a bead mass. We found that reasonable calculations of a cantilever spring constant, k_e, can be performed by assuming that a mass of a probe assembly remains constant and measuring the actual resonant frequency. The correction is done by using a set of Eq. 2.1 with the measured resonant frequency, f_e, and manufacturer-provided values for the resonant frequency, f_m, and spring constant, k_m:

$$k_e = \left(f_e / f_m\right)^2 k_m \tag{2.4}$$

Detection of the cantilever deflection, as it is brought in contact with a surface and scanned over it, can be performed by several methods such as STM,[2] capacitance,[6] interferometry,[7] piezoresistance[8] and others. However, most commercially available instruments use the optical lever detection technique[9] due to its simplicity, reliability and ability to measure simultaneously normal and lateral deflections.[10] A schematic diagram of an optical detection technique is shown in Fig. 2.1. Light from a laser diode is focused on the end of a cantilever (to improve the reflectivity, the back side of the cantilever is coated with a thin layer of gold or aluminium), the reflected light is directed onto a quadrant photo-diode–a position sensitive detector which emits a signal proportional to the position of a laser beam on its active surface. For a vertical deflection, the difference between the voltages of two upper and two lower segments is detected $(V_A+V_B)-(V_C+V_D)$, for a torsion deflection the difference between the signals on the left and the right segments is detected $(V_A+V_D)-(V_B+V_C)$. Optical lever detection is a remote sensing detection system (the light source and the photo diode can be placed away from the cantilever) with high dynamic range.

The operating modes of an SFM can be divided into two categories depending on whether the cantilever or sample surface is oscillated (AC modes) or not (DC modes). DC modes include constant force mode, deflection mode, lateral, or friction force microscopy and force-distance measurements.[12] In constant force mode, a surface is brought in contact with a cantilever and is scanned in an x-y plane, the deflection of a cantilever in z-direction being kept constant by adjusting the position of the z-piezo through a feedback loop. As a result, an image of z-piezo displacement as a function of

(*x, y*) is obtained. Since the deflection of the cantilever is kept constant, the sum of all forces acting in the contact area of the probe tip and surface is kept constant, hence the name "constant force" mode.

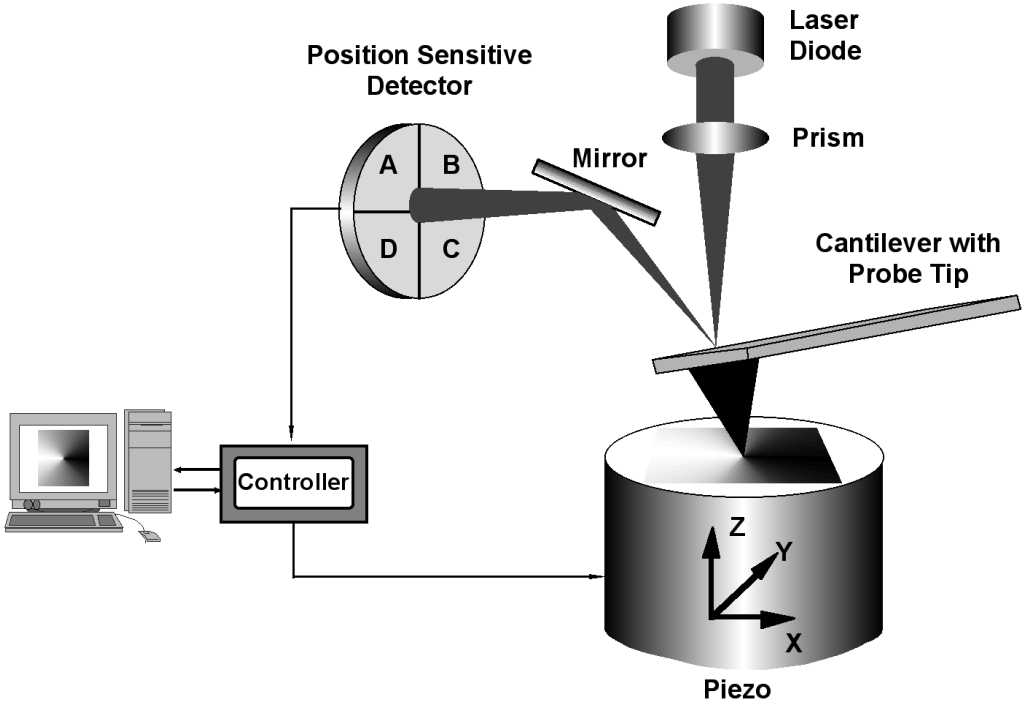

Figure 2.1 *Schematic diagram of a scanning force microscope.*

Deflection of a cantilever, therefore, is not entirely influenced by the surface topographic features, but it is also a product of the tip-surface interaction and the resulting SFM image may vary significantly from the true surface topography. This issue is particularly important when imaging polymer samples, where plastic deformation can easily take place. An applied load of 10nN on a probe tip with an effective radius of 15nm generates a pressure at the centre of contact equal to 480MPa, which exceeds more than 4 times the yield stress of, for example, polystyrene (≈100MPa). The effect of high contact pressures can be seen on the SFM image below (Fig. 2.2), where an area of a polystyrene film was plastically deformed when scanned under higher applied load. It is also important to be aware of capillary forces,[12] when the SFM imaging is done under ambient conditions. Liquid contamination on the surface forms a meniscus with the probe tip generating a capillary force. This Laplace pressure contribution for a concave meniscus can be calculated from the following equation:[13]

$$F \approx 4\pi R\gamma_L \cos\theta \qquad (2.5)$$

where R is the probe tip radius, γ_L surface free energy of the liquid and θ is the contact angle. For an SFM measurement of a hydrophilic surface with a sharp probe (R=15nm), this attractive force may reach 10-15nN, once again generating very high pressures in the contact area. The best way to avoid this problem is to perform measurements under liquids.[14]

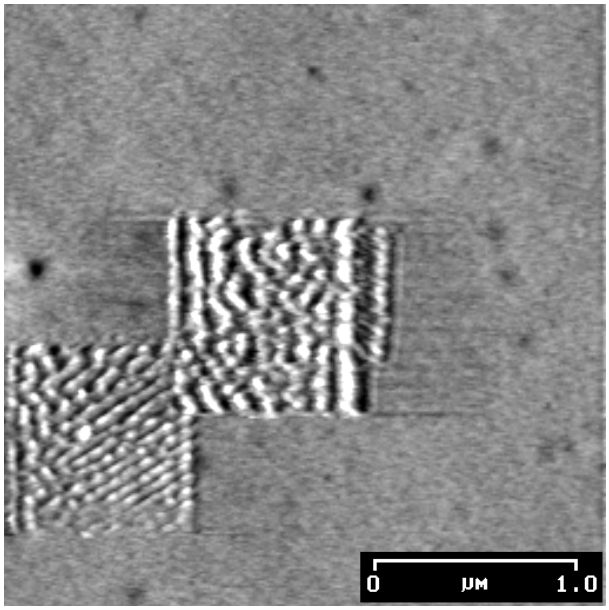

Figure 2.2 *SFM image of a surface of a spin-cast polystyrene film showing damage to the areas that were scanned under loads that exceeded yield stress of the material.*

In deflection mode the feedback loop is switched off and the cantilever deflection is recorded directly from a photodiode. This mode is complementary to the constant force mode, since the information cannot be directly correlated with the surface topography.

In a lateral (friction) force microscopy experiment, a probe or a surface is usually scanned perpendicular to the long axis of a cantilever beam and the resulting torsion of a cantilever is detected by the difference in the signal intensity of the left and the right segments of a photodiode (Fig. 2.3). The sign of the friction signal changes when scanning direction is reversed, generates a so-called friction loop. Since the friction force is sensitive to energy dissipating process as well as the chemical composition of the sample, this technique may be regarded as a spectroscopic method with high lateral resolution. Several features are unique to SFM friction measurements–it simultaneously acquires topography, normal and lateral forces with high precision, friction can be

studied down to an atomic scale, the instrument can be operated in a wear-free regime, and in an ideal situation the small apex of the probe tip represents a single asperity contact. However, it is a challenging task to obtain quantitative frictional data, since the calibration of a lateral spring constant cannot be performed directly.[15]

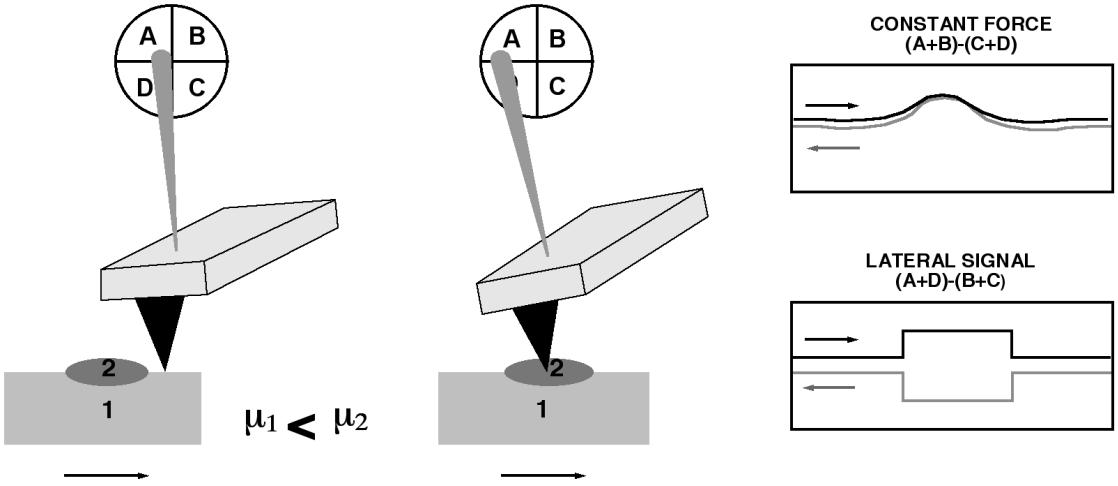

Figure 2.3 *Schematic diagram of a lateral force microscopy(LFM) experiment.*

The lateral force is composed of a friction force and forces due to the change in surface slope[16] (surface topography). Therefore, a friction loop might contain an offset or a slope that has to be accounted for. For a quantitative analysis of the lateral force, as well as for the determination of the dissipated energy, the non-friction offset must be removed by subtracting the scans performed in opposite directions. Amontons' law,[17] in which the friction force, F_{fr}, depends linearly upon the normal force, L, with the slope being equal to the coefficient of friction, μ ($F_{fr.}=\mu L$), is applicable to an SFM experiment, but in a modified form to account for a "residual" force, f_0, which is correlated with adhesion at zero applied load:[18]

$$F_{fr.} = \mu L + f_0. \qquad (2.6)$$

For most surfaces a major contribution to the torsion signal comes from the shear stresses within the contact area, and for a single asperity contact the friction force becomes the product of the interfacial shear strength, τ, and the contact area, A[19]

$$F_{fr.} = \tau A. \qquad (2.7)$$

Determination of contact area will be discussed later in this chapter.

An example of frictional contrast of a phase-separated polymeric surface is shown in Fig. 2.4. A sample of a commercial polyesterurethane block-copolymer (Estane®,

BFGoodrich), which is a thermoplastic elastomer, was prepared by spin-casting of 1 wt.% solution in toluene onto an oxygen-plasma-cleaned Si wafer, followed by 1 hour annealing at 60°C in vacuum. The topographic image (Fig. 2.4A) shows formation of sub-micron size domains on the film surface (the same surface was imaged prior to thermal treatment and showed no signs of phase separation). These domains appear brighter in the topographic image. However, from this image alone we cannot determine whether these domains are composed of a material that is different from that of the surrounding matrix. The subtracted frictional image on the right (Fig. 2.4B) shows a substantial contrast between the domains and the surrounding matrix; note that the contrast is reversed compared the topographic image–while the domains represent surface protrusions, they exhibit lower friction with an SFM probe.

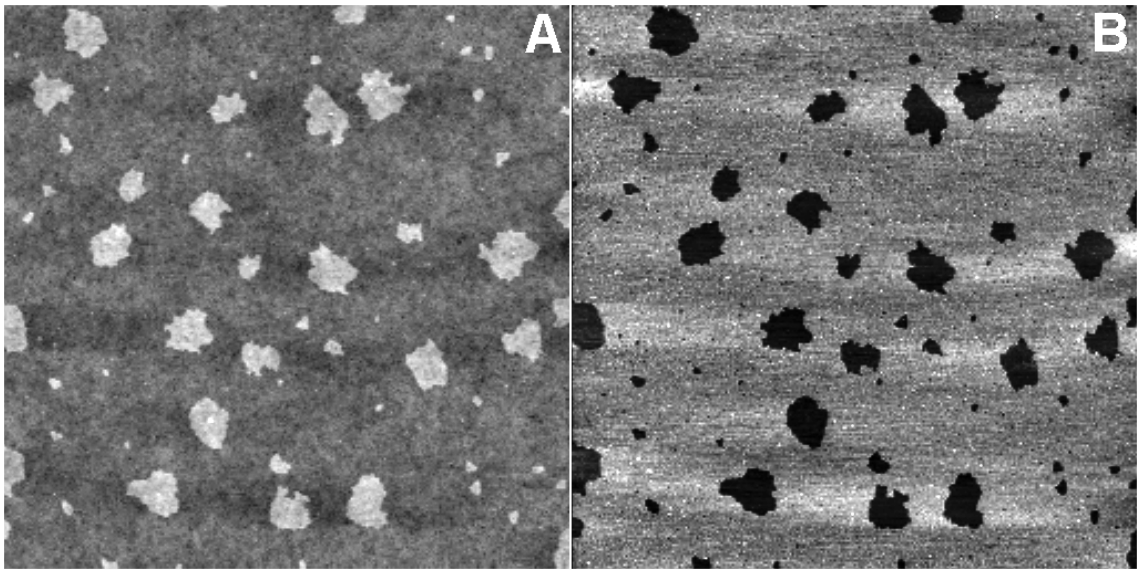

Figure 2.4 *10×10μm^2 a) topographic (z-range 25nm) and b) subtracted frictional images of commercial polyesterurethane spin-cast from 1 wt.% toluene solution and annealed for 1 hour at 60°C in vacuum.*

Since the frictional contrast may be due to chemical (surface energy) and/or physical (molecular weight, viscoelastic behaviour, hardness, degree of crystallinity, etc.) differences, we cannot *identify* the two phases. However, we may conclude that thermal treatment caused material separation at the surface into, at least, two phases.

SFM cantilevers with integrated probes are produced by means of photolithography and are commercially available in a wide range of materials, dimensions and spring constants. However, standard SFM probe assemblies consist of V-shaped cantilevers

made of silicon or silicon nitride with spring constants in the range of 0.01-2.0N/m and integrated silicon or silicon nitride probes with a tip curvature on the order of 10-200nm. The radius of a probe tip plays a crucial role in ultimate image resolution. It can be determined by scanning over a $SrTiO_3$ single crystal, for which the two facet planes form a very sharp edge. Scanning over such a surface produces an image of a probe tip shape.[20] Any defects in the tip, as the one shown in Fig. 2.5B, are convoluted into the surface topography, producing erroneous images.

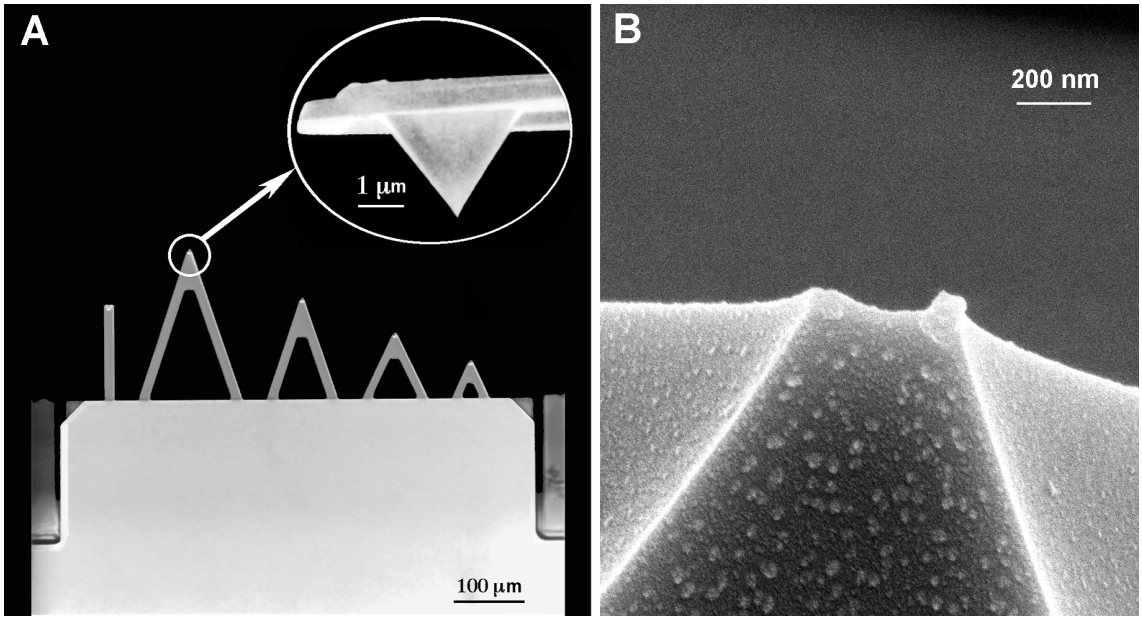

Figure 2.5 *A) Optical microscopy image of a commercial contact mode cantilever assembly and SEM image of a Si_3N_4 probe (Park Scientific Instruments, Sunnyvile, CA). B) High resolution SEM image of a probe tip with a defect.*

Another important operational mode of an SFM instrument involves measuring the deflection of a cantilever as a function of the surface-probe separation[12]. As a result, a cantilever deflection–piezo displacement diagram, commonly known as a "force curve", is obtained. In this experiment, a surface is ramped toward a probe with a *z*-piezo. When the sample force gradient becomes equal to the spring constant of the cantilever, the cantilever jumps in contact with the surface. If we denote U as an interaction potential between the probe tip and the surface, at an equilibrium separation, D, the total force gradient is a convolution of the sample force gradient with the cantilever spring constant k:

$$\text{measured slope} = \frac{k\left(\partial^2 U / \partial D^2\right)}{k + \partial^2 U / \partial D^2}. \qquad (2.8)$$

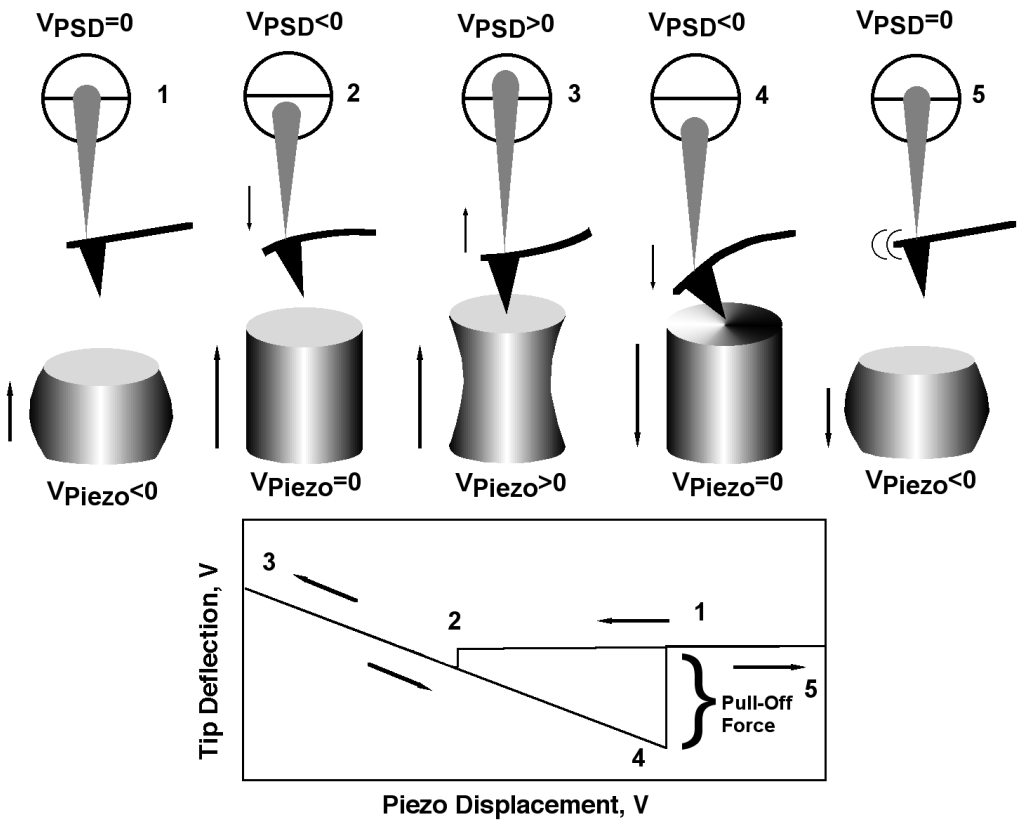

Figure 2.6 *Schematic diagram of a force-separation measurement.*

When the total force gradient (the denominator) becomes equal to zero, the slope becomes infinite, an instability occurs and a cantilever jumps to a surface. The kinetic energy of a "jump to contact" may be sufficient to deform a probe tip or a surface (depending on the elastic moduli of the two and tip geometry) and cause a material transfer from the probe tip to the surface or visa versa. Upon a jump to contact, a surface and a probe tip are moved together in a repulsive regime until the direction of the *z*-piezo movement is reversed. The cantilever will jump away from the surface into an equilibrium position when the spring constant becomes greater than the force gradient, which may now have an additional component due to adhesion. Therefore, a force curve almost always exhibits hysteresis. This hysteresis consists of a mechanical hysteresis due to finite spring stiffness as discussed above, plus an adhesion hysteresis.

The data from a force curve cycle is displayed as an *x*-*y* plot, the *x*-axis representing piezo displacement in nm, the *y*-axis cantilever deflection in volts. To convert the cantilever deflection into nanometres, the slope of the loading part of the curve has to be calculated. If the slope is linear, it may be assumed that no plastic deformation took

place and that the strain in the contact area was constant, the cantilever deflection data is then multiplied by the value of the slope to obtain the deflection in nanometres. To obtain a force-versus-separation curve, the cantilever deflection, z, must be multiplied by the cantilever spring constant value, k, and the separation calculated as the piezo displacement, d, minus the cantilever deflection, z, so that the plot becomes $F=-kz$ as a function of $(d-z)$. Very often, a zero separation is hard to estimate if there is no apparent jump to contact, due to a strong repulsive interaction and low spring stiffness. A vertical displacement of a cantilever between the lowest point in the unloading cycle when the tip snaps off a surface and an equilibrium rest position multiplied by the spring constant of a cantilever is call a "pull-off" force and characterises adhesion and inelastic processes occurring between the tip and the surface.

An example of SFM force-distance curves (force-versus-piezo displacement, in this case) is shown in Fig. 2.7. The force curves were taken under ambient conditions on the two areas of a phase-separated polyesterurethane described above and shown in Fig. 2.4. Force-distance measurements were taken on the surrounding polymer matrix (Fig. 2.7A) and the sub-micron domains (Fig. 2.7B). These data show that the adhesion hysteresis (the area between the approaching and the retracting lines) and the pull-off force are both much greater for the polymer matrix. The results of these measurements in combination with the frictional data are consistent with an important general rule that frictional forces generally correlate with adhesion hysteresis.[21]

Many limitations of the DC modes of an SFM, such as shear stresses in the contact area and instabilities of the cantilever due to a finite stiffness, may be overcome in AC modes in which a cantilever is driven at a certain frequency and amplitude.[22,23,24,25,26] Many new modes have been developed based on the magnitude of these two parameters. The most common is an intermittent contact mode called TappingMode™.[27] It employs stiff cantilevers (k=5–50N/m) that are excited close to their resonant frequency (100-400kHz) by an oscillating piezo, and operate at high amplitudes. The basic idea of this dynamic mode is to replace the tip-surface contacts of possible high local pressures with brief approaches of an oscillating tip. In the vicinity of a surface, the cantilever's amplitude is damped by surface forces–even weak interactions can significantly change this value.

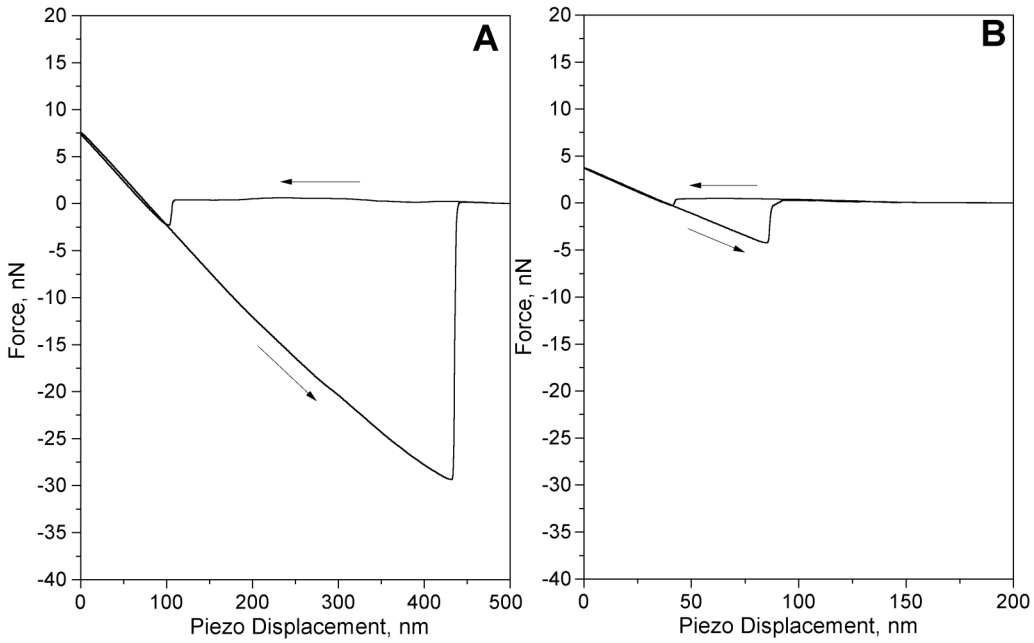

Figure 2.7 *Force-versus-piezo displacement curves measured under ambient conditions with Si_3N_4 probe (k=0.1N/m) on the surface of phase-separated polyesterurethane (Fig. 2.4). A) On the polymer matrix and B) on the sub-micron domains.*

The ratio of the damped to the original amplitude is kept high (80-90%), and the feedback loop uses a constant damped amplitude for adjusting the *z*-piezo position. This technique also allows the phase shift between an oscillator (driver) frequency and that of a cantilever ("phase imaging") to be monitored. Major factors in a phase contrast mechanism are still being debated and are believed to be a result of viscoelastic response and adhesion (energy-dissipating factors) rather than elastic surface behaviour. The intermittent mode reduces the typical operational forces by at least an order of a magnitude, virtually eliminates the shear stresses, and reduces the time of a tip-surface contact by two orders of magnitude.

2.2 Contact Mechanics and Adhesion

In a contact mode SFM a surface and a probe tip are brought together until contact is established. Various attractive and repulsive forces may act in the contact area and its vicinity and may include Van der Waals, electrostatic, hydrophobic, steric and other interactions. Adhesion between a probe tip and a surface may generate an elastic or plastic deformation and a finite contact area is established between the two bodies. Several contact mechanics theoretical models describe the deformation of the two bodies in contact by using continuum mechanics with the assumption that the atomic structure is of little or no importance. These models are derived for static equilibrium

conditions and assume that the materials are elastic and isotropic, that shear forces are absent and that the contact geometry is axisymmetric. In an SFM experiment, the last two assumptions are rarely achieved. Since the cantilever is mounted at a small angle to the surface (≈13º for a Digital Instruments Nanoscope), it bends and generates a torque in the contact area. The first theory of contact mechanics was derived by Hertz[28] with an assumption that there are no surface attractive forces or adhesion. An expression for the contact radius a for the two spheres of radii R_1 and R_2 under an applied load F_{load} in the Hertz model has the following form:

$$a^3 = \frac{RF_{load}}{K}. \tag{2.9}$$

Where R is a combined radius of curvature for the two contacting spheres:

$$R = \frac{R_1 R_2}{R_1 + R_2}. \tag{2.10}$$

K is an effective elastic modulus of the two bodies with Young's moduli E_1 and E_2 and Poisson's ratios ν_1 and ν_2:

$$\frac{1}{K} = \frac{3}{4}\left(\frac{1-\nu_1^2}{E_1} + \frac{1-\nu_2^2}{E_2}\right). \tag{2.11}$$

A prominent contact mechanics model that accounts for short-range forces acting in the contact area was developed by Johnson, Kendall, and Roberts[29] (JKR model). This work was motivated by the study of the adhesional behaviour of windshield wipers. The model considers the work of adhesion in the contact area between the solids and suggests that solids deform locally to form a connective "neck". For a sphere of radius R, work of adhesion W_{12} and applied load F_{load}, the radius of the contact area a is given by

$$a^3 = \frac{R}{K}\left[F_{load} + 3\pi R W_{12} + \sqrt{6\pi R W_{12} F + \left(3\pi R W_{12}\right)^2}\right]. \tag{2.12}$$

This expression for a radius of a contact area of the two elastic solids has several important consequences. When the work of adhesion is absent, the formula reduces to the Hertz model. Under zero applied load the contact radius is finite. Under small negative loads solids adhere until some critical negative force is reached and the bodies jump apart. This pull-off force is given by

$$F_{pull-off} = -1.5\pi W_{12} R. \tag{2.13}$$

An interesting conclusion comes from analysing this expression–the effective elastic modulus has no effect on the magnitude of the pull-off force. One important

shortcoming of this theory is that it predicts an infinite stress at the edge of a contact circle. Nevertheless, the JKR theory has been verified experimentally and found to be adequate for elastic, smooth solids that form an appreciable neck in the contact area.

The work of adhesion enters both Eq. 2.11 and 2.12, and, according to the Dupré equation,[13] the work of adhesion depends on the surface free energies of both surface and probe, γ_1 and γ_2, and their interfacial energy, γ_{12}:

$$W_{12} = \gamma_1 + \gamma_2 - \gamma_{12}. \tag{2.14}$$

This equation, combined with Eq. 2.12, suggests that measurement of pull-off forces with the same probe can be employed to distinguish between a series of materials based on their surface free energies. The situation is more complex for friction measurements, since it has been shown that it is the adhesion hysteresis rather than the adhesion force that is correlated to kinetic friction.[30]

Another contact mechanics model was developed by Derjagin, Muller and Toporov[31] (DMT), with the assumption that there are long-range attractive forces acting outside the contact area. This removes the unrealistic stress distribution at the edge of the contact radius, but may underestimate the actual contact area, since it only assumes Hertzian deformation. The original DMT theory contained errors,[32] but the assumptions and results are still referred to as the DMT model. It works well for stiff materials, weak adhesion forces and small tip radii.[33] In the DMT model the pull-off force is determined by

$$F_{pull-off} = -2\pi W_{12} R. \tag{2.15}$$

The two theories, JKR and DMT, represent two extreme cases of elastic contact. A different approach was undertaken by Barquins and Maugis[34,35] who incorporated viscoelastic response into the fracture mechanics approach to contact mechanics. In this approach, the increase and decrease of contact area is viewed as the opening or closing of a Dugdale-type crack at the contact periphery. The solution is expressed in terms of a dimensionless parameter, λ, which expresses the ratio of the viscoelastic displacement to the range of action of the surface forces. For $\lambda \geq 1$ the JKR theory was found to be a good approximation, while for $\lambda \leq 0.3$ the DMT theory was found to be applicable, for $0.3 \leq \lambda \leq 1$ an exact solution must be solved numerically. More detailed explanation and mathematical expression to calculate λ are given in Chapter 4.

The subsequent chapters of this dissertation will describe applications of scanning force microscopy to the study of thin and ultrathin organic films. These include morphological characterisation of spin-cast semicrystalline and amorphous polymeric films (Section 3.2), high-resolution imaging of the crystalline order of oriented PTFE (Section 3.3), applications of force spectroscopy with chemical sensitivity for non-polar and polar polymeric films (Chapter 4), and the SFM study of oligo- and poly(ethylene glycol) self-assembled monolayers relevant to the inhibition of protein adsorption on the surfaces (Chapter 5).

References

1. Binnig, G.; Quate, C. F.; Gerber, Ch. *Phys. Rev. Lett*. **1986**, *56*, 930.
2. Binnig, G.; Rohrer, H.; Gerber, Ch.; Weibel, E. *Appl. Phys. Lett.* **1982**, *40*, 178.
3. Binnig, G.; Smith, D. P. E. *Rev. Sci Instrum*. **1986**, *57*, 1688.
4. Koleske, D. D.; Lee, G. U.; Wahl, K. J.; Colton, R. J. *Rev. Sci. Instrum*. **1995**, *66*, 4566.
5. Cleveland, J. P.; Manne, S.; Bocek, D.; Hansma, P. K. *Rev. Sci. Instrum*. **1993**, *64*, 403.
6. Neubauer, G.; Cohen, S. R.; Horn, D.; Mate, C. M.; McClelland, G. M. *Rev. Sci. Instrum*. **1990**, *61*, 2296.
7. Martin, Y.; Williams, C. C.; Wickramasinghe, H. K. *J. Appl. Phys.* **1987**, *61*, 4723.
8. Linnemann, R; Gotszalk, T.; Rangelow, I. W.; Dumania, P.; Oesterschulze, E. *J. Vac. Sci. Technol. B* **1996**, *14*, 856.
9. Meyer, G.; Amer, N. M. *Appl. Phys. Lett.* **1988**, *53*, 1045.
10. Mate, C. M.; McClelland, G. M.; Erlandsson, R.; Chiang, S. *Phys. Rev. Lett.* **1987**, *59*, 1942.
11. Burnham, N. A.; Colton R. J In *Scanning Tunneling Microscopy and Spectroscopy: Theory, Techniques, and Applications*; Bonnell, D. A., Ed.; VCH Publishers, Inc.: New York, 1993; Chapter 7.
12. Binggeli, M.; Mate, C. M. *Appl. Phys. Lett.* **1994**, *65*, 415.
13. Israelachvili, J. *Intermolecular and Surface Forces*, 2nd ed.; Academic Press: London, 1992; Chapter 15.

14. Weisenhorn, A. L.; Hansma, P. K.; Albrecht, T. R.; Quate, C. F. *Appl. Phys. Lett.* **1989**, *54*, 2652.
15. Ogletree, D. F.; Carpick, W. R.; Salmeron, M. *Rev. Sci. Instrum*. **1996**, *67*, 3298.
16. Koinkar, V. N.; Bhushan, B. *J.Vac. Sci. Techn. A* **1996**, *14*, 2378.
17. The Amontons' law of friction was first explained with a Cobblestone model by Coulomb in 1785 that attributed friction to the effort required to pull opposing surfaces over a series of inclined planes representing asperities. Coulomb, C. A. *Mem. Math. Phys.* Paris **1785**, *5*, 162.
18. Briscoe, B. J.; Evans, D. C. B. *Proc. R. Soc. , Ser. A* **1982**, *380*, 389.
19. Carpick, R. W., Salmeron, M. *Chem. Rev.* **1997**, *97*, 1163.
20. Sheiko, S. S.; Möller, M.; Reuvekamp, E. M. C. M.; Zandbergen, H. W. *Phys. Rev. Part B* **1993**, *48*, 5675.
21. Israelachvili, J. N.; Chen, Y.-L.; Yoshizawa, H. *J. Adhesion Sci. Technol*. **1994**, *8*, 1234.
22. Spatz, J. P.; Sheiko, S.; Möller, M.; Winkler, R. G.; Reineker, P.; Marti, O. *Nanotechnology* **1995**, *6*, 40.
23. Albrecht, T. R.; Grütter, P.; Horne, D.; Rugar, D. *J. Appl. Phys.* **1991**, *69*, 668.
24. Jarvis, S. P.; Dürig, U.; Lantz, M. A.; Yamada, H.; Tokumoto, H. *Appl. Phys. A* **1998**, *66*, S212.
25. Kolosov, O.; Yamanaka, K. *Jpn. J. Appl. Phys.* **1993**, *32*, L1095.
26. Krotil, H.-U.; Stifter, T.; Waschipsky, H.; Weishaupt, K.; Hild, S.; Marti, O. *Surf. Interface Anal.* **1999**, *27*, 336.
27. Zhong, Q.; Jennis, D.; Kjoller, K.; Elings, V. *Surf. Sci. Lett*. **1993**, *290*, 688.
28. Hertz, H.; Reiner, J. *Angew. Mathematik* **1882**, *92*, 156.
29. Johnson, K. L.; Kendall, K.; Roberts, A. D. *Proc. Ro. Soc. A* **1971**, *324*, 302.
30. Israelachvili, J. N.; Chen, Y.-L.; Yoshizawa, H. *J. Adhesion Sci. Technol.* **1994**, *8*, 1234.
31. Derjagin, B. V.; Muller, V. M.; Toporov, Y. P. *J. Coll. Interface Sci*. **1975**, *53*, 314.
32. Muller, V. M.; Yoshchenko, V. S.; Derjagin, B. V. *J. Coll. Interface Sci*. **1980**, *77*, 92.
33. Pashley, M. D. *Coll. Surf.* **1984**, *12*, 69.
34. Maugis, D.; Barquins, M. *J. Appl. Phys. D*. **1978**, *11*, 1989.
35. Maugis, D. *J. Coll. Interface Sci.* **1992**, *150*, 243.

Chapter 3

Morphological Characterisation of Organic Thin Films

3.1 Introduction

Although mechanical applications of polymers take advantage of their bulk properties, there are numerous technologies in which ultrathin and thin polymer films are used. Applications include resists and interlayer dielectrics in microelectronic fabrication, alignment layers in liquid crystal displays, and lubricants in magnetic information storage devices. Additionally they are incorporated into light emitting diodes, non-linear optical devices, biosensors, etc. Review articles on these subjects can be found in references (1-6).

The main objective of the work described in this dissertation was the attainment of high-lateral-resolution chemically specific information for organic films. In order to employ scanning force microscopy for these investigations, one has to consider the techniques of preparing such films. Several criteria for successful imaging and, most importantly, surface-force measurements are crucial–a film has to be smooth enough so that there is little variation in the contact area between an SFM probe and a surface, the surface chemistry of a film has to be well defined, and the physical properties of the film have to ensure as little plastic deformation as possible. Our first efforts to employ scanning probe microscopy with chemical sensitivity were focused on block copolymers of polyesterurethanes for biomedical applications. Thin films of this material were prepared by means of spin-casting–a conceptually simple process involving the application of a drop of a polymer solution onto a rotating substrate. As will be shown in Section 3.2, despite the obvious simplicity of this process, very complex morphological structures can be obtained that do not meet the above mentioned criteria for successful, chemically sensitive SFM, and many polymer

properties, such as average molecular weight, polydispersity, solvent interactions with polymer constituents, crystallinity, and many others, become important. Spin-casting, however, can provide surfaces suitable for chemically sensitive force measurements and imaging, particularly of amorphous polymers with high glass-transition temperatures.

During the search for other techniques that are capable of producing thin polymer films, a friction deposition method was also considered. The description of this technique and results of the SFM studies are discussed in Section 3.3.

Ultrathin organic films, and specifically monolayers, can be produced by means of self-assembly. Section 3.4 provides a detailed description of the process of self-assembly of thiolates on gold. In this section, examples of high resolution imaging and frictional imaging with chemical sensitivity are also given.

3.2 Preparation and Imaging of Thin and Ultrathin Spin-Cast Polymer Films

A common way of producing thin polymer films is by means of spin-casting (see Fig. 3.1 below). In this conceptually simple process a drop of a polymer solution is applied to a flat substrate that is accelerated to a particular angular speed (rotational speeds commonly fall in the range 1000-8000 rpm). The liquid flows under the centrifugal force and eventually covers the entire surface, then the excess of the liquid is removed and, if the liquid is Newtonian and uniform in viscosity, a film of nearly uniform thickness is formed. The tendency of the liquid film toward uniform thickness as it is thinned by centrifugally-driven radial outflow lies at the heart of the spin-coating process.[7]

When one takes a more careful look at the spin-casting process, it becomes evident that it is, in fact, extremely complex. It involves a transient mechanism of flow and mass transfer, it is a competition between a centrifugally driven thinning of a liquid film and concentration-driven solvent evaporation; falling diffusivity, rising viscosity, shear thinning and changing rheology as solvent evaporates all complicate the process, so it is not surprising that nothing approaching a theory of spin casting has appeared yet.

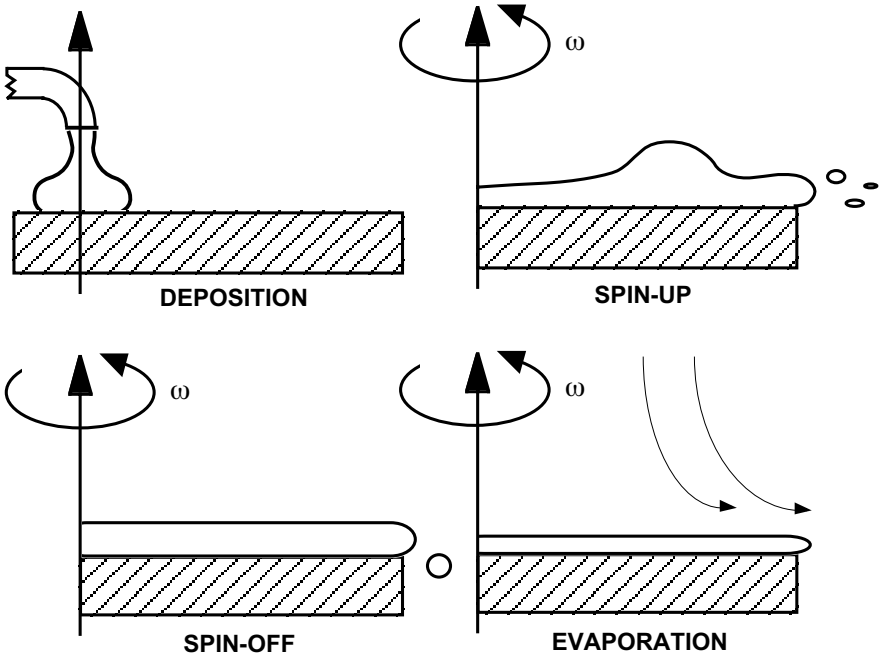

Figure 3.1 *Schematic representation of a spin-casting process. The first three stages (deposition, spin-up and spin-off) are commonly sequential, while spin-off and evaporation overlap.*

However, many experimental and theoretical studies of the separate mechanisms involved in the process have been carried out. As early as 1922, Walker and Thompson[8] described the spin coating technique for producing reproducible films of paint. They found that for Newtonian liquids the final film thickness was independent of the amount of the deposited solution. For a wide range of polymer solutions it was determined[9] that the final film thickness, h_f, correlates with the angular speed as $h_f \sim \omega^{-\lambda}$, where $0.45 \leq \lambda \leq 0.8$. It has also been shown that final film thickness and surface roughness were strongly affected by the initial solution viscosity,[10] solvent volatility,[11] solvent quality, polymer polydispersity and weight average molecular weight.[12] It must be noted that most of the studies referenced were mainly conducted on amorphous glassy polymers, such as polystyrene and poly(methyl methacrylate).

A very interesting consequence of a spin-casting process is that, for high molecular weight polymers, a uniform and continuous film can be obtained with an average film thickness comparable to, or less than, a radius of gyration of unperturbed macromolecules. This implies that molecular conformation of the chains in such systems must be different and this, therefore, leads to a change in physical properties

compared to that of the bulk polymers. It has been shown, for example, that birefringence of polystyrene and polycarbonate films increased significantly as the film thicknesses were reduced, indicating a higher in-plane orientation[13] and chain alignment parallel to the substrate plane. Other factors, such as adhesion to the substrate or presence of residual solvent may significantly change the glass-transition temperature and thermal expansion coefficient of polymer films when compared to the bulk values.[14,15] For semicrystalline polymers it was shown that poly(di-n-hexyl silane) did not crystallise when the film thickness was reduced below 150Å, and the authors suggested that there was a critical nucleation thickness for surface induced crystallization.[16]

Our initial goal was to employ SFM to study interactions, relevant to protein and cell adhesion, of chemically functionalised SFM probes and thin films of modified biocompatible, biodegradable polyesterurethanes (thermoplastic elastomers) produced by means of spin-casting. These polyesterurethanes,[17,18] DegraPols®, were synthesised and studied in the group of Prof. U. W. Suter at the Institute of Polymers (IfP) of the Swiss Federal Institute of Technology (ETH).

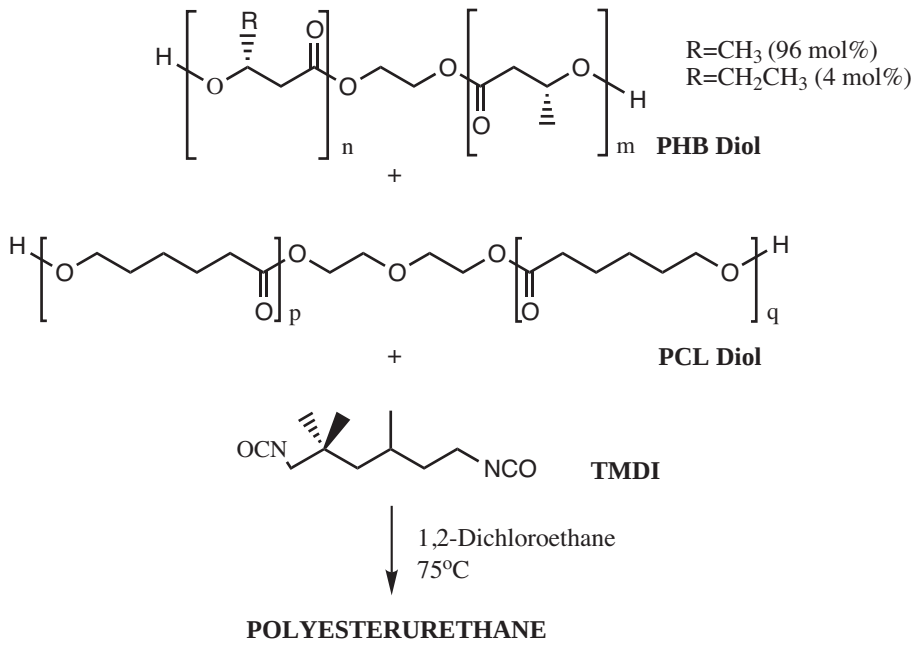

Figure 3.2 *Polymerisation procedure to obtain a block polyesterurethane from PHB-diol, PCL-diol and TMDI.*

Polyesterurethanes are synthesised from dihydroxyterminated low-molecular weight {[(*R*)-3-hydroxybutyric acid]-co-[(*R*)-3-hydroxyvaleric acid]}, PHB diol, (number-average molecular weight M_n=2300 g/mol), dihydroxyterminated poly(ε-caprolactone), PCL diol, (number average molecular weight M_n=2400 g/mol), and junction units of 2,2,4-trimethyl-hexamethylene-diisocyanate, TMDI. The crystallisable PHB diol guaranties the presence of "hard" domains that provide good mechanical characteristics, while the "soft" amorphous PCL-rich domains ensure degradation through hydrolytic cleavage of the ester linkages. Varying the molar fractions of the two diols changes both mechanical properties and degradation time. Many complications are associated with these block copolymers when one attempts to produce thin flat films by spin-casting. Polydispersity of these materials is unknown and is believed to be very high. The presence of both crystalline and amorphous domains complicates solution preparation, since the solvent quality differs significantly for the two components. The presence of water in the solvent induces hydrolytic cleavage and formation of low-molecular-weight species.

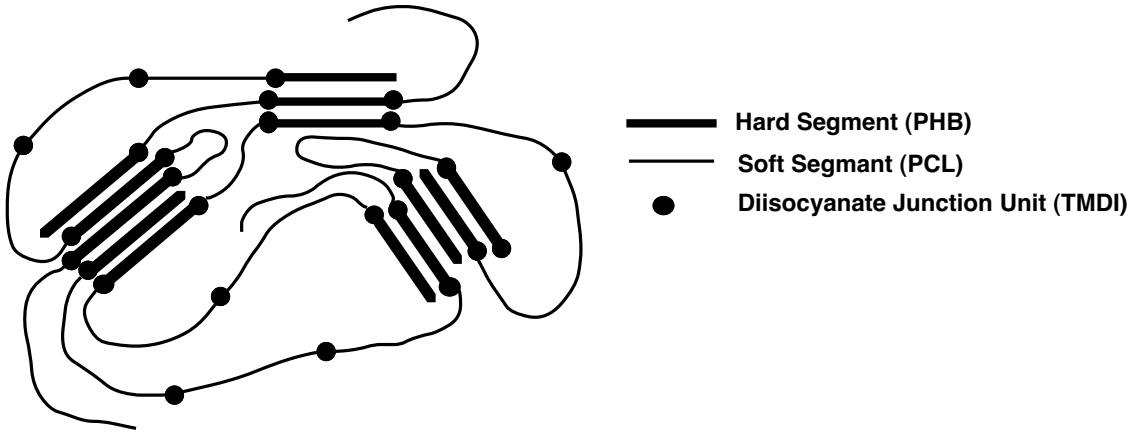

Figure 3.3 *Schematic representation of the polyesterurethane structure.*

During solvent evaporation, the ratio of solvent to non-solvent (if the chosen solvent does not dissolve PHB), as well as the polymer concentration, changes rapidly. Furthermore, a liquid-liquid phase separation with the formation of polymer-rich and polymer-poor phases is certainly anticipated[19] for such a complex system. These effects could lead to a formation of phase-separated structures or to the formation of various semicrystalline domains, depending on the phase from which nucleation and crystallisation takes place.

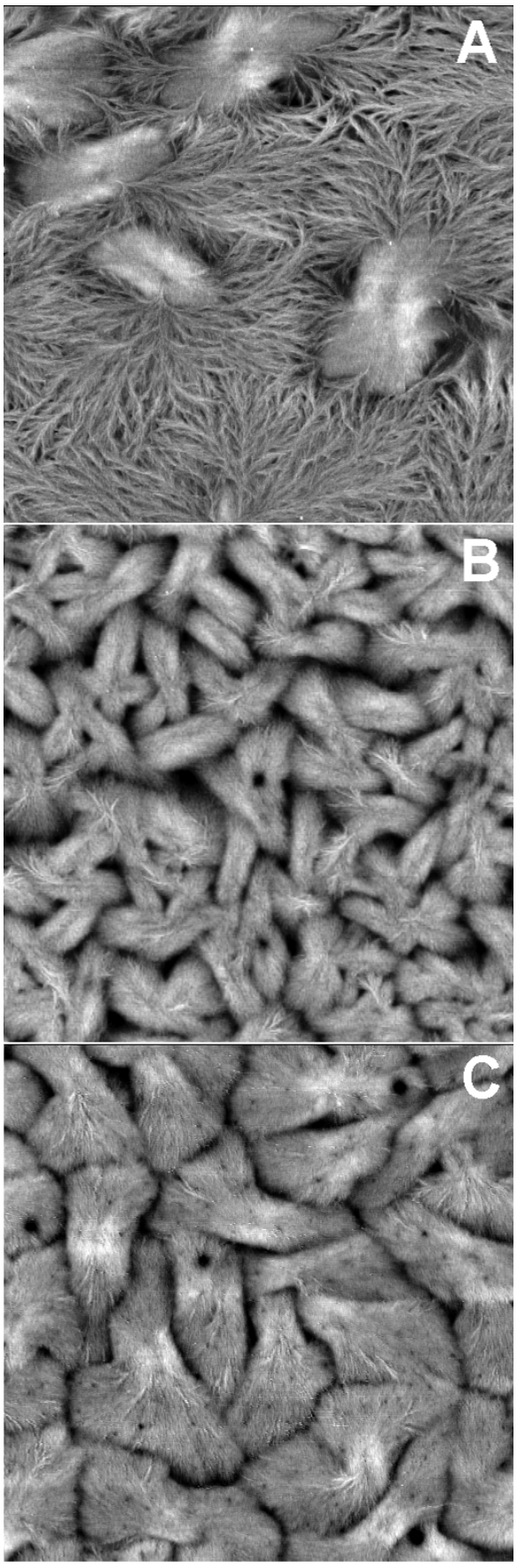

Figure 3.4 *10×10μm^2 SFM images of polyesterurethane thin films spin-cast from a) 1,4-dioxan, b) 2-butanone, and c) tetrahydrofuran. Z-range of the images–60nm.*

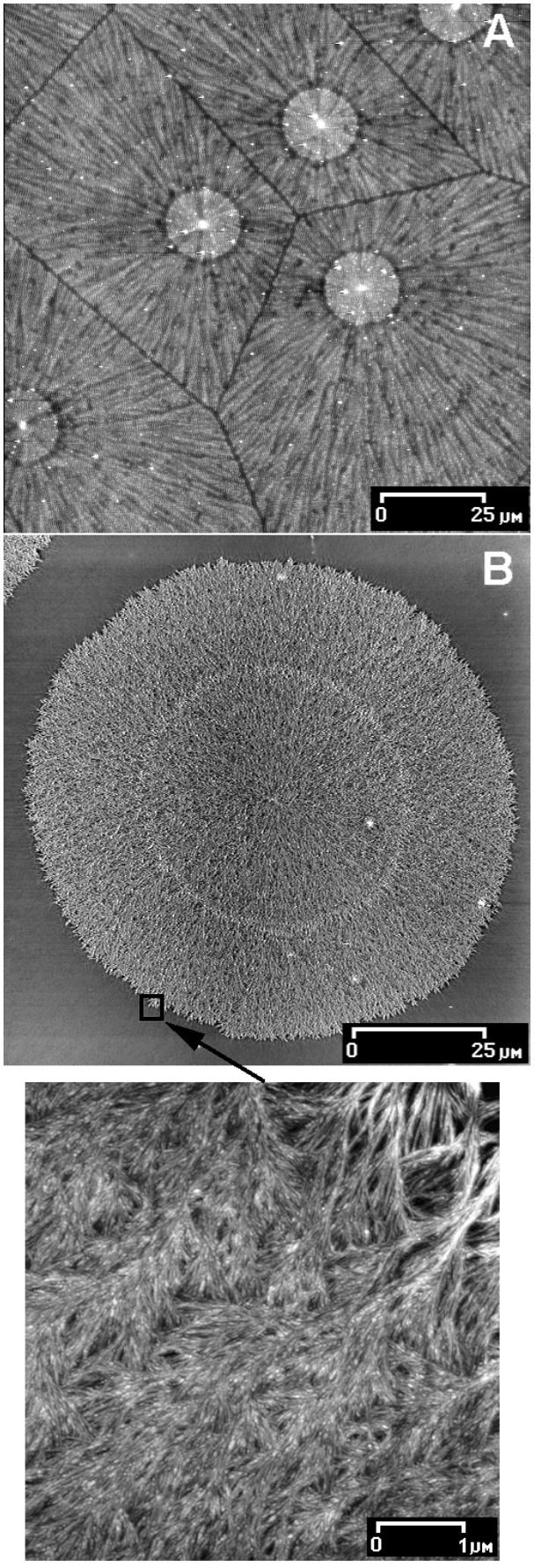

Figure 3.5 *SFM images of the polyesterurethane film spin-cast from a) chloroform and b) 1-methyl-2-pyrrolidinone.*

Since there has been no systematic study of Degrapol® solution behaviour and the availability of the material was very limited, we have only attempted to produce spin-cast films of this polyesterurethane from a range of solvents that had previously been used to "dissolve" the polymer. These experiments were conducted in order to assess the feasibility of using spin-cast films of the polyesterurethane for scanning force microscopy investigation of the polymer interaction with functionalised SFM probes. All solutions were prepared with a concentration of 1 wt.% and spin-cast at 1000 rpm onto oxygen-plasma-cleaned silicon wafers. Scratch tests and ellipsometry revealed that the film thicknesses were in the range of 40-100nm. The figures 3.4 and 3.5 show the complexity and variety of structures of the spin-cast films prepared from a range of solvents. For the films prepared from 1,4-dioxan, 2-butanone (MEK), and tetrahydrofuran (THF), sheaves of lamellae were observed (Fig. 3.4). The morphology appeared very similar for the films prepared from MEK and THF (Fig. 3.4B, C) and consisted of closely packed lamellas. While a similar lamellar structure was also observed for the film prepared from 1,4-dioxan, the lamellae were separated by a fibrillar network spreading radially from them. Spherulitic morphology was observed for the spin-cast films prepared from 1-methyl-2-pyrrolidinone (NMP) and chloroform, with spherulite boundaries being observed for the film prepared from chloroform (Fig. 3.5A).

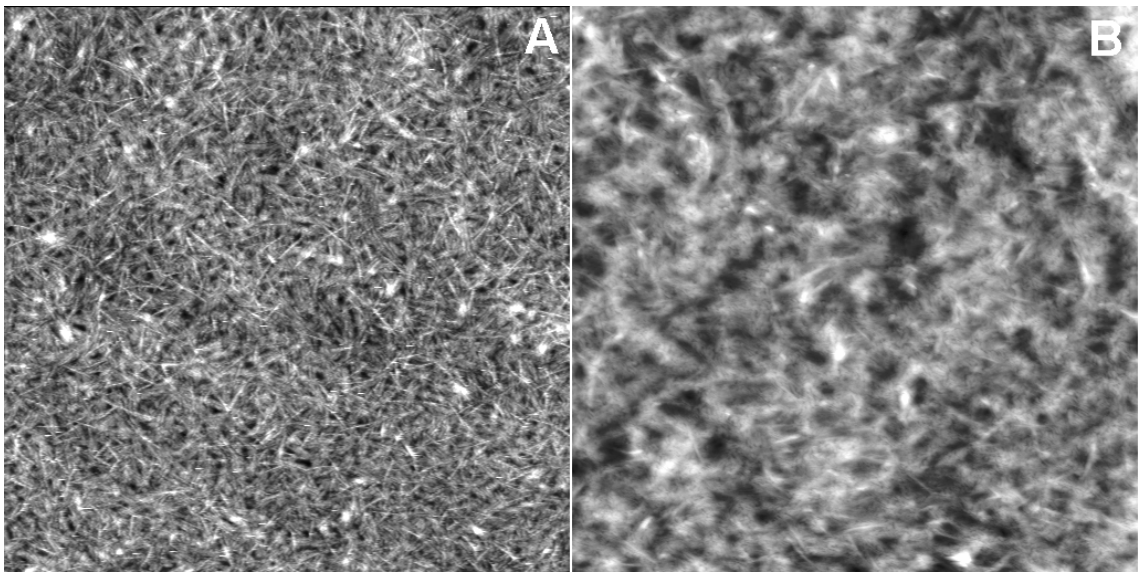

Figure 3.6 *10×10μm^2 SFM images of a) polyesterurethane film spin-cast from toluene solution and b) surface of the inner wall of the melt-extruded tube of the same polymer.*

The morphology of the polyesterurethane film prepared from toluene solution revealed surface morphology with needle-like crystals similar to that of the tubes extruded at 140ºC, suggesting that toluene actually dissolves the semicrystalline PHB-rich domains of the polymer (Fig. 3.6). This complex fibrillar morphology, which leads to high surface roughness (high variations in the contact area between a surface and an SFM probe) and inhomogeneity of surface physical properties (these films are easily damaged under moderate loads) prevented us from using SFM for further investigations of this material.

In a separate study, we used a commercially available non-degradable polyesterurethane, Estane® 54620 from BFGoodrich Chemical (Belgium). Information on the chemical composition of this polymer was very limited. Neither the chemical formula of the polyol nor the molecular weight were available, the chain extender was 1,4-butanol and the linker–4,4,-diphenyl methane di-isocyanite, the melting temperature of the polymer being 170-180ºC. The polymer dissolved readily in toluene. A spin-cast film from 1 wt.% toluene solution exhibited a low-roughness, featureless surface topography (Fig. 3.7A). However, ellipsometric measurement revealed a low refractive index of the film, suggesting a high residual solvent content. To ensure solvent removal, film samples were annealed at 60ºC in vacuum for 2 hours ($T_g \approx 5$ºC) and 24 hours, followed by quenching to room temperature. SFM images of the thermally treated samples revealed that the surface morphology was no longer homogenous. After one hour of annealing (Fig 3.7B), sub-micron size domains appeared on the surface that exhibited lower adhesion to a non-treated Si_3N_4 probe and lower friction signal. At high applied loads the domains could be "wiped away" by the probe without damaging the polymer matrix. This phase separation may be due to a presence of additives and stabilisers common in commercial polymers that migrate to the surface, or due to high polydispersity of the material, which also leads to diffusion of low-molecular-weight species to the interface. Annealing for longer period of time leads to the growth of a fibrillar, sponge-like, structure on the polymer surface (Fig. 3.7C). Clearly, this commercial material could not be further employed in the SFM study, for which defined chemical composition and structure was required.

The choice of polymer solvent plays an important role in defining the surface roughness of the spin-cast film. An example of this effect is shown in Fig. 3.8.

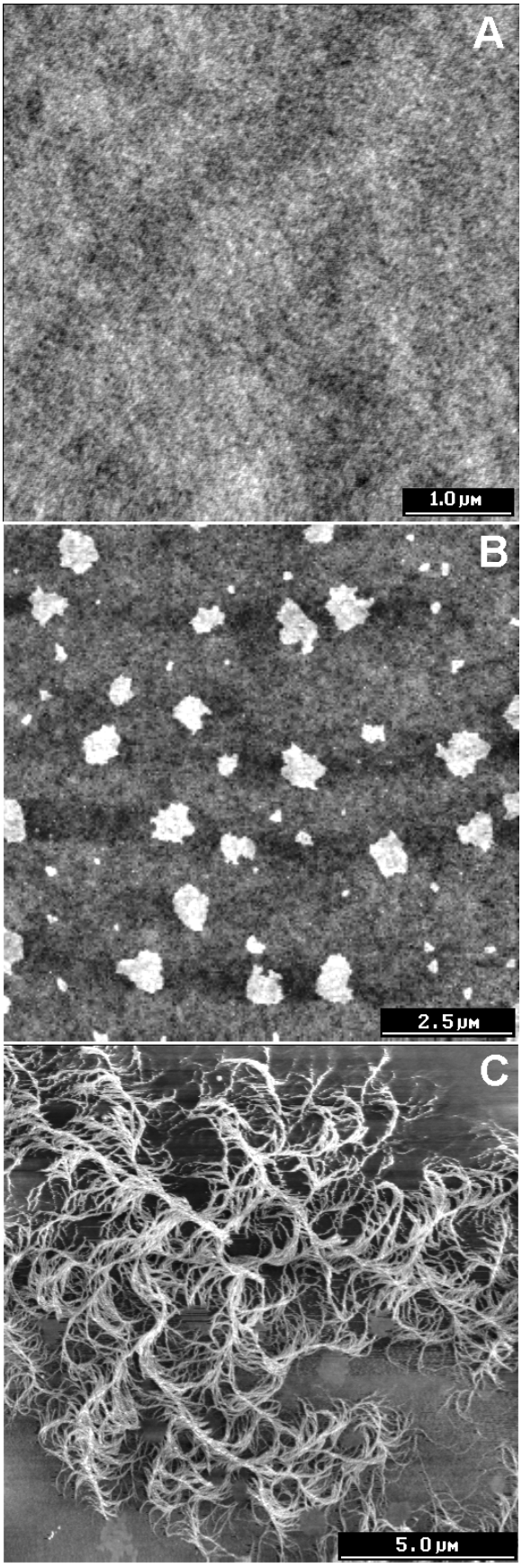

Figure 3.7 *SFM Images of Estane® spin-cast from 1 wt.% toluene solution; a) after spin-casting, no thermal treatment, b) 1 hr. at 60ºC in high vacuum, quenched to room temperature, c) 24 hrs. at 60ºC in high vacuum, quenched to room temperature.*

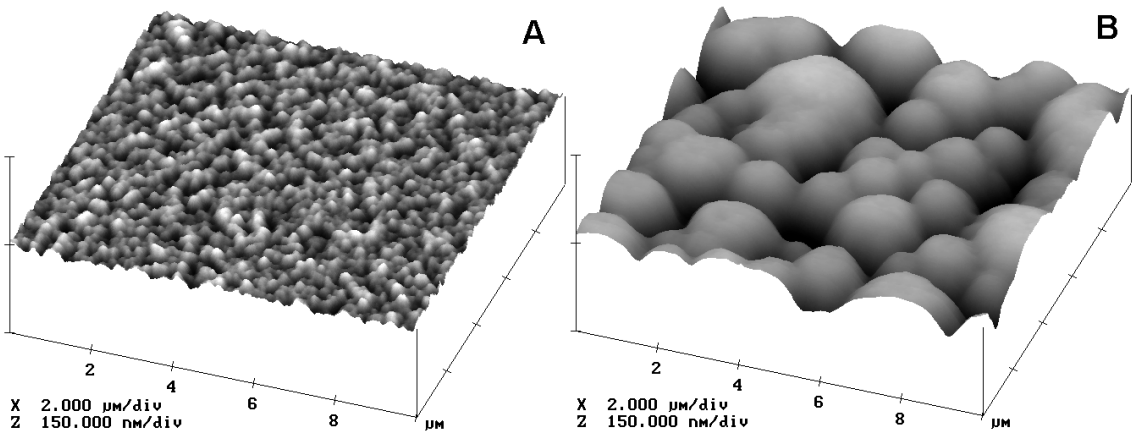

Figure 3.8 *3D 10×10μm2 SFM images of Estane® Spin-cast from a) chloroform (root mean-squared roughness, RMS=3.9nm) and b)1-methyl-2-pyrrolidinone (RMS=20.4nm). Z-range for both images is 150nm.*

Films of Estane® were prepared by spin-casting 2 wt.% solutions in chloroform (Fig. 3.8A) and 1-methyl-2-pyrrolidinone, NMP, (Fig. 3.8B) at 2000rpm onto cleaned Si wafers. The SFM roughness analysis revealed that the surface roughness of the film prepared from NMP was more than 5 times higher than that of the film prepared from chloroform.

After unsuccessful attempts to utilise polyesterurethanes for SFM experiments with chemical sensitivity, we decided to take a step back and analyse polymeric structures that are smooth, chemically well-defined and homogeneous. For this reason, we prepared spin-cast films of amorphous, high-T_g and high-molecular-weight polymers, such as polystyrene, poly(methyl methacrylate), and others. The description of the SFM studies on these polymers is given in the next chapter. These materials can be easily spin-cast from a range of solvents. Annealing above T_g ensures solvent removal, smooth surface topography and homogenous surface structure, and removal of residual stresses in the film. Figure 3.9 shows SFM images of a polystyrene film spin-cast from 1 wt.% toluene solution at 2000rpm. Prior to annealing, the surface topography includes pores that were formed during rapid solvent evaporation. Upon annealing at 120ºC in vacuum a very smooth and uniform surface is achieved, the root mean-squared roughness (RMS) of the annealed surface being ≈0.3nm.

For a study of protein adsorption onto polymer films we coated optical waveguides with polystyrene and poly(acrylonitrile), PAN.

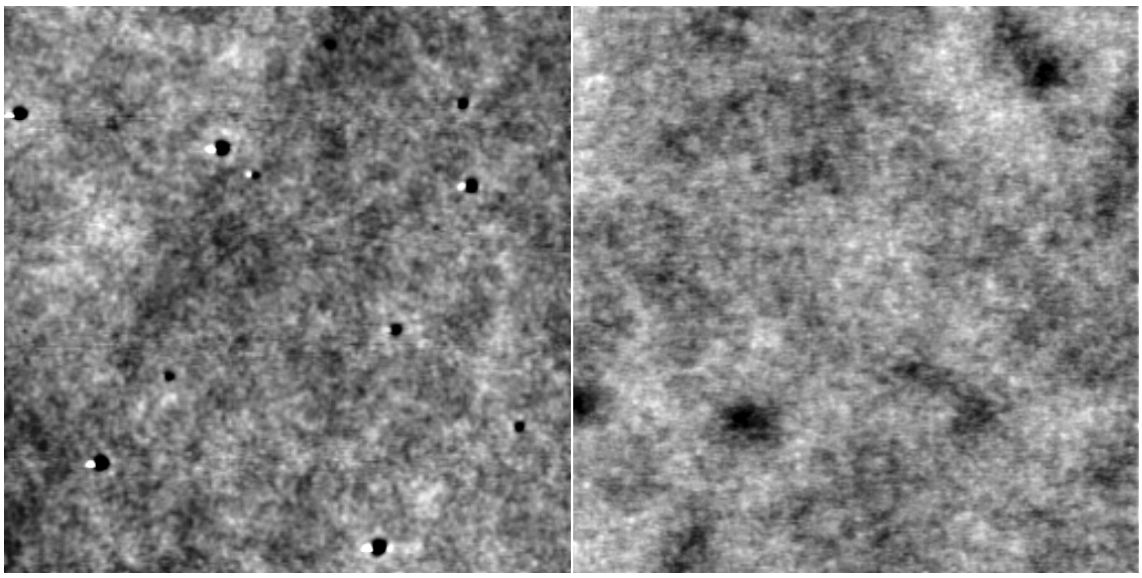

Figure 3.9 *5×5 μm^2 SFM images of polystyrene (M_w=250K g/mol) spin-cast film a) prior to annealing and b) after annealing at 120ºC in vacuum for 4 hrs. Z-range of the two images–10nm.*

This application required that the film thickness should not exceed 15-20nm. This can be achieved by lowering the polymer concentration in the solution and increasing the angular speed during the spin-casting. During an effort to decrease the film thickness to the required range, we observed a very interesting surface network structure for the PAN film spin-cast from 0.02 wt.% solution in *N,N*-dimethylformamid at 5000 rpm.

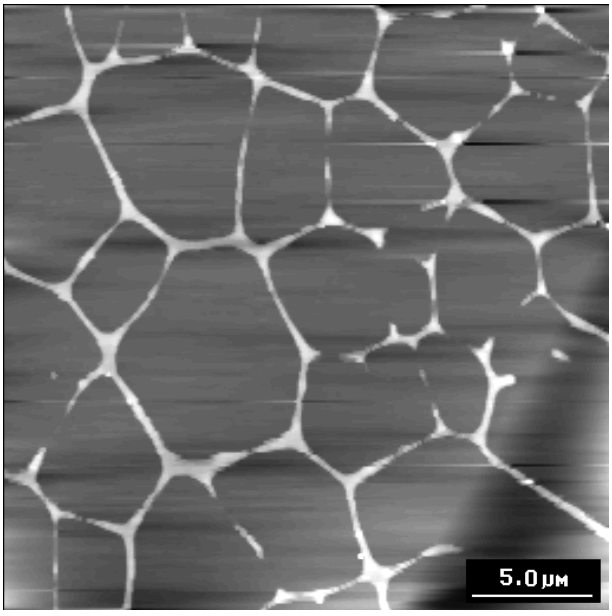

Figure 3.10 *SFM image of PAN film spin-cast onto silicon wafer from 0.02 wt.% solution in N,N-dimethylformamid at 5000 rpm. Z range-50nm.*

This network structure is similar in shape to the boundaries of the spherulitic structures like the one shown in Fig 3.4A. This type of structure is usually referred to as Voronoi tessellation.[20] If points of nucleation (Poisson points) are placed randomly on the surface and are allowed to grow simultaneously at the same rate in circular disks and if the disks are not allowed to impinge on the area of the other and have to deform, the disks evolve into polygons, with the edges equidistant from the two nucleation points and each vertex equidistant from the three nucleation points.[21,22]

This network suggests that, during thinning of the film, a critical film thickness can be reached after which film ruptures over large areas and retreats from rupture points until it runs into another film that retreats from an adjacent location. This mechanism leads to the development of the polymer network which is similar in structure to the domain boundaries of the spherulites in Fig. 3.4A.

3.3 Thin Polymer Films By Means of Friction Deposition

Our interest in finding polymer systems suitable for SFM with chemical sensitivity and, particularly, films of polymers with low refractive index, led us to consider ultrathin polymer films of poly(tetrafluoroethylene), PTFE, prepared by means of friction deposition.[23,24] This surprisingly simple method of rubbing a PTFE bar against a clean flat substrate at constant load and velocity at elevated temperatures (150-350°C) produces highly-ordered, uniaxially oriented crystalline films of PTFE.

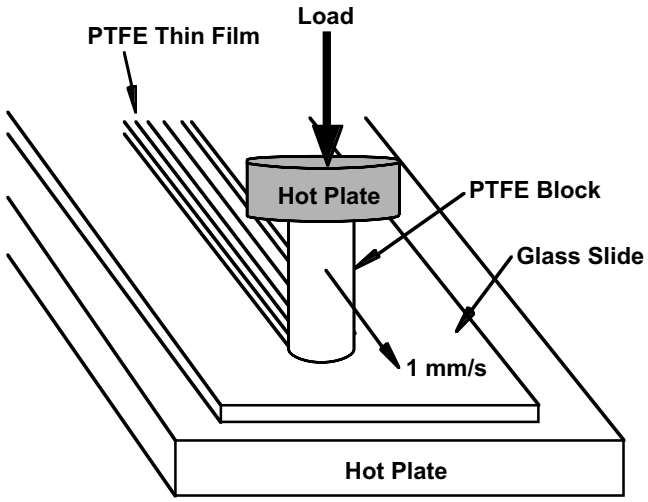

Figure 3.11 *Schematic diagram of friction deposition process of PTFE thin layer.*

Depending on the process parameters, film thickness may vary from several nanometres to several hundreds of nanometres.

The main interest in these uniaxially oriented films lies in their applications as substrates for epitaxial and graphoepitaxial oriented growth of materials,[24,25] including liquid crystals,[26] polymers,[27] small organic molecules,[24] organic dyes[28] and even myosin (the motor protein of muscle) molecules[29] which adhere in an oriented fashion along the PTFE ridges and retain their ability to support the movement of actin filaments.

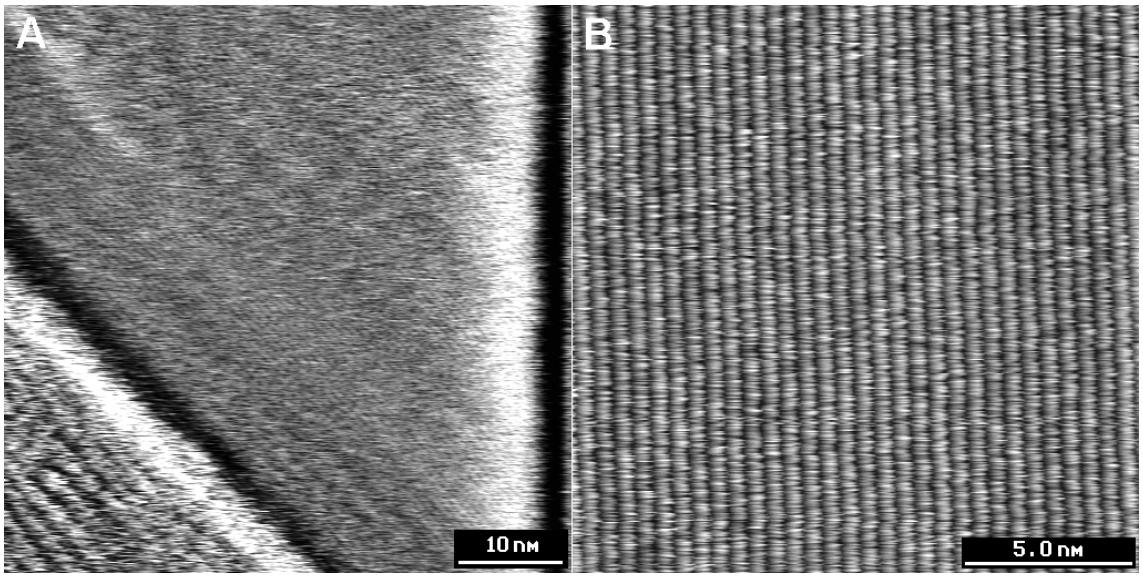

Figure 3.12 *High resolution SFM images of the uniaxially oriented PTFE film.*

This ability of the PTFE films to induce uniaxial orientation of deposited materials has found applications in the design of new light-emitting diodes[30,31] (LEDs), composites for non-linear optics,[32] and flat liquid crystal displays.[33]

Uniaxially oriented films of PTFE have been extensively studied with the SFM,[34,35] since the periodic structure can be easily resolved due to the large Van der Waals diameter of the chains, and the friction anisotropy due to the uniaxial orientation of the PTFE molecules.[36,37]

As was mentioned before, our interest was in studying the adhesion behaviour of oriented films of PTFE with SFM force-distance measurements. We found, however, a very broad distribution of the pull-off forces (Fig. 3.13) due to possible plastic

deformation in the film; high roughness of the grooves and ridges (up to 100nm in height) and, therefore, variability in the contact area; possible transfer of material to the probe tip; and the presence of a static charge on the film surface that was difficult to remove.

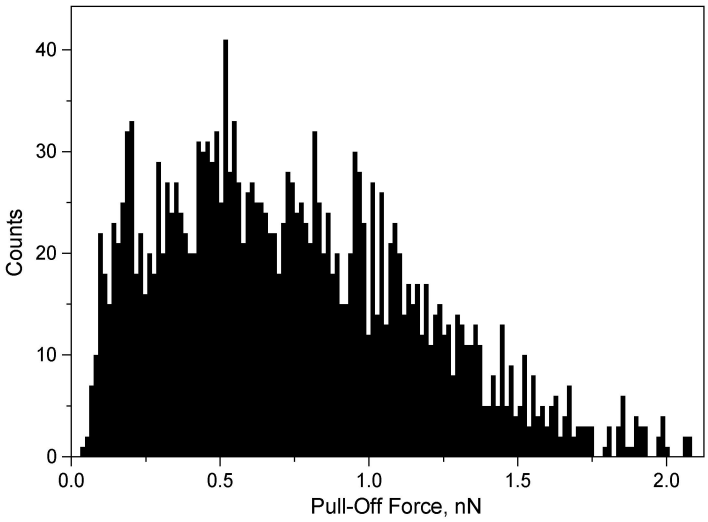

Figure 3.13 *Histogram of the pull-off forces measured between gold-coated probe (k=0.1 N/m) and PTFE film in perfluorodecalin.*

Despite this result, we could not resist an opportunity to visualise with a high-resolution SFM the effects of molecular orientation on the PTFE films. In a first experiment, a uniaxially oriented film of PTFE was briefly exposed to the vapour of tetracosane ($C_{24}H_{50}$). An SFM image (Fig. 3.14) reveals that the molecules of tetracosane orient in between the chains of PTFE due to a smaller chain radius. The fast Fourier transformation (FFT) analysis shown in Fig. 3.14b clearly indicates the presence of two frequencies in the high-resolution image that correspond to the uniaxially oriented chains of PTFE and tetracosane respectively.

In another experiment, a tiny flake of perfluorinated eicosane ($C_{20}F_{42}$) was placed on top of the oriented PTFE film and melted. At first, high resolution imaging revealed that the molecules appeared to be oriented parallel to the PTFE chains and parallel to the substrate plane (Fig 3.15A). The same area was imaged 5 minutes later revealing the CF_3-tails to have a slight tilt out of the PTFE orientation direction and out of the substrate plane, suggesting that the molecules were rearranging and orienting towards the normal to the substrate plane (Fig 3.15B). Imaging after 15 minutes revealed a hexagonal crystal structure of the fluoroeicosane molecules (Fig. 3.15C).

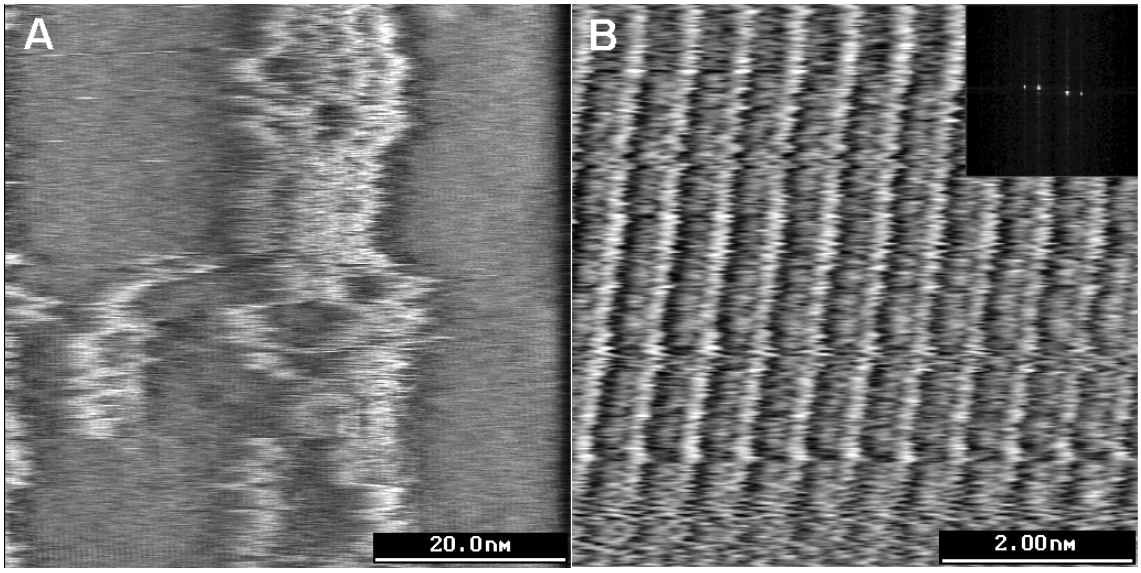

Figure 3.14 *High resolution SFM images of tetracosane molecules oriented in between the chains of the uniaxially oriented PTFE.*

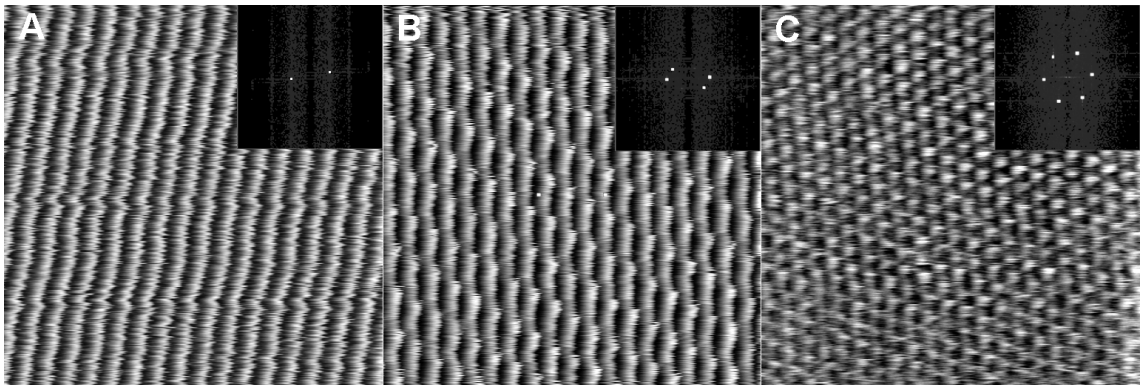

Figure 3.15 *High resolution SFM images and FFT analyses of fluoroeicosane molecules on uniaxially oriented PTFE a) scanned immediately after deposition, b) 5 min after deposition c) 15 min after deposition.*

These images indicate that, due to a large volume of the deposited molecules, the effect of the epitaxial orientation of fluoroeicosane on the PTFE layer is not sufficient to prevent the molecules at the air interface from reorienting perpendicular to the surface normal in order to minimise surface free energy (surface tension of $–CF_3$ group is 15mN/m while that for the $–CF_2–$ is 23mN/m).[38]

3.4 Self-Assembled Monolayers of Alkanethiols

Fundamental studies of adhesion, friction, biocompatibility, wetting, and other related phenomena require chemically and structurally well-defined surface models of thin and ultra-thin organic or metallo-organic films, for which surface free energy, functional

group density, conformational order and other parameters can be systematically varied and characterised. When a scanning force microscope is employed in these studies, the chemical composition of an SFM probe becomes of great importance and the probes need to be chemically defined in order to obtain meaningful results. A highly effective approach to modifying SFM probes and producing surfaces of ultrathin, chemically and structurally well-defined films is by means of self-assembly. Self-assembled monolayers (SAMs) are formed spontaneously by wetting an appropriate substrate with a solution of an active surfactant in an organic solvent or by vapour-phase adsorption of the active molecules onto the substrate. There are many types of molecules that form SAMs, including organosilanes on hydroxylated surfaces of silicon oxide, aluminium oxide and glass;[39] alkanethiols on gold,[40] silver,[41] and copper;[42] alcohols and amines on platinum;[43] carboxylic acids on aluminium oxide;[44] and alkanephosphates on oxides.[45] In this thesis, the adsorption of SAMs of ω-substituted alkanethiols onto gold and silver are described and, therefore, a more detailed discussion is devoted to that subject.

Formation of alkanethiol SAMs on Au(111) has been investigated, and a two-step adsorption process has been proposed.[46] In a first step, the molecules are thought to rapidly physisorb onto the gold surface, following a Langmuir-type adsorption isotherm. In a second step, the molecules rearrange, lateral attractive Van der Waals interactions between the alkyl chains drive the molecules to pack into crystalline domains, the sulphur atoms bind to gold (chemisorption), and an ordered monolayer is formed with the chains oriented close to the surface normal. Chemisorption of alkanethiols on gold yields the gold thiolate species[39] via the reaction:

$$RS - H + Au_n^o \Rightarrow RS^- - Au^+ + \frac{1}{2}H_2 + Au_n^o .$$

The binding energy of alkanethiols on gold has been determined to be approximately 120 kJ/mol.[47] The binding of the sulphur atoms occurs in a highly ordered manner at the three-fold hollow site of the gold atoms,[48] producing a $(\sqrt{3}\times\sqrt{3})R30°$ lattice structure on Au(111). Since the distance between the sulphur atoms is greater than the diameter of the hydrocarbon chains, the chains tilt about 30° from the surface normal to maximise the attractive intermolecular Van der Waals interactions. However, the chemical reaction mechanism is not completely understood, hydrogen evolution, for example, has yet to be detected.

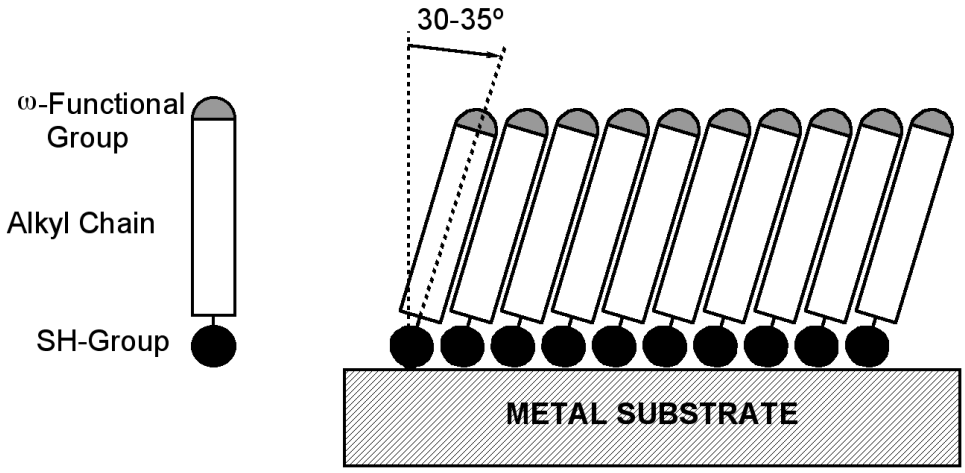

Figure 3.16 *Self-Assembled Monolayer of alkanethiols on a gold surface.*

Figure 3.17 shows high-resolution SFM images of Au(111) surface with the measured Au-Au distance of 2.8±0.1nm and hexadecanethiolate on gold with the nearest neighbour distance of 4.9±0.1nm, in accordance with previously published results.[49] Surface patterning with SAMs of alkanethiols can be performed from the vapour-phase by the elegant "micro-contact printing" (μCP) technique.[50] In this method, an elastomeric stamp (usually made from poly(dimethylsiloxane), PDMS) bearing a 3D-patterned surface is inked with a thiol solution, the solvent is allowed to evaporate, and the stamp is placed onto the gold substrate. Thiol molecules transfer onto gold in the areas of contact, forming a SAM. The formation of SAMs using this method is very rapid, "high quality" SAMs being formed within several seconds of contact time.[51] However, the adsorption mechanism in this case is not well understood.[52] The "stamped" gold surface can subsequently be placed into a solution of another thiol with a different surface functional group to form a patterned surface with alternating surface chemical properties. The SFM probes can also be modified with SAMs of thiols yielding tips with well-defined chemical and structural compositions (the probes are coated with gold and subsequently immersed into thiol solution).

If a surface, patterned with different functional groups, is now scanned in friction mode with a chemically modified probe, contrast in the friction signal usually arises from the difference in the extent of interaction between the probe and the surface functionalities. This method, therefore, provides chemically sensitive information of the surface composition with high lateral resolution.

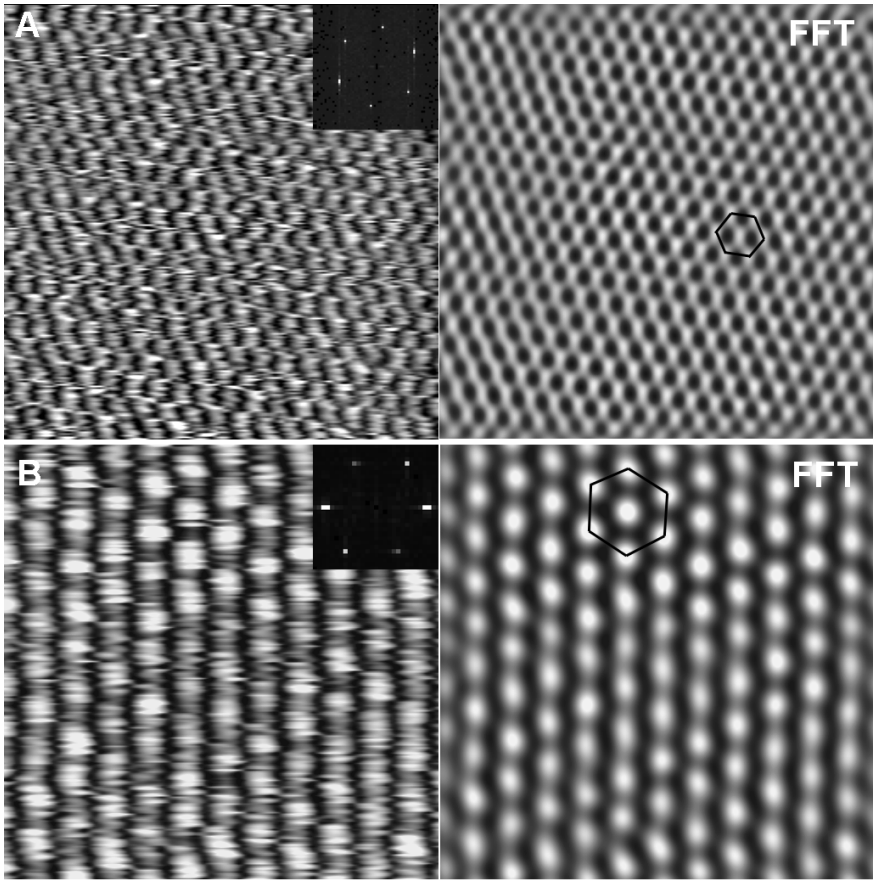

Figure 3.17 *5×5nm^2 SFM raw and FFT-filtered images of a) thermally evaporated gold surface and b) SAM of hexadecanethiol on gold obtained by immersion into 1mM solution in ethanol for 20 minutes.*

It was first developed in the group of Prof. C. M. Lieber at Harvard University and received the name of "chemical force microscopy", CFM.[53] Most CFM measurements have been performed on the surfaces patterned with SAMs of thiolates of similar chain lengths and different ω-group functionalities. For these systems it has been shown that microscopic friction could be directly correlated to the adhesive forces (the pull-off forces measured with an SFM), since the mechanical properties of the two phases were similar. It must be noted that it is only when the elastic and crystalline properties of the two phases are similar that the contrast in a friction mode experiment can be directly correlated with the chemical composition, and the two phases easily identified. It has been shown, for example, that for phase-separated Langmuir films of perhydroarachidic acid ($C_{19}H_{39}COOH$) and fluorinated carboxylic ether acid ($C_9F_{19}C_2H_4$-O-C_2H_4COOH), friction signal was found to be higher for fluorinated molecules, since they are present in a more liquid-like state.[54] Even if the surface functional group of the two constituents is the same, the frictional signal might depend strongly upon the chain length of the

molecules in the monolayer, revealing frictional contrast due to differences in mechanical properties.[55]

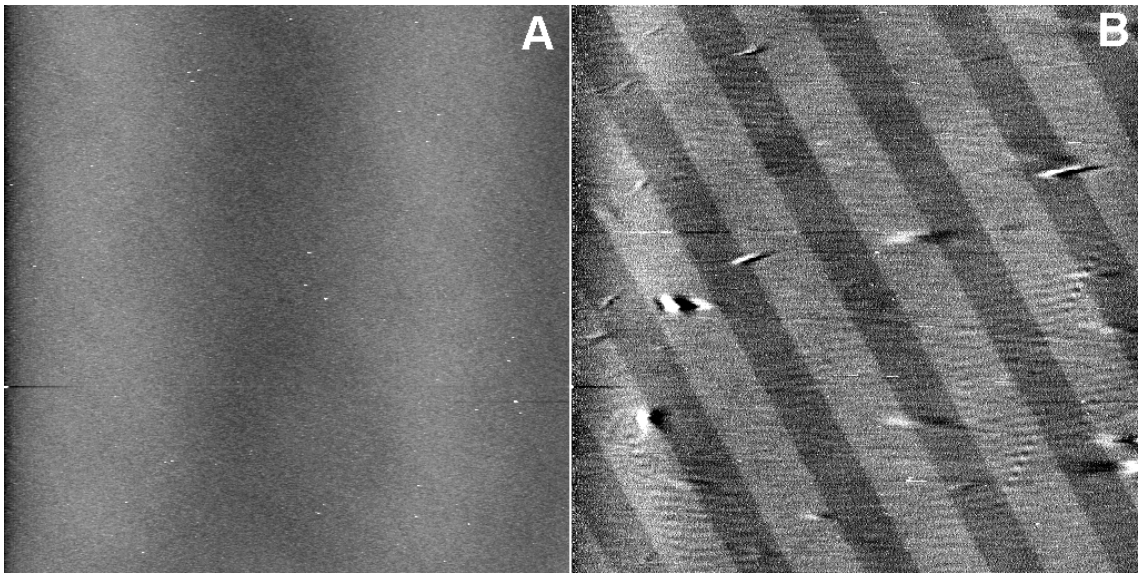

Figure 3.18 *100×100μm² SFM a) height and b) friction images of gold patterned with C16 and EG3-OMe thiols.*

An example in Figure 3.18 shows an SFM image of the gold surface patterned with monolayers of hexadecanethiol (C16) and (1-mercaptoundec-11-yl)-tri(ethylene glycol) methyl ether, EG3-OMe ($SH\text{-}C_{11}H_{22}\text{-}(O\text{-}CH_2\text{-}CH_2)_3\text{-}OCH_3$), imaged with a hexadecanethiol-functionalised probe (C16-probe) in an aqueous 1mM KNO_3. While there is no contrast in the "height" image due to similar chain lengths, the subtracted (Chapter 2.1) friction image shows significant contrast that allows the chemically different regions to be distinguished. In this particular case, the force-distance measurements reveal an attractive force upon approach for the C16/C16 pair, while that for the C16/EG3-OMe pair was found to be repulsive; the pull-off forces were, therefore, found to be much stronger for the C16/C16 pair than for C16/EG3-OMe pair. Combining adhesion and friction information, we may conclude that the lighter areas on the friction image represent regions of the EG3-OMe SAM. A study of the oligo- and poly(ethylene glycol)-terminated SAMs on gold and silver will be discussed in more detail in Chapter 5.

3.5 Conclusions

Scanning force microscopy investigation of polymeric thin films prepared by means of spin-casting revealed that, despite the apparent simplicity of the process, complex

polymer morphologies can be obtained. A diverse field of parameters and process conditions have to be accounted for in order to achieve desirable surface morphological properties: polymer chemical structure, molecular weight, polydispersity, solvent quality, phase behaviour, solvent vapour pressure, spinning conditions, solution viscosity, solution concentration, substrate cleanliness, all have to be considered when preparing thin films by spin-casting.

The complex (fibrilar) surface morphology of biocompatible polyesterurethanes prevented a chemically sensitive SFM study of these systems. Spin-casting of well-defined amorphous polymers, however, provided the means of generating surface morphologies of the desired roughness and homogeneity for SFM investigations.

Force spectroscopy and frictional imaging with chemical sensitivity of spin-cast semicrystalline and amorphous polymeric thin films are described and discussed in Chapter 4. The conformational differences of oligo- and poly(ethylene glycol)-terminated SAMs on gold and silver and the relevance of these conformational effects to resistance to protein adsorption are studied with SFM and covered in Chapter 5.

References

1. Swalen, J. D. In *Organic Thin Films: Structure and Applications*; Curtis W. F. Ed.; ACS Symposium Series Vol. 695; ACS, Washington, D.C., 1998; Chapter 1.
2. Ulman, A. *Organic Thin Films and Surfaces: Direction for the Nineties*; Academic Press: San Diego, 1995.
3. Swalen, J. D. *J. of Molecular Electronics* **1986**, 2, 155.
4. Allara, D. L. *Biosensors and Bioelectronics*; Elsevier: Amsterdam, 1995; Vol.10, 771.
5. Knoll, W. *Encyclopedia of Applied Physics*; VCH Publishers: Brooklyn, NY, 1996; Vol. 14, 569.
6. *Organic Thin Films for Waveguiding Non-linear Optics*; Kajzar, F., Swalen J. D., Eds.; *Advances in Non-linear Optics*; Gordon and Breach Publisher: Amsterdam, 1996; Vol. 3.
7. Bornside, D. E.; Macosko, C. W.; Scriven, L. E. J. *Imag. Techn.* **1987**, *13*, 122.

8. Walker, P. H.; Thompson, J. G. *Proc. Am. Soc. Test. Mat*. **1922**, *22*, 464.
9. Meyerhofer, D. *J. Appl. Phys*. **1978**, *49*, 3993.
10. Chen, B. T. *Polym Eng. Sci*. **1983**, *23*, 831.
11. Gu, J.; Bullwinkell, M. D.; Campbell, G. A. *J. Appl. Polym. Sci*. **1995**, *57*, 717.
12. Spangler, L. L.; Torkelson, J. M.; Royal, J. S. *Polym. Eng. Sci*. **1990**, *30*, 644.
13. Prest Jr., W. M.; Luca, D. J. *J. Appl. Phys.* **1979**, *50*, 6067.
14. Wu, W. L.; van Zanten, J. H.; Orts, W. J. *Macromol.* **1995**, *28*, 771.
15. Wallace, W. E.; van Zanten, J. H.; Wu, W. L. *Phys. Rev. E* **1995**, *52*, R3329.
16. Frank, C. W.; Rao, V.; Despotopopoulou, M. M.; Pease, R. F. W.; Hinsberg, W. D.; Miller, R. D.; Rabolt, J. F. *Science* **1996**, *273*, 912.
17. Hirt, T.; Neuenschwander, P.; Suter, U. W. *Macromol. Chem. Phys*. **1996**, *197*, 1609.
18. Ciardelli, G.; Kojima, K.; Lendlein, A.; Neuenschwander, P.; Suter, U. W. *Macromol. Chem. Phys*. **1997**, *198*, 2667.
19. Flory, P. J. *Principles of Polymer Chemistry*; Cornell University Press: Ithaca, 1953; Chapter 13.
20. Voronoi, G. J. *Reine Angew.* **1908**, *134*, 198.
21. Prager, S.; Talmon, Y. *Nature* **1977**, *267*, 333.
22. Stange, T. G.; Mathew, R.; Evans, D. F. Hendrickson, W. A. *Langmuir* **1992**, *8*, 920.
23. Pooley, C. M.; Tabor, D. *Proc. R. Soc. London A* **1972**, *329*, 251.
24. Wittmann, J. C.; Smith, P. *Nature* **1991**, *352*, 414.
25. Fenwick, D.; Smith, P.; Wittmann, J. C. *J. Mater. Sci*. **1996**, *31*, 128.
26. Yang, C. Y.; Yang, Y.; Hotta, S. *Mol. Cryst. Liq. Cryst*. **1995**, *270*, 113.
27. Yan, S.; Petermann, J. *Polymer Bulletin* **1999**, *43*, 75.
28. Tanabe, K.; Shijoiri, M. *Dyes Pigments* **1997**, *2*, 121.
29. Suzuki, H.; Oiwa, K.; Yamada, A.; Sakakibara, H.; Nakayuama, H.; Mashiko, S. *Jpn. J. Appl. Phys*. **1995**, *34*, 3937.
30. Greiner, A. *Polym. Adv. Mat*. **1998**, *9*, 371.
31. Bastiaansen, C. W. M.; Caseri, W.; Darribere, C.; Dellsperger, S.; Heffels, W.; Montali, A.; Sarwa, C.; Smith, P.; Weder, C *Chimia* **1998**, *52*, 591.
32. Saujanya, C.; Dhumal, A.; Mitra, A. *J. Appl. Polym. Sci*. **1999**, *74*, 3522.
33. Campoli, F.; Beccherelli, R.; d'Alessandro, A. *Displays* **1999**, *20*, 191.

34. Hansma, H.; Montamedi, F.; Smith, P.; Hansma, P. K.; Wittmann, J. C. *Polymer* **1992**, *33*, 647.
35. Dietz, P.; Hansma, P. K.; Ihn, K. J.; Montamedi, F.; Smith, P. *J. Mat. Sci*. **1993**, *28*, 1372.
36. Schonherr, H.; Vancso, G. J. *Polymer* **1998**, *39*, 5705.
37. Schonherr, H.; Vancso, G. J. *Macromol*. **1997**, *30*, 6391.
38. Wu, S. in *Polymer Handbook*, 3rd. ed.; Brandrup, J., Immergut, E. H., Eds.; J. Wiley & Sons, Inc.: New York, 1989, Chapter 4.
39. Ulman, A. *An Introduction to Ultrathin Organic Films: From Langmuir-Blodgett to Self-Assembly*, Academic Press, Inc.: San Diego, 1991; Part 3.
40. Nuzzo, R. G.; Allara, D. L. *J. Am. Chem. Soc*. **1983**, *105*, 4481.
41. Ulman, A. *J. Mat. Ed*. **1989**, *11*, 205.
42. Stewart, K. R.; Whitesides, G. M.; Godfried, H. P.; Silvera I. F. *Surf. Sci*. **1986**, *57*, 1381.
43. Troughton E. B.; Bain, C. D.; Whitesides, G. M.; Nuzzo, R. G.; Allara, D. L.; Porter, M. D. *Langmuir* **1988**, *4*, 365.
44. Allara, D. L.; Nuzzo, R. G. *Langmuir* **1985**, *1*, 45.
45. Brovelli, D.; Hähner, G.; Ruiz, L.; Hofer, R.; Kraus, G.; Waldner, A.; Schlösser, J.; Oroszlan, P.; Ehrat, M.; Spencer, N. D. *Langmuir* **1999**, *15*, 4324.
46. Bain, C. D.; Troughton E. B.; Tao, Y.-T.; Evall, J.; Whitesides, G. M.; Nuzzo R. G. *J. Am. Chem. Soc.* **1989**, *111*, 321.
47. Nuzzo, R. G.; Fusco, F. A.; Allara, D. L. *J. Am. Chem. Soc*. **1987**, *109*, 2358.
48. Sellers, H.; Ulman, A.; Shnidman, Y.; Eilers, J. E. *J. Am. Chem. Soc*. **1993**, *115*, 9389.
49. Alves, C. A.; Smith, E. L.; Porter, M. D. *J. Am. Chem. Soc.* **1992**, *114*, 1222.
50. Xia, Y.; Whitesides, G. M. *Annu. Rev. Mat. Sci*. **1998**, *28*, 153.
51. Larsen, N. B.; Biebuyck, H. A.; Delamarche, E.; Michel, B. *J. Am. Chem. Soc*. **1997**, *119*, 3017.
52. Eberhardt, A. S.; Nyquist, R. M.; Parikh, A. N.; Zawodzinski, T.; Swanson, B. I. *Langmuir* **1999**, *15*, 1595.
53. Noy, A.; Vezenov, D. V.; Lieber, C. M. *Annu. Rev. Mat. Sci*. **1997**, *27*, 381.
54. Overney, R. M.; Meyer, E.; Frommer, J.; Guntherodt, H.-J. Fujihira, M. *Langmuir* **1994**, *10*, 1281.
55. Xiao, X.; Hu, J.; Charych, D. H.; Salmeron, M. *Langmuir* **1996**, *12*, 235.

Chapter 4*

Force Spectroscopy of Polymer Surfaces

4.1 Introduction

Scanning force microscopy and lateral force microscopy techniques (SFM and LFM) have, since their development in the 1980s,[1,2] shown considerable promise as methods for nanometre-scale, surface-chemical analysis, since they can provide quantitative, spatially resolved, chemically dependent information on interactions between the scanning probe and sample surfaces. This feature has been exploited by many researchers, using approaches such as chemical modification of probe tips for the recognition of specific surface groups,[3-8] or by monitoring the pH-dependence of the tip-surface interaction[9-11]. The majority of such studies have involved self-assembled monolayers (SAMs) on flat gold surfaces[12], which provide an idealised test surface, presenting a well-ordered, highly concentrated plane of functionality. The usefulness of SAMs as models for polymer surfaces is limited, however, since issues such as complex surface morphology, disorder, mechanical properties, and solvent interactions significantly complicate the issue with actual polymers, making chemical imaging extremely challenging.[6,13,14] In this chapter, the study of the adhesion and friction between a series of polymer film surfaces and chemically well-defined SFM tips will be discussed. This work was undertaken to evaluate the feasibility of employing SFM for chemical imaging of heterogeneous polymer systems, such as phase-separated blends, analogous to the "chemical force microscopy" developed for SAMs.[11]

---

*This chapter is reproduced in part from:
Feldman, K.; Tervoort, T. A.; Smith, P.; Spencer, N. D. *Langmuir* **1998**, *14*, 372-378.

Below, a systematic study of SFM-adhesion measurements on polymeric surfaces is described. We have endeavoured to control as many of the complicating parameters on polymer surfaces as possible, such that the SFM adhesion measurements were primarily due to the dispersion component of the Van der Waals and H-bonding interactions between the tip and the polymer surface. Using an embryonic "force spectroscopy" approach, polymers could be distinguished by virtue of their differing hydrophobicities/hydrophilicities or, for purely hydrophobic systems, on the basis of their optical refractive index. By capitalising on the intimate relationship between adhesion and friction, these phenomena can be rendered visual by means of lateral force microscopy (LFM), enabling high-spatial-resolution chemical imaging of heterogeneous polymer systems–a challenging analytical task for conventional ultrahigh vacuum surface chemical imaging methods.

4.2 Van der Waals Interaction

Interaction between a polymer surface and an SFM probe consists chiefly of the Van der Waals interaction. The non-retarded Van der Waals interaction free energy between two surfaces is described by:[15]

$$W(D) = -\frac{A}{12\pi D^2} \text{ per unit area} \tag{4.1}$$

where D is the separation between two bodies and A is the Hamaker[16] constant. The Hamaker constant is defined as

$$A = \pi^2 C \rho_1 \rho_2 \tag{4.2}$$

where C is a coefficient in the atom-atom pair potential, and ρ_1 and ρ_2 are the number densities of atoms per unit volume in the two bodies. The Derjagin approximation,[17] which gives the force between two spheres of radii R_1 and R_2 as a function of separation D in terms of the energy per unit area of the two planar surfaces allows one to obtain a force law for any given geometry of the two interacting bodies:

$$F(D) = 2\pi\left(\frac{R_1 R_2}{R_1 + R_2}\right) W(D). \tag{4.3}$$

The most interesting aspect of this formula is that it shows that the geometry of the two surfaces dictates the distance dependence of the force.

The non-retarded Hamaker constant can be calculated according to Israelachvili's simplification[15] of the Lifshitz theory.[18] Hamaker constant, A_{Total}, consists of the two

terms $A_{\nu=0}$ and $A_{\nu>0}$. The first term corresponds to the dipole-dipole (Keesom) and the dipole-induced-dipole (Debye) interaction, while the second term corresponds to the dispersion (London) interaction. For the two macroscopic phases 1 and 2 interacting across a medium 3, with the respective static dielectric constants (ε_1, ε_2, ε_3) and optical refractive indexes (n_1, n_2, n_3) the Hamaker constant is given by:

$$A_{Total} = A_{\nu=0} + A_{\nu>0} \approx \frac{3}{4}kT\left(\frac{\varepsilon_1 - \varepsilon_3}{\varepsilon_1 + \varepsilon_3}\right)\left(\frac{\varepsilon_2 - \varepsilon_3}{\varepsilon_2 + \varepsilon_3}\right) + \\ + \frac{3h\nu_e}{8\sqrt{2}} \frac{\left(n_1^2 - n_3^2\right)\left(n_2^2 - n_3^2\right)}{\left(n_1^2 + n_3^2\right)^{0.5}\left(n_2^2 + n_3^2\right)^{0.5}\left\{\left(n_1^2 + n_3^2\right)^{0.5} + \left(n_2^2 + n_3^2\right)^{0.5}\right\}} \qquad (4.4)$$

where the electronic absorption frequency, ν_e, is assumed to be equal for all three components ($\nu_e = 3\times10^{15}$Hz). The consequence of this relationship is that a close match between the dielectric constants of tip, sample and medium leads to a suppression of the first term, with the result that dispersion forces (determined by the optical refractive index) play the dominant role in determining the tip-sample interaction. In fact, if the refractive index of the intervening medium is intermediate between that of the other phases, a negative Van der Waals interaction can result.[19] A liquid environment, therefore, can be used to tune the Van der Waals forces between the probe and the surface[20a] and make the interaction repulsive, so that the adhesion between the probe and surface is minimised, and the possibility of the sample damage is reduced. This is a valuable approach that others have used for DNA imaging,[20b] for example. Another important consequence of Eq. 4.4 is that the Hamaker constant can be readily calculated based only on the two bulk properties, the static dielectric constant and the refractive index, for the two bodies interacting across medium.

Equations 4.1 and 4.4 can be combined to provide an estimate of the work of adhesion and the Lifshitz-Van der Waals contribution, γ^{LW}, to the total surface free energy, when two surfaces are in contact ($D=D_0$). It was shown by Israelachvili[15] that the cut-off separation of D_0=0.165nm yields surface energy values in good agreement with the measured values for a wide range of liquids and solids, except for highly polar H-bonding liquids:

$$\gamma^{LW} = \frac{1}{2}W(D_0) = \frac{A}{24\pi(0.165nm)^2}. \qquad (4.5)$$

Surface free energies calculated from Eq. 4.5 can than be used to predict the pull-off forces for one of the contact mechanics theories described in Chapter 2.

4.3 Effects of Polymer Molecular Weight

An important consideration in the SFM experiments on the polymer surfaces is the effect of the polymer molecular weight. It has been shown by several groups[21,22] that, when films are produced from polymers of low molecular weight, adhesion and friction measurements become strongly dependent upon the molecular weight. For example, a decrease in the pull-off force upon the number of force-distance cycles at one point has been demonstrated[21] for atactic polystyrene (PS) films of average M_w=1,890 g/mol and M_w=23K g/mol, suggesting an ageing process, while there was no change for the polystyrene film of M_w=284K g/mol. The values of the pull-off forces were found to be greater for the lower molecular weight PS samples. While the authors do not provide an explanation, it is possible that this effect is due to the greater number of free chain ends available to interact with the SFM tip, the chain ends are not entangled and therefore more mobile, allowing for better adherence to the tip. Friction measurements were also found to be strongly dependent upon the molecular weight, only for the PS film of M_w=284K g/mol was the friction coefficient found to be close to the macroscopic value. The maximal variation of the dynamical modulus with the molecular weight between the smallest and the highest M_w in the study was about 15%, while variation in the friction coefficient had a factor of two. These results can be explained by drawing an analogy with the crazes in vitreous polymers,[23,24] for which the type of failure is strongly dependent upon the molecular weight: fragile fracture for the high molecular weight polymers occurs by chain scission of the fibrils; ductile fracture by plastic flow for the intermediate and low molecular weight polymers that occurs through disentanglement in the active zone. It is, therefore, proposed that for the intermediary molecular weights the change from static to dynamic friction occurs at a smaller force threshold through the disentanglement of the chains, resulting in a smaller friction coefficient. To avoid the mentioned complications associated with the mechanical behaviour of polymers of the intermediary molecular weight, only high molecular weight polymers were used in this study.

4.4 Choice of Medium for the SFM Measurements

The manipulation of surface forces by a suitable choice of medium is central to the experiments in the present study. In the case of polymers, the choice of a suitable medium is greatly restricted by potential interactions, as a solvent, for example, with the polymer surface. In view of these constraints, we have chosen perfluorinated decalin ($C_{10}F_{18}$), PFD, as a measurement medium: employment of this non-polar liquid, which displays both a low dielectric constant and a low refractive index, and is inert towards most polymers, greatly facilitates the measurement of the dispersion component of the Van der Waals forces between the probe tip and the polymer surface.

An example of the effect of different media on force-distance measurements is shown in Figure 4.1 for the case of a poly(methyl methacrylate)-surface (PMMA) scanned with an oxygen-plasma-treated SiO_x probe in water, isopropanol and PFD. The SiO_x probe is negatively charged at neutral pH (isoelectric point, IEP≈3),[25] most polymer surfaces also acquire a negative charge in aqueous environment,[26] and the force-distance measurements in water exhibit a repulsive double-layer interaction. For low surface potentials (ψ<25mV) the electrostatic force per unit area between two bodies bearing effective surface charge densities σ_1 and σ_2 is described by the following equation:[27,28]

$$F_{el} = \frac{2}{\varepsilon\varepsilon_0}\left[\left(\sigma_1^2 + \sigma_2^2\right)e^{-2\kappa D} + \sigma_1\sigma_2 e^{-\kappa D}\right] \qquad (4.6)$$

where $1/\kappa$ is the so-called Debye length and D is the separation. It is seen from Eq. 4.6 that, even if the polymer surface does not carry an effective charge in aqueous environment and remains electrostatically neutral (σ_2=0), a charge on the surface of a hydroxylated SiO_x probe ($\sigma_1 \neq 0$) would lead to a repulsive electrostatic force and overall interaction between the two surfaces would be described by the Derjagin-Landau-Verwey-Overbeek (DLVO) theory[29,30] of colloidal stability. From Figure 4.1 it is also clear that PFD (n=1.317) leads to a far greater tip-sample interaction (both pull-on and pull-off force) than isopropanol (n=1.378), when used as the intervening medium between a SiO_x (n=1.480) tip and a PMMA (n=1.482) surface. The higher pull-off forces and therefore greater signal-to-noise ratio obtained in force-distance measurements under PFD thus facilitates comparisons between different polymer samples. Calculations (Tables 4.1-4.3) show the interaction to be overwhelmingly dominated by the dispersion component for all polymers used in this study, due to the

low refractive index, n, of PFD, and the similarity of its dielectric constant, ε, to those of the surrounding solid phases.

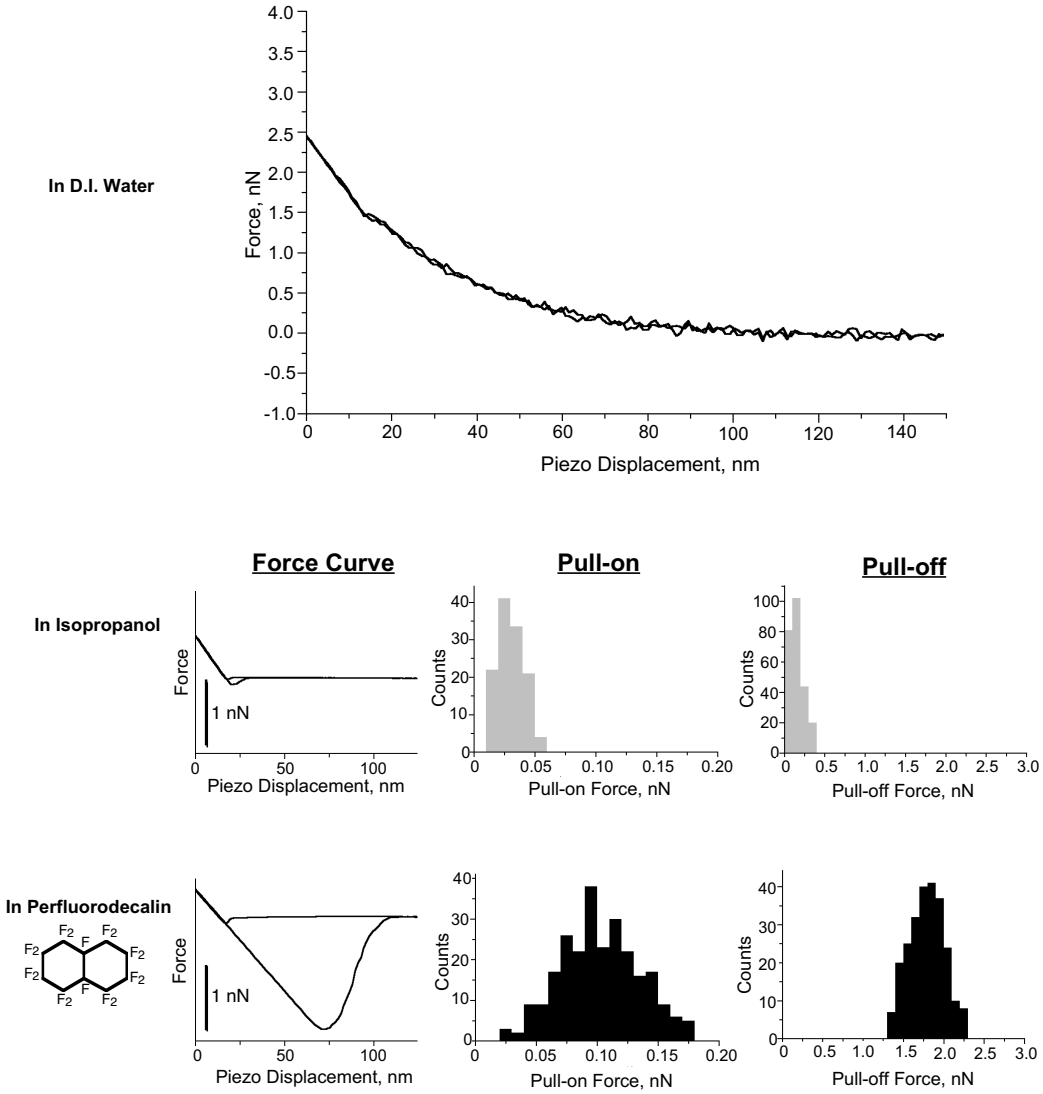

Figure 4.1 *Comparison of force curves, pull-on, and pull-off forces between a SiO_x probe (k=0.01N/m) and a PMMA surface in water, isopropanol, and perfluorodecalin.*

To explore the use of PFD as a contrast-enhancing medium in force-distance measurements on polymer surfaces, two series of polymers were chosen for the experiments: a first series consisting of non-polar polymers with different refractive indices, and a second series in which polymers of different hydrophobicities/hydrophilicities were selected.

4.5 Force Measurements

Force-distance measurements and lateral-force imaging were performed with a scanning probe microscope (Nanoscope™ III Multimode™, Digital Instruments, Santa Barbara, USA) equipped with a liquid cell and enclosed in a thermally equilibrated environment. Up to 1280 force-distance curves at adjacent locations were collected for each sample. Prior to the measurements, the films were briefly placed under an α-radiation source, ^{210}Po (NRD, Inc., USA) to ensure that the static charge, which is likely to be present on the polymer surfaces, was removed and did not contribute to the overall forces measured. Following each set of experiments on a given series of polymers, the initial measurements were repeated, in order to check that the tip was unaltered and intact. Reproducibility was found to be within 15%.

In order to determine the influence of time-dependent effects on the pull-off force for the polymer systems investigated, both load-dependent and frequency-dependent experiments were carried out (0.25–5.5nN applied load and 0.1 to 5Hz for loading-unloading cycles). Figure 4.2 represents the load- and frequency-dependent measurements performed with a gold-coated probe on polystyrene in perfluorodecalin. As is seen from the figure, at moderate loads and low frequency of the approaching-retracting cycle there is no increase in the pull-off force, as would be anticipated in the case of a plastic deformation, for which the increase in the contact area should lead to a greater pull-off force. As it is seen from Fig 4.2B, the pull-off forces were found to decrease by ≈25% over the measured frequency range. This effect, however, is largely due to hydrodynamic damping of the cantilever deflection at higher frequencies–a compliant cantilever does not return to the same rest position during the retracting cycle, which leads to the onset of the hysteresis in the force-distance graph and, therefore, to a decrease in the pull-off force value. To avoid this problem, we decided to perform measurements at low frequency (0.5 Hz), below the onset of hysteresis. Refractive index and film thicknesses were measured by ellipsometry (Type L-116C, Gaertner Sci. Corp., Chicago, USA) using a 70° angle of incidence, and a He-Ne laser. Static water-contact angle measurements were carried out using a contact angle goniometer (Ramé-Hart, Inc., Mountain Lakes, USA). We chose perfluorodecalin (PFD), $C_{10}F_{18}$, (Fluorochem, UK) as a medium for all SFM and LFM experiments, both

for the reasons discussed in detail above and because PFD is not a solvent for any of the materials examined in this study.

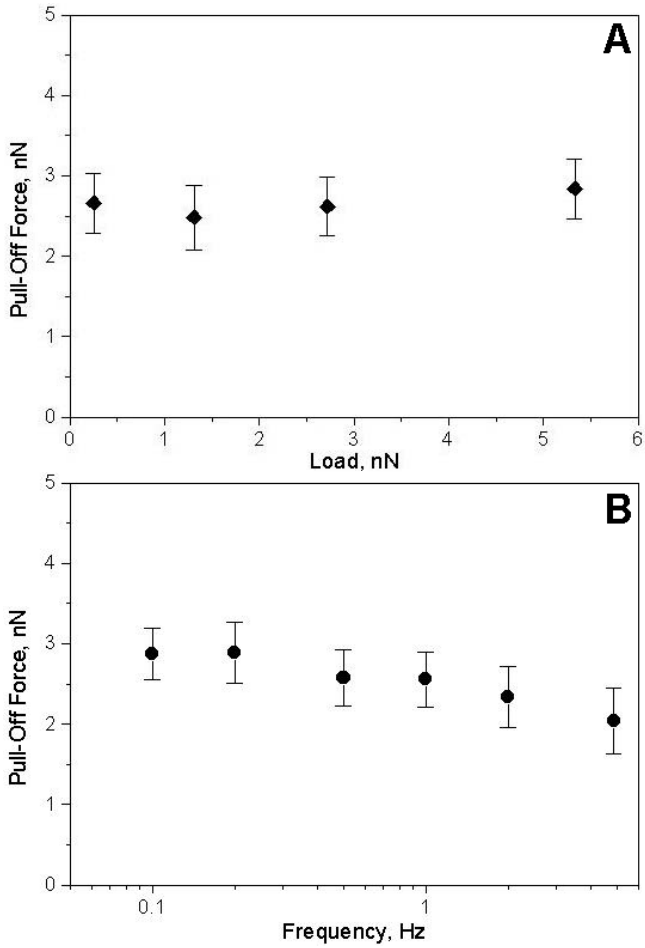

Figure 4.2 *Dependence of the pull-off force upon a) the applied load (at 0.5Hz) and b) frequency of the approaching-retracting cycle (at 3nN applied load) measured on PS film with gold-coated probe (k=0.12N/m) in perfluorodecalin.*

Additionally, PFD is convenient to use in SFM experiments because of its relatively low vapour pressure (P_v=0.88 kPa), high boiling point (T_b=141ºC) and non-toxicity.

4.6 Probes for Force Spectroscopy

Two classes of SFM probe-tip surfaces were used in this work: polar and non-polar. Polar tips were either oxygen-plasma-treated Si_3N_4 Microlevers™ (Park Scientific Instruments, USA) or Si_3N_4 cantilevers (Digital Instruments, USA) with attached COOH-functionalised glass spheres (Bioforce Laboratory, USA). The non-polar tips were either gold-coated Si_3N_4 Microlevers™ or Si_3N_4 cantilevers with attached ≈7.5μm-diameter polystyrene beads (Bioforce Laboratory, USA). Sharpened Microlevers™

were chosen because of their low spring constants (down to 0.007N/m), providing high sensitivity to the measured pull-off forces and a small (10-20nm, according to manufacturer's specifications) tip radius. Spring constants of the oxygen-plasma-treated and gold-coated Microlevers™ were calibrated by the method developed by Cleveland *et al.*[31] Oxygen-plasma treatment of the Microlevers™ was carried out in a radio-frequency plasma cleaner (Harrick Scientific Corp., USA) operated at 40W with an oxygen feed. The isoelectric point of the resulting tips was at approximately pH≈3 (measured by the method of Marti *et al*[9]), suggesting that the surface consisted chiefly of SiO_4. The gold-coated tips were prepared by thermal deposition of a 4-nm chromium adhesion layer, followed by 20nm of gold in a Balzers MED-010 coater operated at 2×10^{-5} mbar. A single tip of each type was used to measure all polymer surfaces within a given series, to ensure that the spring constant and tip radius was kept constant between samples.

4.7 Non-Polar Polymer Series

A first series of thin (hydrophobic) polymer films consisted of atactic polystyrene, PS (average M_w=250K g/mol, Polysciences, Inc., USA), isotactic polypropylene, i-PP (average M_w=250K g/mol, Aldrich Chem. Co., Inc., USA), poly(vinylidene fluoride), PVDF (average M_w=534K g/mol, Aldrich Chem. Co., Inc., USA) and poly(tetrafluoroethylene-co-hexafluoropropylene), FEP (Polymer Technology Group, ETH-Zürich). i-PP, PVDF, and FEP were first prepared from foils made by pressing powders between aluminium sheets above their corresponding melting temperatures. The films obtained were then pressed between plasma-cleaned silicon wafers (once again, above their melting temperatures) to achieve low surface roughness, the films were than quenched in liquid nitrogen. It must be noted, however, that due to the crystallisation of i-PP and PVDF upon cooling, the attainment of a comparable surface roughness to that of the silicon wafer was not anticipated; nevertheless, film root mean-squared roughnesses (RMS) of ≈3nm were attained. In addition, these polymers have glass transition temperatures of about -22°C and -38°C respectively, meaning that additional chain rearrangements and an increase in crystallinity may take place during their subsequent storage at room temperature.

The effect of thermal treatment was studied on the film of i-PP that was first prepared as discussed above (quenched from the melt in liquid nitrogen) and than kept at 100°C overnight in a vacuum oven to ensure high degree of crystallinity. Histograms of the pull-off forces measured for the two i-PP films with a gold-coated probe under perfluorodecalin are shown in Fig. 4.3. The pull-off forces were found to be 0.56±0.21nN for the quenched sample and 0.72±0.05nN for the annealed film.

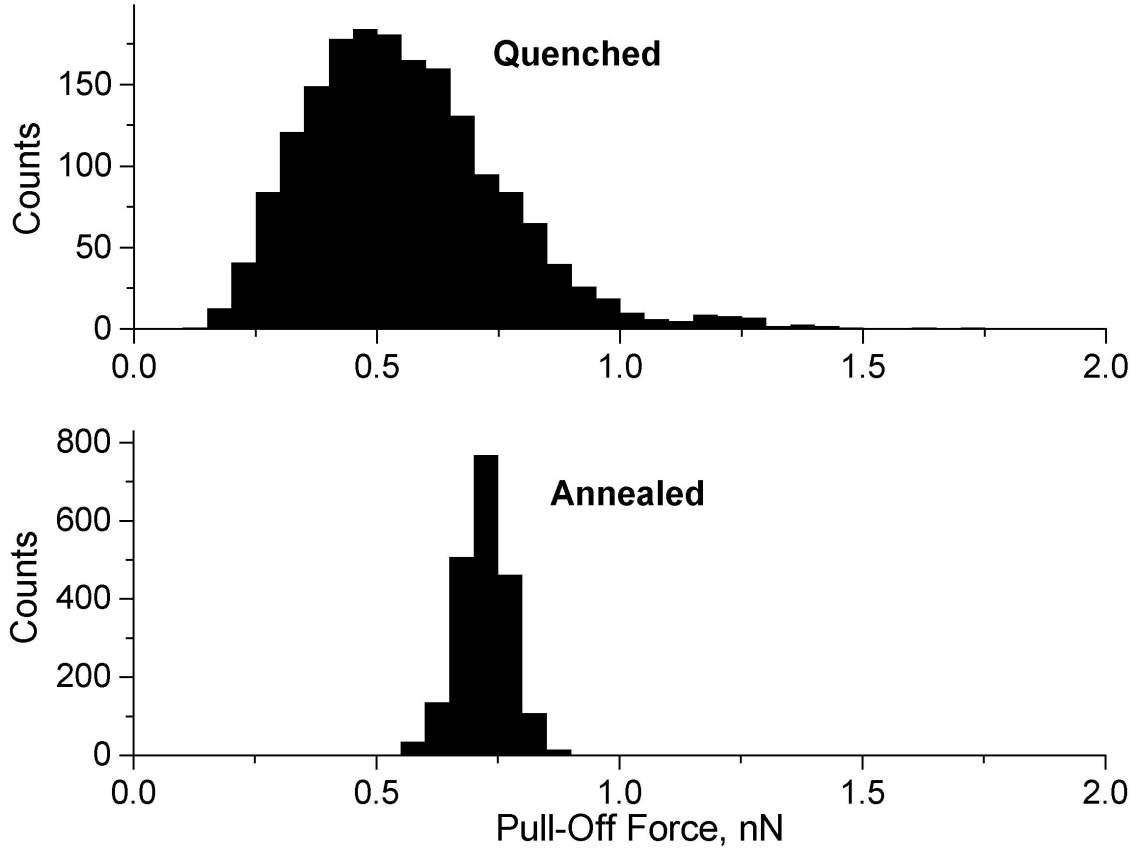

Figure 4.3 *Histogram of the pull-off forces measured with gold-coated probe (k=0.01N/m) under perfluorodecalin on i-PP film that was quenched from the melt and, subsequently, annealed at 100°C overnight.*

There was not only an increase in the average pull-off force value but also a dramatic decrease in the distribution of the pull-off forces with the distribution changing from the Poisson-like for the quenched i-PP film to the Gaussian-like for the annealed specimen. An increase in the value of the average pull-off force for the mostly crystalline i-PP is due to an increase in the chain density that, in turn, causes an increase in the refractive index of the material ($n_{annealed}$=1.501>$n_{quenched}$=1.487). A higher refractive index leads to a larger Hamaker constant value (Eq. 4.4) and, subsequently, to an increase in the value of the work of adhesion for the polymer surface–probe tip system (Eq. 4.5).

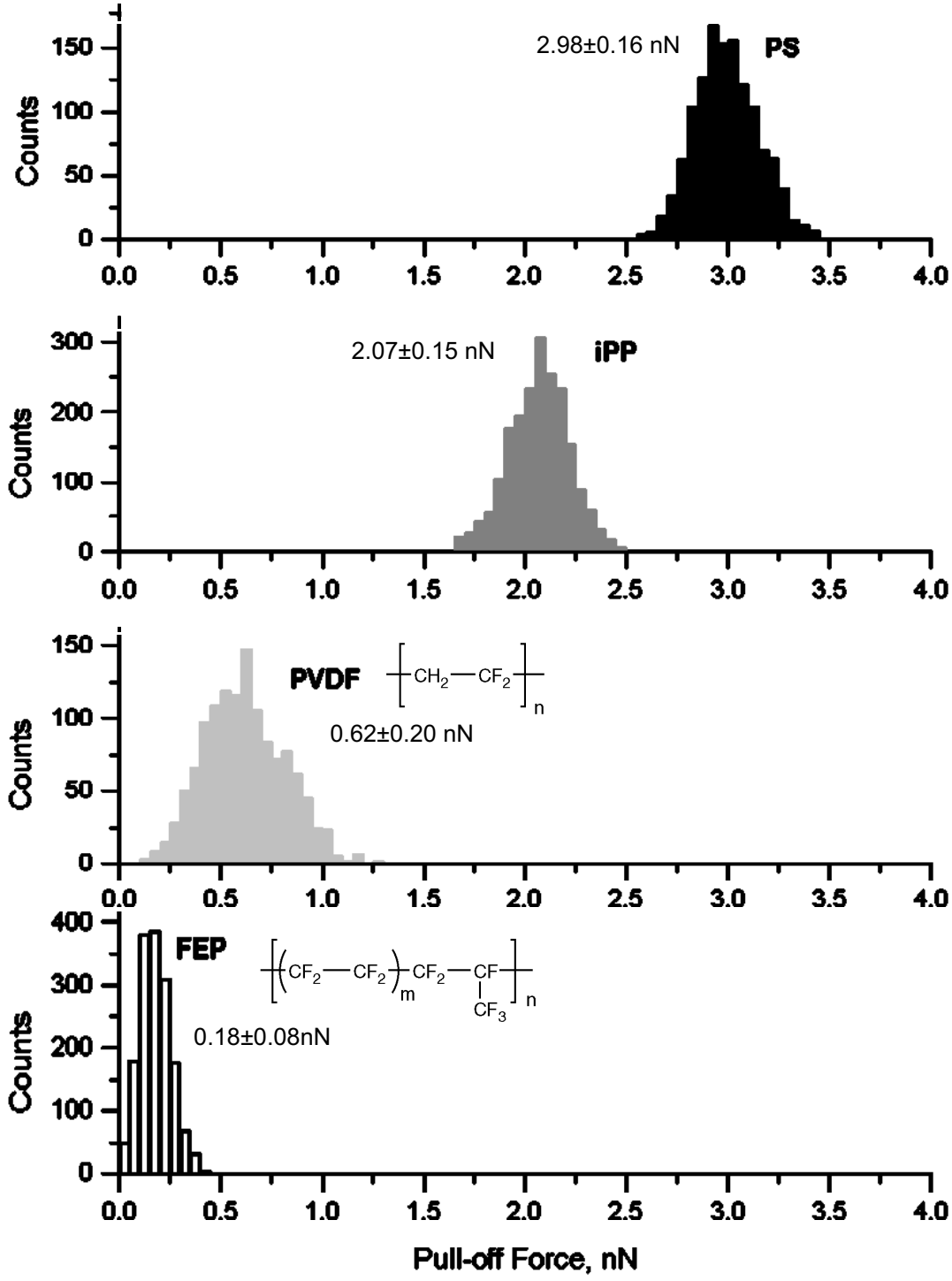

Figure 4.4 *Histograms of pull-off forces measured between a SiO_x probe (k=0.01N/m) and PS, i-PP, PVDF, and FEP surfaces in perfluorodecalin.*

Since the same probe was used to measure both surfaces (effective probe tip radius was kept constant), the difference in the value of the average pull-off force is proportional to the work of adhesion. The change of the type and the width of the distribution of the pull-off forces can be attributed to the change in the mechanical properties when the i-PP is annealed and becomes uniformly more crystalline. The Poisson distribution of the pull-off forces becomes indicative of plastic deformation or other energy-dissipating processes that lead to a dependence of the pull-off force upon the tip velocity during the force-curve cycle, applied load, time of contact and contact area. It also indicates that the surface mechanical properties are not uniform. Another example of such a distribution has been shown in Chapter 3.3 for a PTFE film prepared by friction deposition.

The non-polar series of polymers was investigated, in order to limit the interaction between an SFM probe and polymer surfaces to only the *dispersion* (London) component of the Van der Waals force. Adhesional forces were measured between a SiO_x probe and a set of non-polar polymers that provided a range of refractive indexes (as measured): polystyrene (1.582), isotactic polypropylene (1.501), poly(vinylidene fluoride) (1.407) and poly(tetrafluoroethylene-co-hexafluoropropylene) (1.348). The histograms of the pull-off forces, measured with a SiO_x probe, are shown in Figure 4.4 and tabulated with the calculated values for adhesion energy in Table 4.1. The Hamaker constants for these systems were derived from equation 4.4, as described above; the work of adhesion, *W*, was calculated from Eq. 4.5. Figure 4.4 shows that for all four polymer surfaces, the distributions of the pull-off forces were of a Gaussian type, suggesting that there was little if any plastic deformation during the SFM experiment.

Polymer	Measured Refractive Index, n	Dielectric Const., ε	$A_{v=0}$, $J\times10^{21}$	$A_{v>0}$, $J\times10^{21}$	A_{Total}, $J\times10^{21}$	Calc. Work of Adhesion, mN/m	Calc. Pull-Off Force (DMT), nN (ranking)	Measured Pull-Off Force, nN (ranking)
FEP	1.348	2.1	0.17	1.48	1.65	1.6	0.39 (4)	0.18±0.08 (4)
PVDF	1.407	8.4	1.12	4.09	5.21	5.1	1.23 (3)	0.62±0.20 (3)
i-PP	1.501	2.5	0.31	8.11	8.42	8.2	1.98 (2)	2.07±0.15 (2)
PS	1.582	2.5	0.31	11.44	11.75	11.4	2.76 (1)	2.98±0.16 (1)

Table 4.1 *Calculated and Measured Values for Interactions Between the Second Series of Polymers and a SiO_x Probe.*

Plotting measured pull-off forces, F, vs calculated work of adhesion values, W, should yield a slope of $1.5\pi R$, if the Johnson-Kendall-Roberts theory[32] of contact mechanics (JKR) holds for our system (or $2\pi R$ if Derjagin-Muller-Toporov theory[33] (DMT) is a more appropriate model[34]). The JKR theory assumes that the two elastic solids form a connective neck in the area of contact with the short-range forces acting in the contact area, while the DMT theory assumes Hertzian type of contact with long-range forces acting outside the contact area. The two theories represent two limits of the elastic contact mechanics. A new theory of the transition between the JKR and DMT limits was proposed and a dimensionless parameter, λ, was introduced:[35]

$$\lambda = \frac{2.06}{D_0}\left(\frac{W^2 R}{\pi K^2}\right)^{1/3} \tag{4.6}$$

where W is the work of adhesion, K is the effective elastic modulus (Eq 1.10), R is the tip radius and D_0 is the equilibrium interatomic distance (D_0=0.165nm).

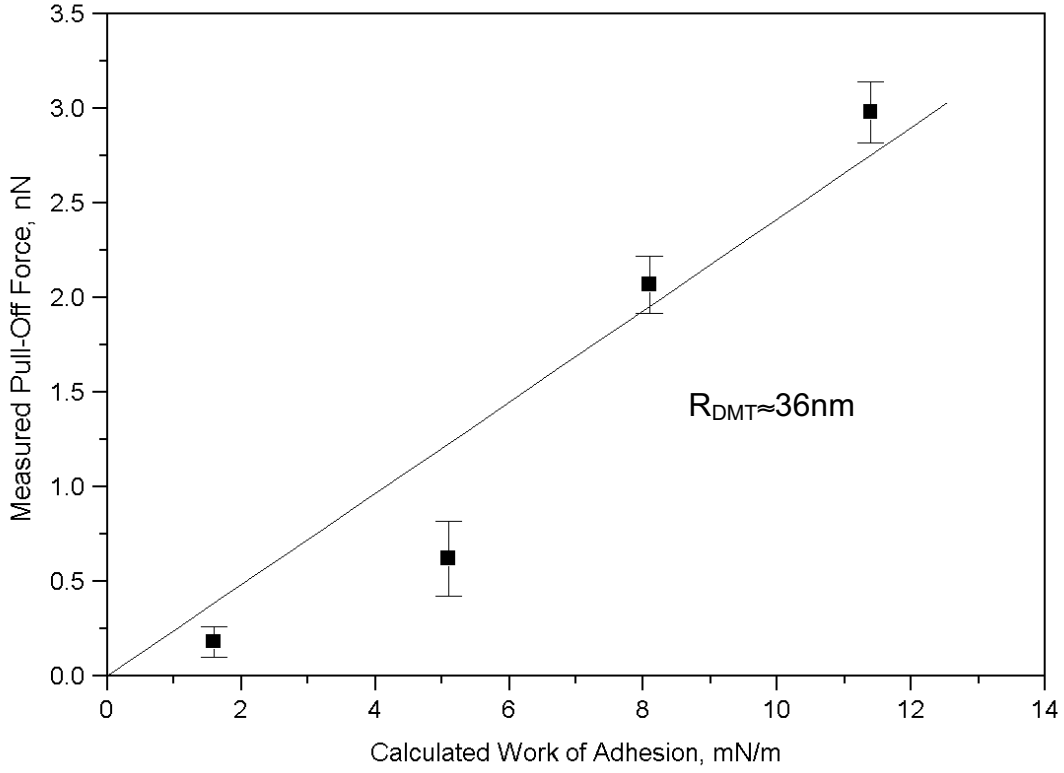

Figure 4.5 *Comparison of measured pull-off forces and calculated work of adhesion for interactions between a SiO_x probe and PS, i-PP, PVDF, and FEP surfaces in perfluorodecalin.*

For $\lambda \geq 1$ the JKR theory was found to be a good approximation, while for $\lambda \leq 0.3$ the DMT theory was found to be applicable. For the series of non-polar polymers, the value

of λ was found to be 0.4 (for PVDF) or less, we, therefore, used the DMT equation of the pull-off force ($F_{pull\text{-}off}=-2\pi WR$). The results (Figure 4.5) indicate that for this first polymer series, F scales linearly with W, with a corresponding tip radius of ≈36nm. In other words, in the case of non-polar polymers, SFM pull-off force results obtained under PFD scale quite well with adhesion energies predicted from Lifshitz theory.

4.8 Polar Polymer Series

A second series of thin films consisted of glassy polymers with different hydrophobicities/hydrophilicities: polystyrene, PS (average M_w=250K g/mol, Polysciences, Inc., USA), polyacrylonitrile, PAN (average M_w=500K g/mol, Polysciences, Inc., USA), poly(methyl methacrylate), PMMA (average M_w=350K g/mol, Aldrich Chem. Co., Inc., USA), and polyacrylic acid, PAA (average M_w=450K g/mol, Aldrich Chem. Co., Inc., USA).

Thin films of the second polymer series were prepared by spin casting 2 wt. % solutions (PS and PMMA in toluene, PAN in N,N-dimethyl formamide and PAA in methanol) onto plasma-cleaned silicon wafers at 1000rpm, followed by drying in a vacuum oven at 120ºC and 0.03 mbar for 24 hours. All polymers of the second series are fully or highly amorphous and have glass transition temperatures of ≈100°C. Annealing above T_g ensured low surface roughness of the films and evaporation of the solvents. The thicknesses of the produced films were on the order of 50-100nm, as measured by ellipsometry. The measured surface roughness of all films was close to that of the silicon substrates.

The histograms of the distributions of pull-off forces measured between SFM probes and polymer surfaces in PFD (Figures 4.6, 4.7, 4.8) clearly indicate two trends: one for the non-polar tips (virtually identical results were obtained for both the gold and the polystyrene probes), where the adhesion is strongest for the polystyrene sample and weakest for the poly(acrylonitrile); and the other for the polar probes (again, very similar results being obtained for the SiO_x- and COOH-coated tips), where the strongest adhesion is observed with the polyacrylic acid surface, and the weakest with the polystyrene.

The Hamaker constants and the work of adhesion for the second series were calculated as described above. Pull-off forces were calculated using the DMT theory, $F=-2\pi WR$, where, for this second set of polymer films, the effective radius, R, of a sharpened tip was given a typical value of 20nm.[36] These results highlight both the promise and the difficulties of this approach to polymer surface characterisation. In the case of the non-polar probes, the measured ranking in adhesion is roughly similar to that calculated for the PS-sphere probe (Table 4.3). Presumably surface roughness of the PS-sphere is at least partially responsible for the significant disparities in absolute values. In the case of the polar probes, the measured order of adhesion is entirely different from the values calculated from the Lifshitz theory (Table 4.2). It must be borne in mind, however, that many important surface properties of polymers are not taken into account by the calculation: PAA, with its free carboxyl groups, might reasonably be expected to form hydrogen bonds with hydroxyl species on the SiO_x tip. This effect would not, of course, be accounted for in the Lifshitz formalism. In the case of PMMA, which generally displayed strong interactions with both polar and non-polar probes, surface rearrangement[37] could lead to a preferential orientation of either methyl or methacrylate groups towards the interface, depending on the nature of the approaching probe, thus increasing the strength of the interaction in both situations.

Polymer	Measured Water Contact Angle, °	Measured Refractive Index, n	Dielectric Constant[40], ε	$A_{\nu=0}$, J×10^{21}	$A_{_>0}$, J×10^{21}	A_{Total}, J×10^{21}	Calculated Work of Adhesion, mN/m	Calculated Pull-Off Force, nN (ranking)	Measured Pull-Off Force, nN (ranking)
PAN	64±2	1.356	6.5	0.99	1.84	2.83	2.8	0.26 (4)	1.32±0.15 (3)
PMMA	68±2	1.482	3.6	0.60	7.31	7.91	7.7	0.73 (3)	1.84±0.16 (2)
PAA	H_2O Soluble	1.506	5.0	0.83	8.32	9.15	8.9	0.84 (2)	2.13±0.14 (1)
PS	91±2	1.582	2.5	0.31	11.44	11.75	11.4	1.08 (1)	0.66±0.10 (4)

Table 4.2 *Calculated and Measured Values for Interactions Between the First Series of Polymers and a SiO_x Probe (R assumed to be 20nm). The calculated pull-off forces are measured from DMT theory.*

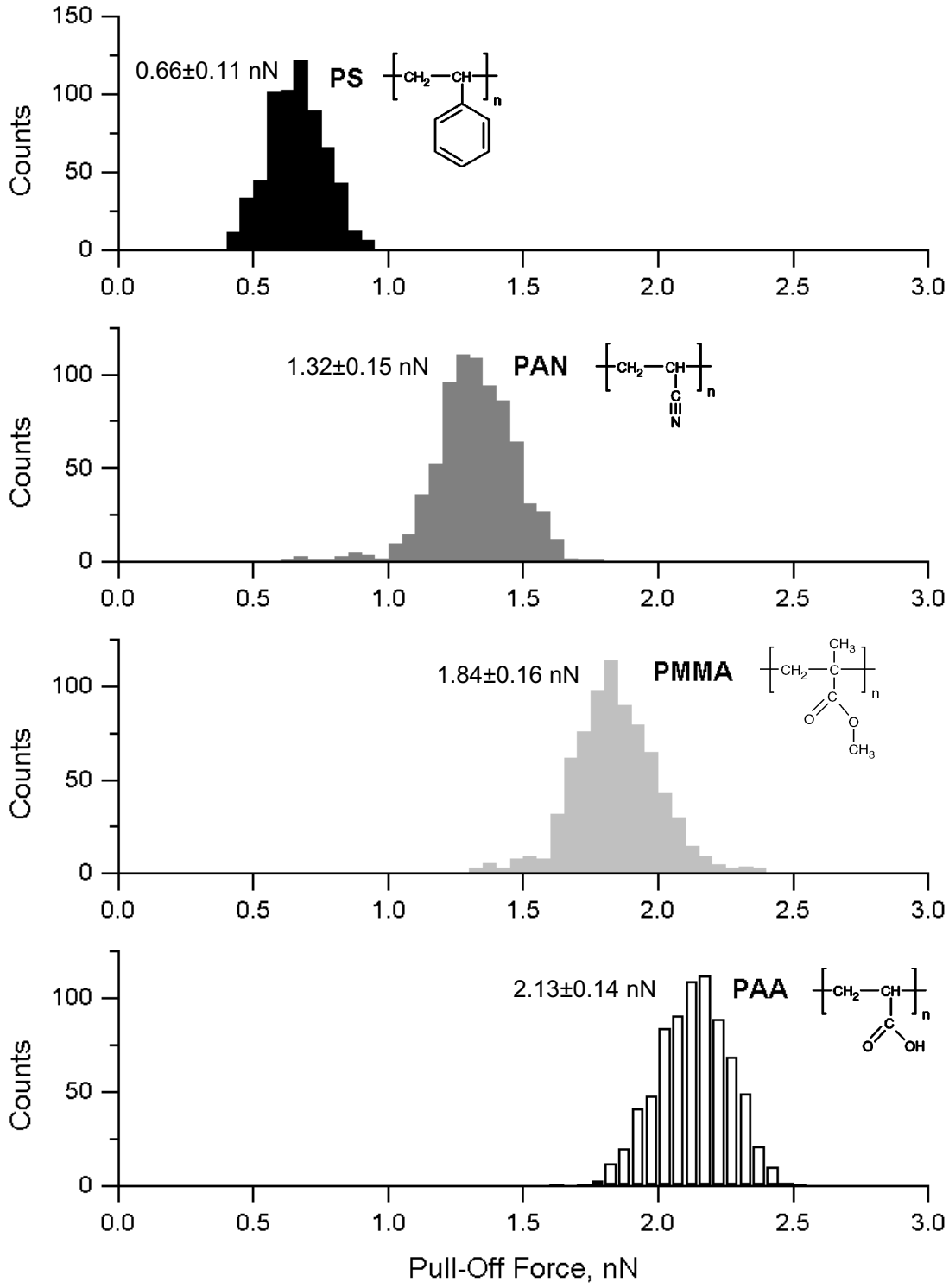

Figure 4.6. *Histograms of pull-off forces measured between a SiO_x probe (k=0.01N/m) and PS, PAN, PMMA, and PAA surfaces in perfluorodecalin.*

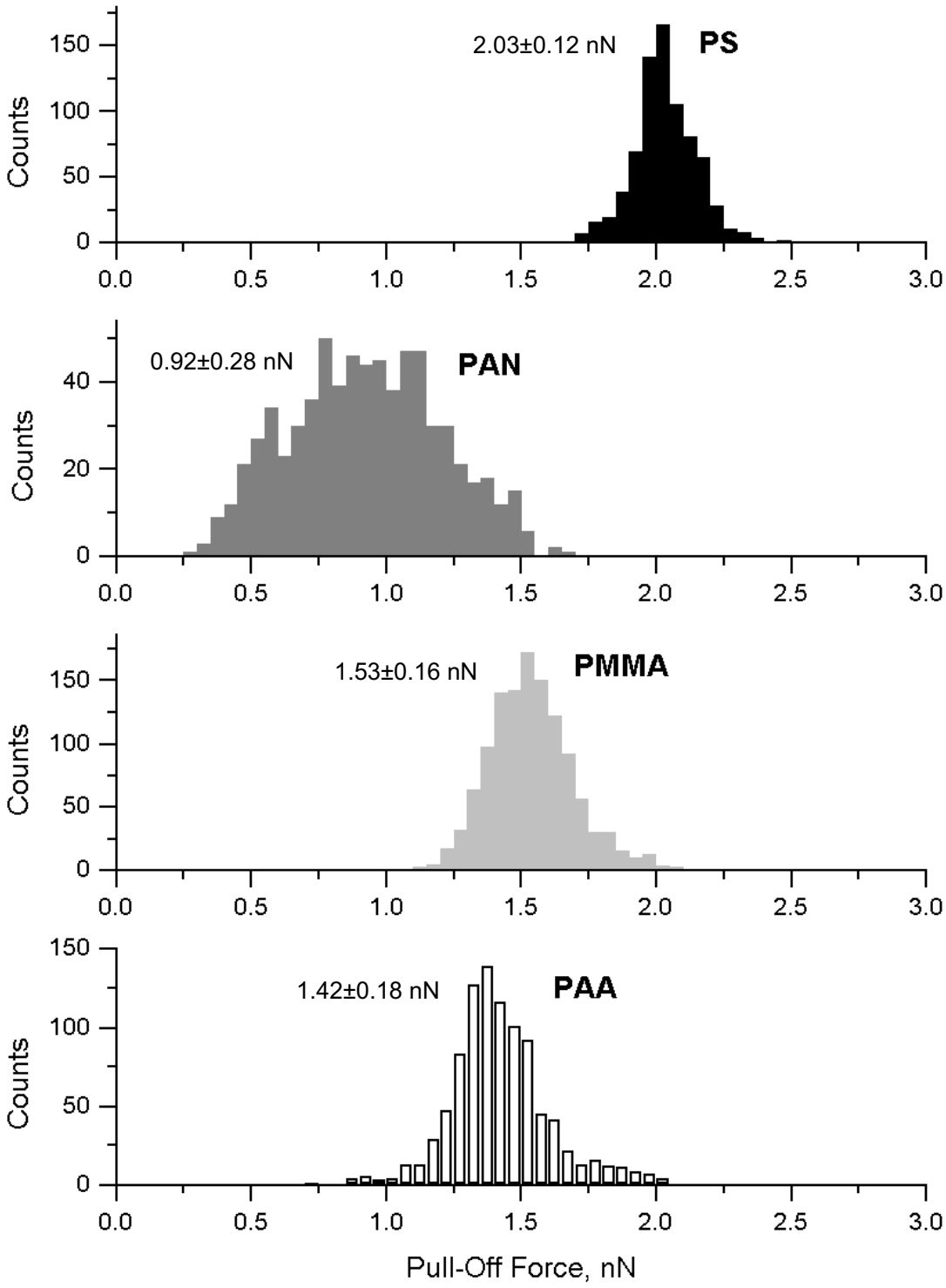

Figure 4.7 *Histograms of pull-off forces measured between a gold probe (k=0.05N/m) and PS, PAN, PMMA, and PAA surfaces in perfluorodecalin.*

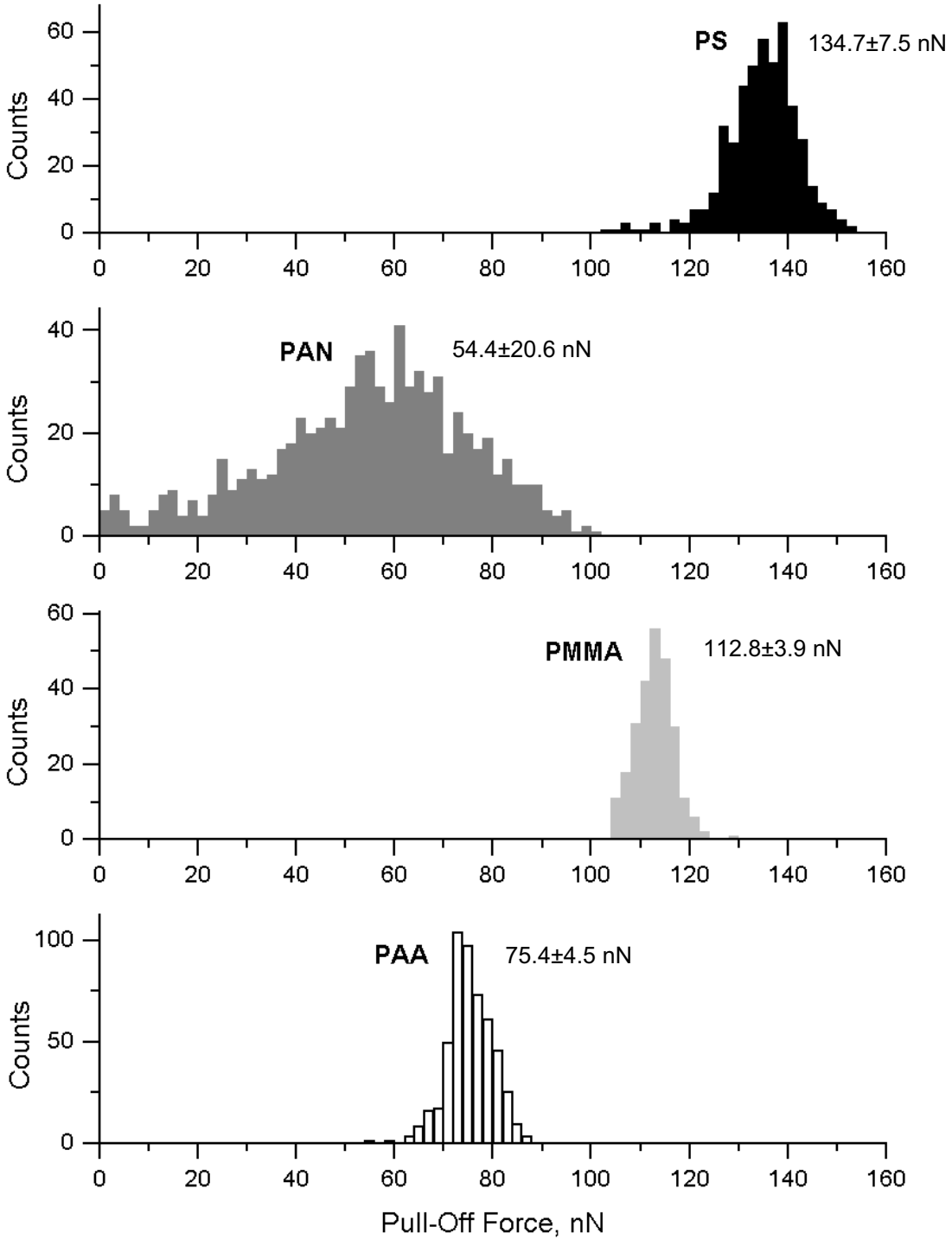

Figure 4.8 *Histograms of pull-off forces measured between a polystyrene sphere (radius 3.75μm) probe (k=0.38N/m) and PS, PAN, PMMA, and PAA surfaces in perfluorodecalin.*

Although our experiments were carried out at room temperature, some 80°C below the bulk T_g, simulations by Mansfield and Theodorou[38] and experimental work by Kambour[39] (rapid craze healing of PMMA at room temperature) show that mobility at the surface is greatly enhanced over the corresponding bulk value, thus increasing the feasibility of rearrangement. Furthermore, the Van der Waals interaction of PFD with the polymer surfaces (all of which are wetted by PFD) presumably enhances surface mobility. The correspondence between the calculations and the measured interactions between PAN and the non-polar probes is quite good, providing that the measured (ellipsometry, thin film), rather than the literature (bulk) values for the refractive index are used.The measured refractive index value is lower (1.356) than that in the literature (1.518). Frank *et al*[41] have shown that the physical properties of spin-cast thin polymer films can differ substantially from those of corresponding bulk samples. In particular, these authors observed solvent incorporation to be higher in spin-cast films. This could account for the deviations of our refractive index measurements from literature values, in particular for PAN, where the presence of a small oxygen signal in XPS analysis of the film suggests that traces of solvent (N,N-dimethyl formamide) were indeed present. By reducing the density, solvent incorporation lowers the refractive index, which, in turn, leads to a decrease in the Hamaker constant, as shown in Eq. 4.4, and therefore affects the Van der Waals interaction.

Polymer	Measured Refractive Index, n	Dielectric Constant, ε	$A_{v=0}$, $J\times10^{21}$	$A_{v>0}$, $J\times10^{21}$	A_{Total}, $J\times10^{21}$	Calculated Work of Adhesion, mN/m	Calculated Pull-Off Force (DMT), nN (ranking)	Measured Pull-Off Force, nN (ranking)
PAN	1.356	6.5	0.33	2.91	3.24	3.2	55.7 (4)	54.4±20.6 (4)
PMMA	1.482	3.6	0.20	11.57	11.77	11.5	202.6 (3)	112.8±3.9 (2)
PAA	1.506	5.0	0.27	13.17	13.44	13.1	231.4 (2)	75.4±4.5 (3)
PS	1.582	2.5	0.10	18.11	18.21	17.7	313.6 (1)	134.7±7.5 (1)

Table 4.3 *Calculated and Measured Values for Interactions Between the First Series of Polymers and a PS Particle (R≈3.75 μm) Probe.*

The Lifshitz theory is insufficient to account for the behaviour of the second polymer series, in particular when examined with the polar probes. However, since the SiO_x-probe is known to contain hydroxyl groups, it was attempted to correlate the adhesion measurements with the behaviour of water on the surface as measured by water contact

angle (see Table 4.2). The water contact-angle measurements were observed to correlate reasonably well with pull-off forces for the second polymer series and the polar probes, suggesting that the SFM-Van der Waals approach could potentially be used to provide local hydrophobicity/hydrophilicity information, and thus to differentiate between polymer surfaces, as an alternative to the method described by Sinniah *et al*.[6]

Differences in tip radius would account for the difference in the SiO_x-PS pull-off forces derived from the two series of measurements (Figures 4.4 and 4.6), given that the spring constants for the cantilevers appeared to be very similar. Imaging the tip used for the first polymer series (tip radius 50nm) by field-emission scanning electron microscopy showed that it was, indeed, somewhat flattened. The tips for the second polymer series measurements had been taken from a different area of the wafer, and were presumably closer to specifications (20nm). This illustrates another difficulty with attempts to obtain quantitative analytical data with SFM, and the need for independent measurements of tip properties.

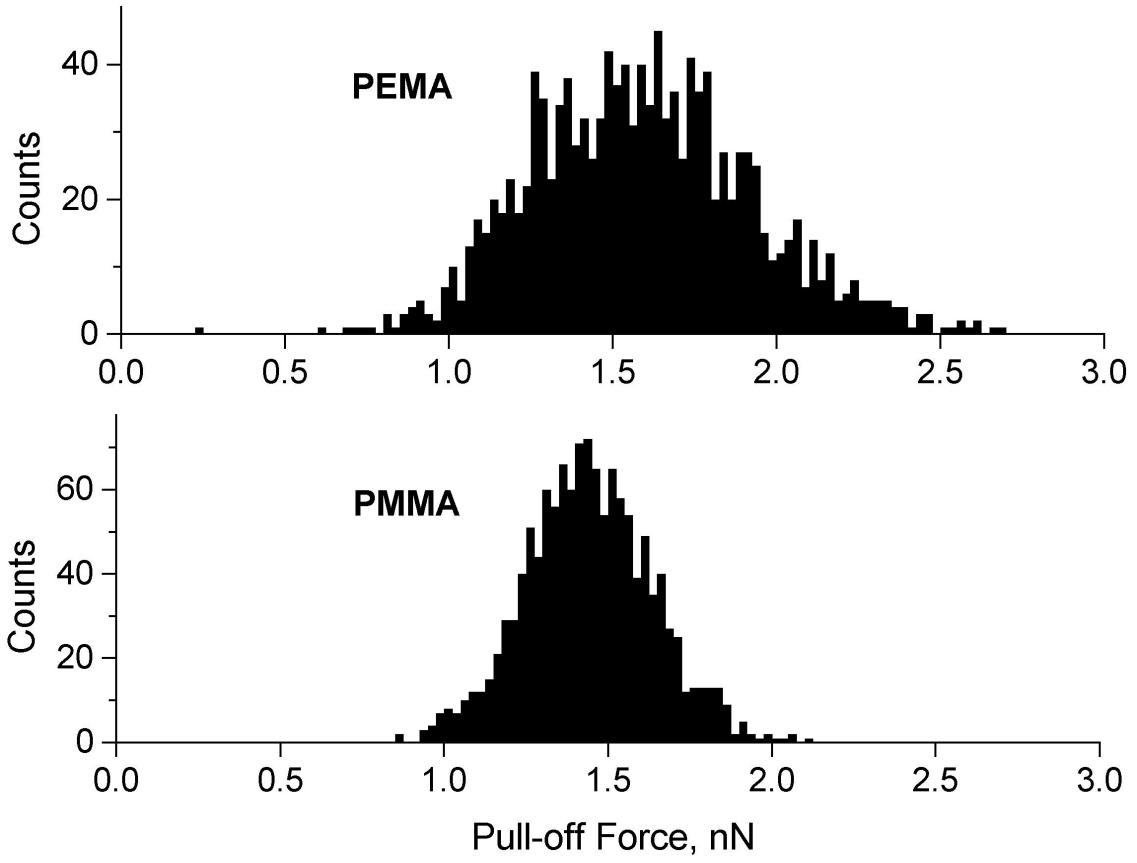

Figure 4.9 *Histograms of the pull-off forces measured between a SiO_x probe (k=0.03N/m) and surfaces of PEMA and PMMA in perfluorodecalin.*

To further elucidate the hypothesis stated above that there might be an enhanced mobility of the side groups (for example, in case of PMMA), we have compared the pull-off forces measured between a SiO_x probe and surfaces of PMMA and poly(ethyl methacrylate), PEMA (M_w=515K g/mol, Aldrich Chem. Co., Inc., USA). PEMA has a glass transition temperature (T_g=63°) lower than that of PMMA and similar refractive index. The fact that the T_g is lower for PEMA suggests that the ether ethyl side group should be more mobile than the ether methyl group of PMMA that, in turn, should lead to a stronger adhesion (greater pull-off forces) with a polar SiO_x probe. The results are shown in Fig. 4.9 and indicate that the average pull-off force is indeed greater for the PEMA surface (1.59±0.34nN) than for the PMMA surface (1.44±0.19nN), however, the distribution of the pull-off forces is also broader.

4.9 Frictional Measurements

The histograms in Figures 4.6 and 4.7 demonstrate that the chemical nature of the probe tip determines, for example, whether it is PS or PMMA that exhibits the greater adhesional force between the tip and the polymer surface. Given that frictional forces are generally commensurate with adhesion hysteresis[42] (which usually varies monotonically with pull-off force), we would also expect to see a reversal of contrast between the two tip classes in lateral force microscopy (frictional) images of PS-PMMA blends. It is worth noting that in our measurements the polymers of similar molecular weights and similar bulk elastic moduli (3200MPa and 3300MPa for PS and PMMA, respectively) were employed. Frictional contrast between PS and PMMA has been reported in the literature with the results being somewhat contradictory.[43,44] The authors in ref. 43 reported that for an applied load of 10nN frictional signal was found to be lower for PS (M_w=902K g/mol) than for PMMA (M_w=109 g/mol). The same authors observed the reversal of contrast upon decreasing the applied load,[45] suggesting differences in the dynamic properties of the two materials. The authors in ref. 44 reported lower friction on the areas of PMMA (M_w=12K g/mol) than on the areas of PS (M_w=19,6 g/mol). It is clear that for polymers with intermittent molecular weights close to the molecular weight of entanglement (for PS M_e=10K), the friction behaviour of the two materials is quite complex and non-linear load dependence is anticipated. Therefore, while all these measurements revealed contrast between the two polymers in SFM friction measurements, the nature of the contrast was primarily due to the nanomechanical differences between the two polymers.

We prepared a blend by spin-coating a 2 wt.% solution of PS and PMMA (1:10 wt. ratio) onto a Si wafer; the resulting film was annealed at 140°C overnight to ensure substantial phase separation. The film was imaged in PFD in frictional mode with both SiO_x- and gold-coated tips at zero applied load (the load being due to the work of adhesion only). Both height and frictional (loop-subtracted) images are shown in Figure 4.10.

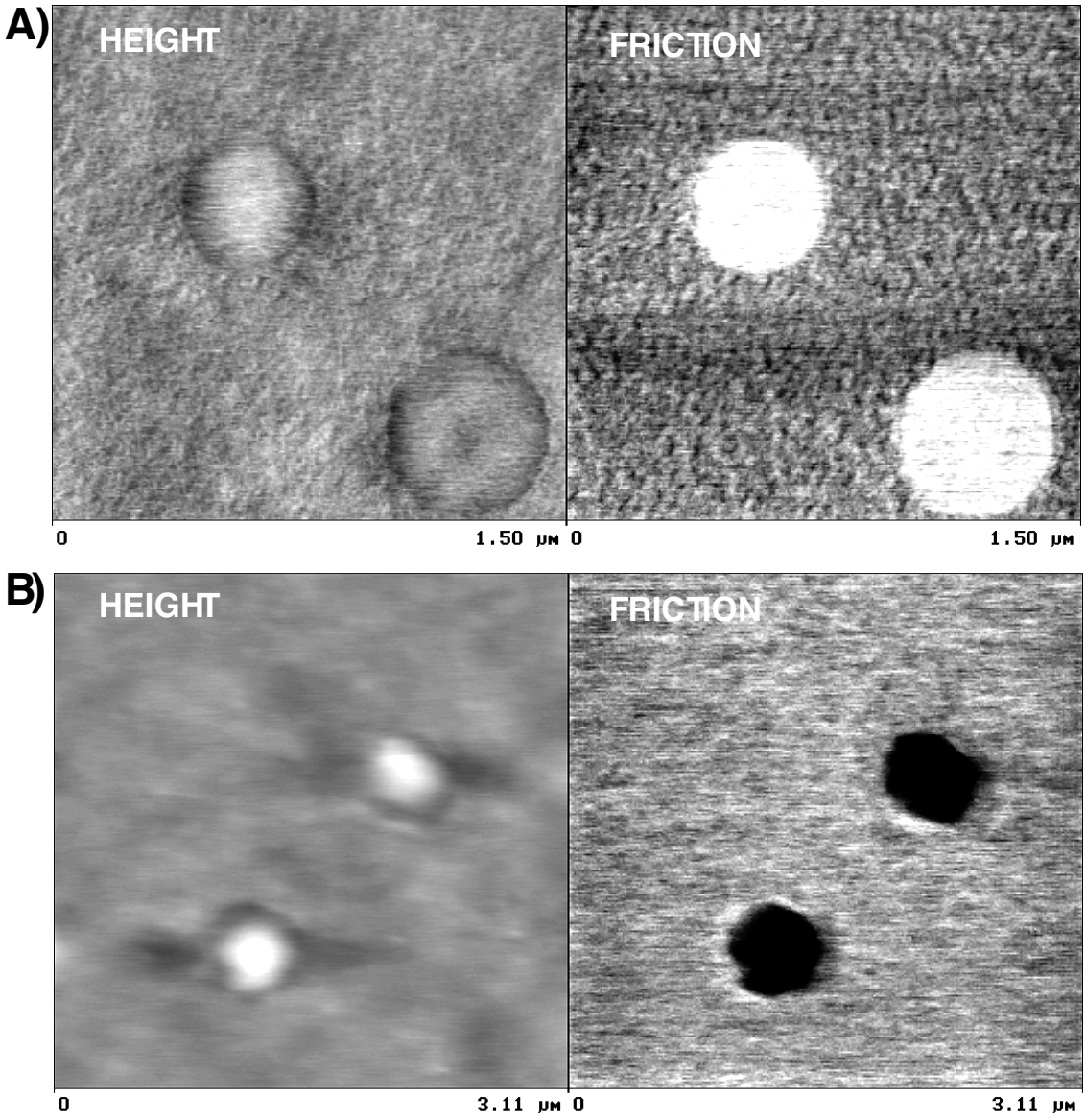

Figure 4.10 *Height (SFM) and friction (LFM) images of a spin-cast polystyrene:poly(methyl methacrylate) polymer blend [PS:PMMA (1:10 w:w)], obtained with a) Gold-coated and b) SiO_x tips under perfluorodecalin.*

These images clearly reveal the tip-dependent reversal of the frictional contrast for the two polymers: friction was lower for PS-SiO_x than for PMMA-SiO_x, and higher for PS-Au than for PMMA-Au.

4.10 Conclusions

Surface nanochemical imaging of polymers with SFM is clearly an analytical challenge, in that the chemically induced properties are convoluted with many other factors, such as disorder, mechanical properties, surface dynamics and morphology. Nevertheless, when these other factors are carefully controlled, it appears that SFM may be used to distinguish, in the case of non-polar systems, between areas of differing optical refractive index, as manifested by the London component of the Van der Waals force. In the case of polar systems, the approach can distinguish between regions of different hydrophilicity. By imaging in frictional mode (LFM), this same information could be used to provide a high-spatial-resolution chemical map of many heterogeneous polymer systems, especially in cases where mechanical properties of the components are similar. It was found that, due to its low refractive index, the use of perfluorinated decalin as a medium in SFM experiments significantly enhanced the differences in pull-off forces measured on various polymer surfaces.

References

1. Binnig, G.; Quate, C. F.; Gerber, Ch. *Phys. Rev. Lett.* **1986**, *56*, 930.
2. Mate, C. M.; Erlandsson, R.; McClelland, G. M.; Chiang, S. *Phys. Rev. Lett.* **1987**, *59*, 1942; Overney, R.; Meyer, E. *MRS Bulletin,* **1993**, *May*, 26.
3. Frisbie, C. D.; Rozsnyai, L. F.; Noy, A.; Wrighton, M. S.; Lieber, C. M. *Science* **1994**, *265*, 2071.
4. Lee, G. U.; Kidwell, D. A.; Colton, R. J. *Langmuir* **1994**, *10*, 354.
5. Akari, S.; Horn, D.; Keller, H.; Schrepp, W. *Adv. Mater.* **1995**, *7*, 549.
6. Sinniah, S. K.; Steel, A. B.; Miller, C. J; Reutt-Robey, J. E. *J. Am. Chem. Soc.* **1996,** *118*, 8925.
7. Green, J.-B. D.; McDermott, M. T.; Porter, M. D.; Siperko, L. M. *J. Phys. Chem.* **1995**, *99*, 10960.
8. Han, T.; Williams, J. M.; Beebe, T. P. *Analytica Chimica Acta* **1995,** *307,* 365.

9. Marti, A.; Hähner, G.; Spencer, N. D. *Langmuir* **1995**, *11*, 4632.
10. Hähner, G.; Marti, A.; Spencer, N. D. *Tribology Letters* **1997**, *3***,** 359.
11. Vezenov, D. V.; Noy, A.; Rozsnyai, L. F.; Lieber, C. M. *J. Am. Chem. Soc*. **1997**, *119*, 2006.
12. Bain, C. D.; Evall, J.; Whitesides, G. M. *J. Am. Chem. Soc.* **1989**, *111*, 7155.
13. Schönherr, H.; Vancso, G. J. *Polymer Preprints* **1996**, *37 (2),* 612.
14. Aimé, J. P.; Elkaakour, Z.; Odin, C.; Bouhacina, T.; Michel, D.; Cuély, J.; Dautant, A. *J. Appl. Phys.***1994,** *76,* 754.
15. Israelachvili, J. *Intermolecular and Surface Forces*, 2nd ed.; Academic Press: London, 1992; Chapter 11.
16. Hamaker, H. C. *Physica* **1937**, *4*, 1058.
17. Derjagin, B. V. *Kolloid Zeits*. **1934**, *69*, 155.
18. Lifshitz, E. M. *Sov. Phys.* **1956**, *JETP 2*, 73.
19. Burnham, N. A.; Colton, R. J. *Force Spectroscopy* In *Scanning Tunneling Microscopy and Spectroscopy: Theory, Techniques, and Applications*; Bonnell, D. A. Ed.; VCH Publishers, Inc.: New-York, 1993; Chapter 7.
20. (a) Hutter, J. L.; Bechoefer, J. *J. Appl. Phys*. **1993**, *73*, 4123. (b) Hansma, H. G., Sinsheimer, R. L.; Li, M.-Q.; Hansma, P. K. *Nucleic Acids Research* **1992**, *20***,** 3585.
21. Kopp-Marsaudon, S.; Nony, L.; Michel, D. Aimé, J. P. in *Microstructure and Microtribologyof Polymer Surfaces*; Tsukruk, V. V., Wahl, K. J., Eds.; ACS Symposium Series 741: Washington, DC, 1999; Chapter 8.
22. Marti, O.; Hild, S. in *Microstructure and Microtribologyof Polymer Surfaces*; Tsukruk, V. V., Wahl, K. J., Eds.; ACS Symposium Series 741: Washington, DC, 1999; Chapter 12.
23. De Gennes, P. G. *Europhys. Lett*. **1991**, *15*, 191.
24. Kramer, E. J.; Berger, L. L. *Adv. Pol. Sci.*, **1990**, *91*, 1.
25. Iler, R. K. *The Chemistry of Silica*; Wiley & Sons, Inc.: New York, 1979; Chapter 4.
26. Garbassi, F., Morra, M., Occhiello, E. *Polymer Surfaces: From Physics to Technology*, John Wiley & Sons Ltd: Chichester, 1994; Chapter 1.
27. Parsegian, V. A.; Gingell, D. *Biophys. J*. **1972**, *12*, 1192.
28. Butt, H.-J. *Biophys. J*. **1991**, *60*, 777.
29. Derjagin, B. V.; Landau, L. *Acta Physicochim. URSS* **1941**, *14*, 633.

30. Verwey, E. G. W.; Overbeck, J. J. G. *Theory of the Stability of Lyophobic Colloids*; Elsevier: Amsterdam, 1948.
31. Cleveland, J. P.; Manne, S.; Bocek, D.; Hansma, P. K., *Rev. Sci. Instr.* **1993**, *64*, 403.
32. Johnson, K. L., Kendall. K., Roberts, A. D. *Proc. R. Soc. Lond. A.* **1971**, *324*, 301.
33. Derjaguin, B. V., Muller, V. M., Toporov, Yu. P. *J. Coll. Interf. Sci.* **1975**, *53*, 314.
34. Burnham, N. A., Kulik, A. J., Oulevey, F., Mayencourt, C., Gourdon, D., Dupas, E., Gremaud, G. In *Micro/Nanotribology and Its Applications*; Bhushan B., Ed.; NATO ASI Series E: Applied Sciences; Kluwer Academic Publishers: Dordrecht, 1997; Vol. 330, p 421.
35. Maugis, D. J. *J. Coll. Interf. Sci*. **1992**, *150*, 243.
36. Manufacturer's specifications: Park Scientific Instruments, Sunnyvale, CA, USA.
37. Garbassi, F.; Morra, M.; Occhiello, E. *Polymer Surfaces: From Physics to Technology*; John Wiley & Sons Ltd: Chichester, 1994; Chapter 1.
38. Mansfield, K. F.; Theodorou, D. N. *Macromol.* **1991**, *24*, 6283.
39. Kambour, R. P. *J. Polym. Sci.* **1964**, *2*, 4165.
40. *Polymer Handbook*, 3rd ed.; Brandrup, J., Immergut, E. H., Eds.; J. Wiley & Sons, Inc.: New-York, 1989.
41. Frank, C. W.; Rao, V.; Despotopoulou, M. M.; Pease, R. F. W.; Hinsberg, W. D.; Miller, R. D.; Rabolt, J. F. *Science* **1996**, *273*, 912.
42. Israelachvili, J. N.; Chen, Y.-L.; Yoshizawa, H. *J. Adhesion Sci. Technol.* **1994**, *8*, 1234.
43. Krausch, G.; Hipp, M.; Böltau, M.; Marti, O.; Mlynek, J., *Macromol.* **1995**, *28*, 260.
44. Motomatsu, M.; Mizutani, W.; Nie, H.-Y.; Tokumoto, H. In *Forces in Scanning Probe Microscopy*; Güntherodt, H.-J., Anselmetti, D., Meyer, E., Eds.; NATO ASI Series E: Applied Sciences; Kluwer Academic Publishers: Dordrecht, 1995; Vol. 286, p 331.
45. The use of nanomechanical measurements is, of course, an alternative approach to that described in this paper for the chemical imaging of polymers. We believe, however, that it is likely to be more prone to ambiguity, due to the dependence of mechanical properties on processing conditions.

Chapter 5*

Force Spectroscopy of Oligo- and Poly(ethylene Glycol) Self-Assembled Monolayers

5.1 Introduction

Self-assembled monolayers (SAMs) of alkanethiolates on metal surfaces constitute a class of molecular assemblies formed by the spontaneous chemisorption of long-chain functionalised molecules on the surface of solid substrates.[1,2] Due to their ease of preparation, long-term stability, controllable surface chemical functionality, and high, crystal-like, two-dimensional order, SAMs represent suitable model surfaces to study molecular adsorption, adhesion, wetting, lubrication and the interaction of proteins and cells with artificial organic surfaces. The latter phenomena are of crucial importance to the fields of biomaterials, biosensors, and medical devices.

5.2 Protein Resistance of OEG- and PEG-Grafted Surfaces

The outstanding protein-resistant properties of poly(ethylene glycol) (PEG)-containing surfaces have been recognized for a long time and extensive experimental and theoretical work has been carried out to elucidate the physics underlying these properties.[3-6] Jeon *et al*[5] considered the balance between steric repulsion, Van der Waals attraction, and hydrophobic interaction between protein in solution and the PEG surface. They found that the net force determining the adsorption of the PEG-presenting surface

*This chapter is reproduced in part from:
Feldman, K.; Hähner, G.; Spencer, N. D.; Harder, P.; Grunze, M. *J. Am. Chem. Soc*. **1999**, *121(43)*, 10134-10141.

depends on the thickness of the grafted chains and their surface coverage. The steric repulsion has an osmotic (due to the solvation of the polymer chains) and an elastic (due to the conformational entropy of the PEG chains) component; these components become effective when the protein reaches the interphase by diffusion and compresses the PEG layer. The Van der Waals contribution to the attractive force was found to be smaller than the hydrophobic interaction between the protein and the hydrophobic surface, so only the latter was considered to compete with the steric repulsion effect. Protein resistance was only observed for the room-temperature stable hydrated phase of PEG in its helical (gauche–trans–gauche) conformation, and not for the high-temperature dehydrated amorphous phase.[7] The "steric repulsion" effect that prevents protein adsorption onto PEG chains attached to a surface is related to the positive free energy associated with compression (and therefore restriction of conformational freedom) and concomitant desolvation when the protein tries to attach to the surface. In a laterally densely packed film with only a few ethylene glycol units per chain attached to the surface, the steric repulsion will be (in absolute terms) smaller because of conformational constraints and the reduced hydration energy per chain and unit surface. The resistance to protein adsorption of oligo(ethylene glycol)-terminated self-assembled monolayers (SAMs), as first described by Prime and Whitesides,[8] suggests that this "protein-resistant" property is inherent in the composition and molecular conformation of the ethylene glycol chains. Prime and Whitesides compared and correlated the surface composition of different functionalised alkanethiolate SAMs with the amount of protein adsorbed from a single-component protein solution and found that both the hydroxyl- and the methoxy-terminated oligo(ethylene glycol) (OEG) SAMs both showed protein resistance, even when the surface layer was diluted with *n*-alkanethiol molecules up to a surface coverage of 35% of OEG-terminated moieties. These results demonstrate that resistance to protein adsorption is insensitive to the surface density of OEG groups over a substantial range of surface compositions.

5.3 Methoxytri(etheylene Glycol) Thiolates: Conformational Effects

The protein adsorption characteristics of the methoxytri(ethylene glycol) undecanethiolate (EG3-OMe) SAMs are strongly sensitive to the substrate used.[9] While the monolayers self-assembled on Au are protein resistant, those self-assembled on Ag

are not. Fourier transform infrared reflection-absorption spectroscopic (FTIRAS) experiments show that the SAMs on Au and Ag differ in the conformation of the OEG tail.[9] On gold a conformation with spectral characteristics typical of helical and amorphous PEG is found, whereas the spectra observed on the Ag substrates resemble those for the planar all-*trans* conformation of stretched PEG samples (Fig. 5.1). The different conformation and higher packing density in the Ag-supported monolayer is due to the formation of an incommensurate solid phase with nearly upright chains and a perceptibly smaller lattice spacing, as confirmed by calculation of the lowest-energy monolayer configurations on Au and Ag.[10] Good agreement is found between the experimental and calculated vibrational spectra of the lowest-energy SAM configurations on Au and Ag using these structural models.[11]

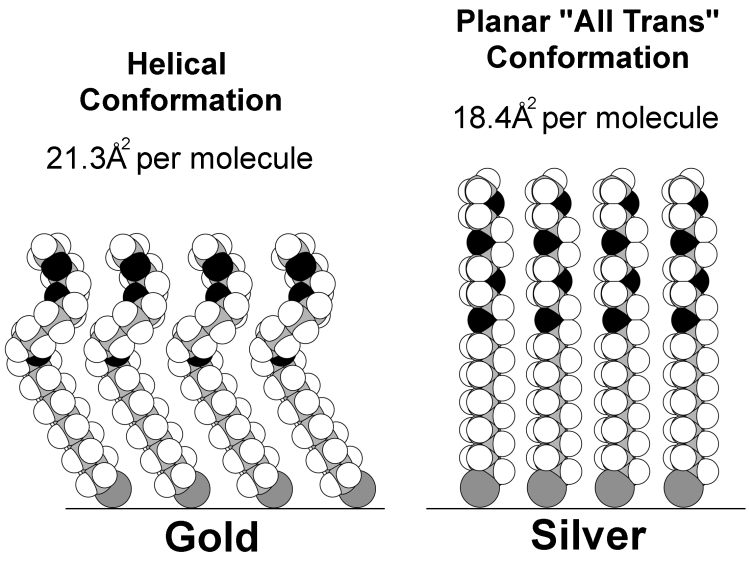

Figure 5.1 *Molecular cross-sections for the helical EG3-OMe on gold with a ~30° tilt of the alkyl chain and a perpendicular orientation of "all-trans" EG3-OMe on silver.*

To interpret the protein-resistance properties of the SAMs containing the helical conformers, the presence of a stable interphase water layer preventing the SAM from direct contact with protein molecules was postulated from *ab initio* 6-31G SCF calculations of the microscopic structure of the SAM/water interphase region.[12] The observed difference in protein adsorption between the helical and planar SAM phases is assumed to be caused by a difference in the structural organization of water near the SAM surface. Calculations show that the helical SAM phase easily accommodates water molecules, which act as a template for further adsorption of water via a hydrogen bridge-bonding network. The resulting interphase water layer is tightly bound to the

helical or amorphous SAM surface, thereby preventing direct contact between the surface and the protein. In contrast, the denser SAM phase on silver does not allow water molecules to form strong hydrogen bonds with oxygen atoms in the EG3-OMe strands. As a result, no interphase water layer capable of hindering protein adsorption is formed. Similar explanations have been given in the literature[13] to correlate the inertness of some hydrophilic surfaces towards protein adsorption with the contact angles of water.

Force measurements have been performed with scanning probe techniques to study protein properties and protein-surface interactions. Apart from specific recognition and specific interactions,[14-20] single-molecule force spectroscopy,[21] adhesion forces between ligand-receptor pairs,[22,23] and protein adsorption onto polymer surfaces[24] have also been reported in the literature. However, the importance of the different chemical regions (neutral or charged) in a protein with respect to the net interaction of the macromolecule with a surface is still being debated.[25]

In this Chapter, force-distance measurements between fibrinogen-modified probes and the surfaces of tri(ethylene glycol)-terminated ($-S(CH_2)_{11}(OCH_2CH_2)_3OCH_3$) alkanethiolate monolayers (further in the text referred to as EG3-OMe) on gold and silver are described. These measurements, obtained with a commercial AFM, demonstrate the good correlation between these experiments and fibrinogen adsorption data obtained by FTIR.[9] Subsequently, results obtained with charged (oxidised/hydroxylated) or hydrophobised (hexadecanethiol-derivatised) probes are reported. These experiments are conducted in order to elucidate qualitatively the different contributions and relevance of charged or hydrophobic patches in fibrinogen (the protein used in this study) to the resulting interactions with tri(ethylene glycol)-terminated SAMs on gold or silver. Furthermore, the force-distance measurements for the OEG SAMs and PEG end-grafted surfaces are compared to emphasise that the nature of the repulsive forces originating from the short-chain oligomers is unique and not related to a “steric repulsion” effect.

5.4 Experimental

5.4.1 Materials

EG3-OMe (1-Mercaptoundec-11-yl)tri(ethylene glycol) methyl ether was prepared according to a general procedure developed by Prime and Whitesides.[88] 11-bromoundec-1-ene was added dropwise to a solution of tri(ethylene glycol) methyl ether in THF with 2 equivalents of NaH and the solution was stirred overnight. Non-consumed NaH was reacted with isopropanol. The solvent was removed and the remaining product was purified by column chromatography. A solution of the olefin in methanol containing four equivalents of thiolacetic acid and 10mg of AlBN was irradiated for 6h under an atmosphere of nitrogen with a 450W, medium pressure mercury lamp. Concentration of the reaction mixtures by rotary evaporation at reduced pressure followed by purification by chromatography on silica gel gave the thioacetate. The latter was refluxed overnight in 0.5M HCl in methanol and the solution purified by column chromatography. The purity of the thiol was checked with NMR and mass spectroscopy.

(1-Mercaptoundec-11-yl)poly(ethylene glycol) methylether (average M_w=2K g/mol) was prepared analogously to a general procedure for mercaptoundecyl oligo(ethylenglycol) described by Prime and Whitesides.[88] The following changes were made: PEG 2000 monomethylether as a starting material was dried over molecular sieve 48 h before use. For the coupling reaction to the alkyl chain, 2 eq. 11-bromoundec-1-ene were added to a solution of PEG 2000 monomethylether in dry THF with 2 eq. NaH and the mixture stirred overnight. Purification of the different synthetic steps was carried out by column chromatography on silica gel with chloroform/methanol 1:3 as eluent. Purity and molecular weight distribution of the thiol were checked by NMR and MALDI mass spectrometry (M_n (number average) =2199, M_w (weight average) =2224; Mw/Mn =1.01).

5.4.2 SAM Preparation

Polycrystalline gold (99.99%, Balzers Materials, Liechtenstein) and silver (99.99+%, Aldrich Chem. Co., Milwaukee, WI) substrates were prepared by thermal evaporation of these metals onto plasma-cleaned pieces of singly polished silicon (100) wafers (MEMC Electronic Materials, Inc., St. Peters, MO) in a BAL-TEC (Balzers,

Liechtenstein) MED-020 coating system operated at $3\text{-}5\times10^{-5}$ mbar. Evaporation of a 5-nm chromium adhesion layer was followed by deposition of a 100-nm layer of gold or silver at a rate of 0.5nm/s. Coated substrates were immediately immersed into 2-mMol thiol solutions in ethanol. Upon removal from the thiol solution, the SAMs were rinsed with pure ethanol and dried with nitrogen. Characterisation of SAMs involved static water-contact-angle measurements with a contact-angle goniometer (Ramé-Hart, Inc., Mountain Lakes, NJ) and film-thickness measurements by ellipsometry (Type L-116C, Gaertner Science Corp., Chicago, IL) with a 70° angle of incidence of a He-Ne laser. Results of water-contact-angle measurements were in agreement with those reported earlier:[9] 63°±2° for the EG3-OMe SAMs on *both* gold and silver. Representative films were checked by FTIR with respect to their overall quality and molecular conformation.

5.4.3 SFM Measurements

Force-distance measurements and imaging were performed with a Nanoscope IIIa scanning force microscope (Digital Instruments, Inc., Santa Barbara, CA) equipped with a liquid cell. We monitored the temperature inside the cell with a K-type thermocouple. The temperature was in the range of 27–30ºC during our measurements. Force-distance curves were collected with a cycle frequency of 0.3–0.5Hz. All liquids introduced into the liquid cell were filtered with 0.22µm 'millex-GV', low-protein-binding filters (Millipore, Bedford, MA). Manufacturer-provided nominal values of the cantilevers' spring constants, k_0, and frequencies, ω_0, were used to calculate the actual spring constant, k, by measuring resonant frequencies, ω, of the probes according to the equation:

$$k = k_0\left(\omega / \omega_0\right)^2 \tag{5.1}$$

assuming that the effective mass of the cantilevers is constant. Prior to force-versus-distance measurements, 100-nm and 500-nm z-calibration gratings (TGZ-type, NT-MDT, Zelenograd, Russia) were scanned in contact mode to ensure proper calibration of the z-piezo. Piezo-displacement cantilever-deflection curves were converted into force-distance curves according to the procedure described in ref. 89. Zero separation corresponds to the detection point of the hard-wall potential, i.e., there is no absolute measure for the distance between tip and surface. Force-versus-distance measurements of each series of samples were performed with the same probe to minimise the error in distance due to variability in the spring-constant value.

5.5 SFM Imaging of EG3-OMe SAMs on Gold and Silver

In establishing possible differences between the EG3-OMe SAMs on gold and silver, we first recorded $3\times3\mu m^2$ SFM images of the two surfaces in TappingMode™ with a 5% reduction in the set-point amplitude (Fig. 5.2). A surface-roughness analysis revealed no significant differences between the root-mean-square (RMS) roughness values of the two surfaces, which were both found to be around 1.6nm. Since the protein adsorption experiments were conducted using fibrinogen, which is known to have an extremely high surface activity,[26] one would not expect roughness to be a factor influencing the surface affinity of fibrinogen. However, it is helpful to be able to exclude surface roughness as a possible variable in our experiments.

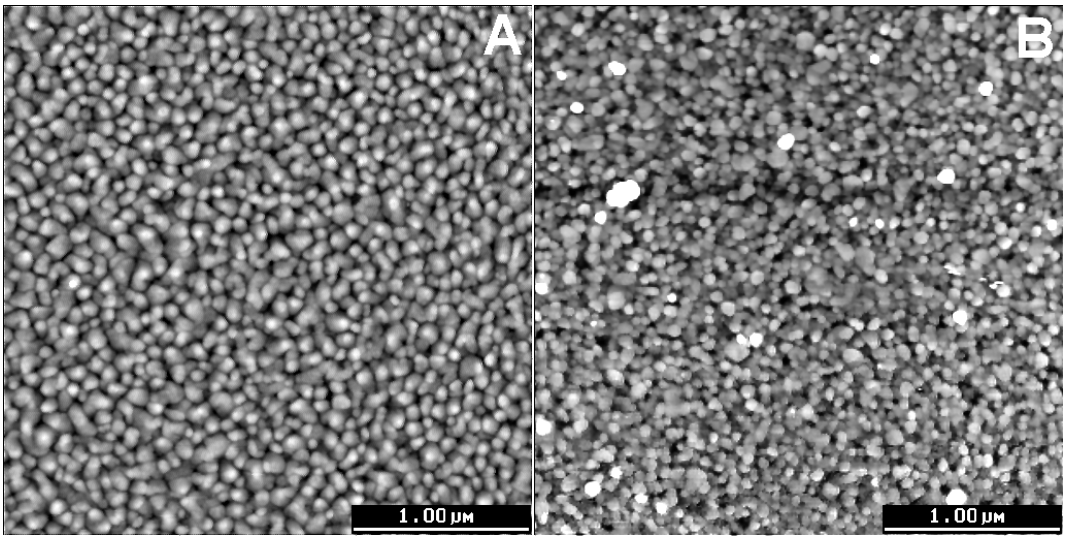

Figure 5.2 *$3\times3\mu m^2$ SFM images of EG3-OMe SAMs on a) gold and b)silver in TappingMode™ with a 5% reduction in the set-point amplitude. Z-range 50nm.*

To establish whether the EG3-OMe monolayers form ordered crystalline films on the two substrates, high-resolution SFM imaging of the EG3-OMe SAMs on gold and silver was performed. The images revealed periodic structures on both substrates (Fig 5.3). The periodic structure on Au(111) was found to be consistent with the commensurate hexagonal $(\sqrt{3}\times\sqrt{3})R30°$ structure of the SAM overlayer[27] with a tail-group spacing of ≈5Å. The structure on Ag(111) was also found to be consistent with previously reported results,[28] which had suggested that the SAM overlayer formed a commensurate hexagonal $(\sqrt{7}\times\sqrt{7})R11°$ structure with a lattice spacing of ≈4.7Å.

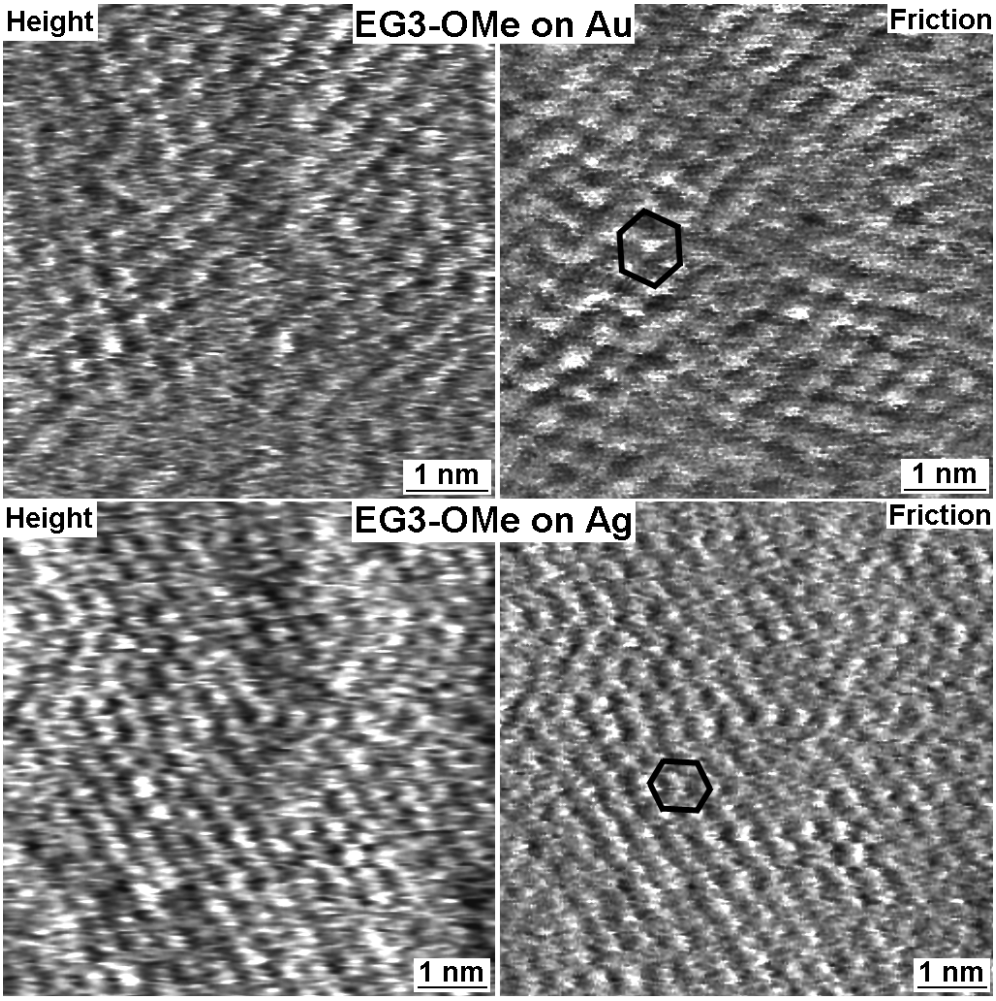

Figure 5.3 *SFM images of the EG3-OMe monolayers on gold and silver.*

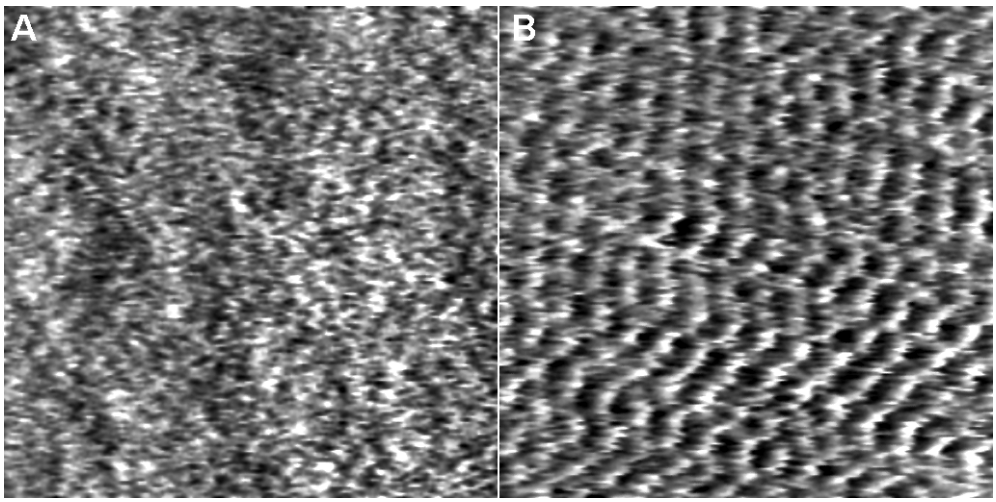

Figure 5.4 *SFM 7×7nm^2 height images of the EG3-OMe monolayer on a) gold and b) silver taken at identical scanning conditions with an applied load of 0.5nN.*

It must be noted, however, that imaging of the periodic structure of the SAM on gold was only possible in a vary narrow range of effective loads (the effective load is mainly due to adhesion, the applied load being close to zero). When both surfaces were scanned

under identical conditions with an applied load of 0.5nN, the periodic structure was no longer observed for the EG3-OMe monolayer on gold, while the EG3-OMe periodicity in the silver system remained (Fig. 5.4). These results indicate that the monolayer on silver is highly crystalline and robust. The periodicity revealed for the SAM on gold at zero applied load might be either due to the periodic structure of the OEG tails or that of the underlying, crystalline hydrocarbon (undecanethiolate) backbone. It is therefore unclear whether the OEG tails of the monolayer on gold are in fact in an ordered crystalline or in an amorphous state.

5.6 SFM Measurements With Fibrinogen-Modified Probes

The resistance of surfaces toward protein adsorption is often tested with the solutions of fibrinogen.[8,9] Fibrinogen is a plasma protein that has received much attention due to its dual functionality in thrombosis (formation of a blood clot). The conversion of fibrinogen to fibrin and the subsequent polymerisation of fibrin is a key step in blood clot formation. Fibrinogen also serves as an adhesive agent in the aggregation of platelets, which occurs simultaneously with fibrin polymerisation in the development of a hemostatic blood clot.[26] Fibrinogen is a "sticky" protein, having a strong tendency to adsorb onto various surfaces.

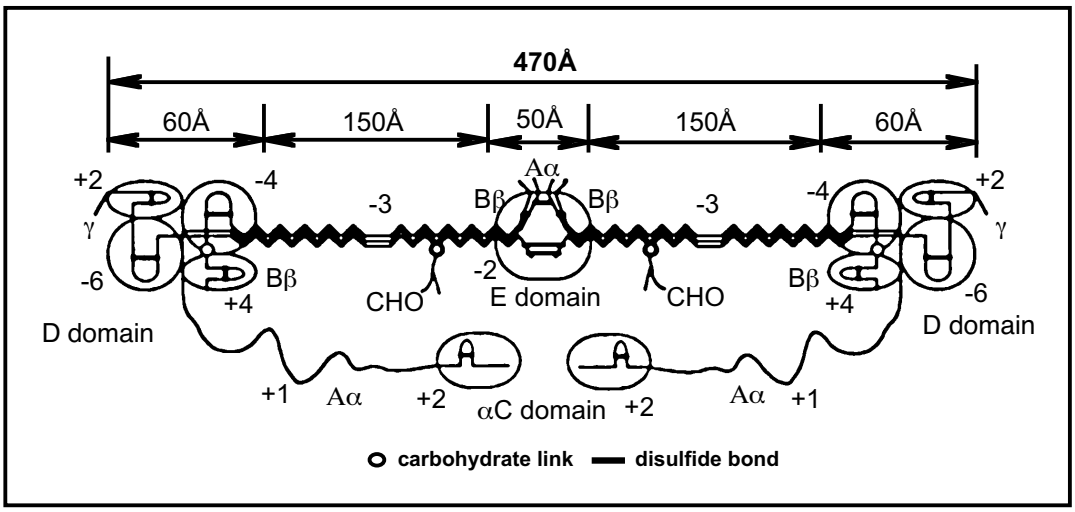

Figure 5.5 *Molecular model of fibrinogen and its individual domains showing net charges on individual domains and sub-domains. Adapted from ref. 26.*

The high surface activity of fibrinogen results in its binding strongly to both hydrophilic and hydrophobic surfaces.[29] Fibrinogen is a massive molecule (M_w=340K g/mol) with many molecular domains (Fig. 5.5); the structurally distinguishable regions of

fibrinogen are: a lone central E domain, two distal D domains, two α helical coiled coils, two αC domains, and a pair of junctions between them. Two distinct mechanisms of fibrinogen film formation on hydrophilic and hydrophobic substrates has been recently proposed.[30] It has been shown that on hydrophobic substrates film formation proceeds through formation of a network of clusters, implying a strong protein-protein interaction.

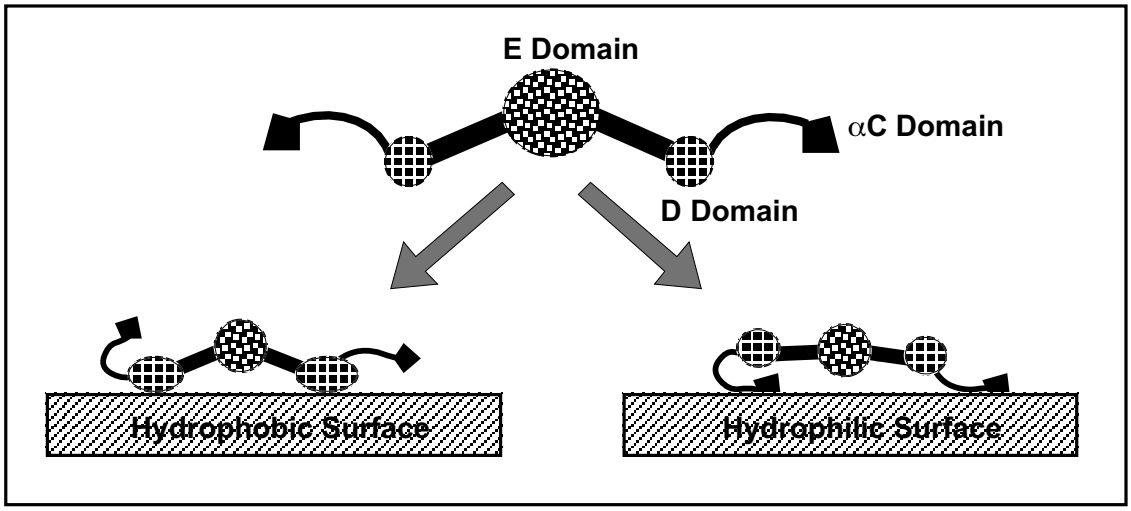

Figure 5.6 *Schematic representation of fibrinogen adsorption to hydrophobic and hydrophilic surfaces. Adapted from ref. 30.*

The growth mechanism on hydrophilic substrates occurs through a homogeneous increase in the number of nuclei across the surface and gives no indication of significant intermolecular interactions. The authors proposed that binding to a hydrophobic substrate occurs through D domains with the final film structure having strong intermolecular interactions and tight binding to the surface (Fig. 5.6). In fact, a fibrinogen film on a hydrophobic surface could not be eluted with a surfactant solution.[30] On a hydrophilic substrate, a fibrinogen film forms via αC domains, the proteins being loosely bound and easily eluted with a surfactant solution. The elution of surface-bound fibrinogen with a surfactant solution has been previously correlated with the protein affinity for platelets–a loosely bound layer is more active than a tightly bound one,[31] therefore, strong interaction with a hydrophobic substrate is indicative of a possible protein denaturation, with a change in the structural and biological properties. Therefore, we decided to adsorb fibrinogen onto hydrophilic oxygen-plasma-treated Si_3N_4 probes to ensure high surface activity of a fibrinogen coating on the probe.

Adsorption of fibrinogen onto SFM probes was conducted according to the following protocol: Si_3N_4 probes (Digital Instruments, Inc., Santa Barbara, CA), previously cleaned with water-enriched oxygen plasma were placed in phosphate-buffered saline solution (PBS) containing 0.01M phosphate buffer, 0.0027M KCl and 0.137M NaCl (solution obtained by dissolving PBS tablets, P-4417, Sigma Chem. Co., St. Louis, MO). Fraction I fibrinogen from human plasma (F-4883, Sigma Chem. Co., St. Louis, MO) was dissolved in PBS solution at a concentration of 2mg/ml. This solution was then added to that containing SFM probes to achieve a final concentration of fibrinogen of approximately 1mg/ml. After one hour of adsorption, more PBS solution was added, followed by aspirating the liquid with a vacuum line to remove any fibrinogen film that may have formed at the liquid-air interface. This procedure was repeated several times, to ensure that upon removal of the probes from the solution no fibrinogen film was transferred from the air/water interface onto the probes.

Each set of samples was measured with only one probe, to ensure that the observed changes in the tip-surface interaction were not due to variability in cantilever stiffness or probe-tip radius, although the latter might be affected by the number of loading-unloading cycles. The force-distance measurements with the fibrinogen-preadsorbed probes were conducted in the following manner: at least 64 force-distance curves were collected in PBS solution, both at the same point and at adjacent locations.

Figure 5.7 shows representative force-separation curves measured with a fibrinogen-modified probe in PBS solution on a series of surfaces including mica (hydrophilic) (Fig. 5.7A), hexadecanethiol-covered gold (hydrophobic) (Fig. 5.7B), a protein-resistant EG3-OMe monolayer on gold (Fig. 5.7C) and a protein-adsorbing EG3-OMe film on silver (Fig. 5.7D). According to FTIR measurements, the latter adsorbed about 20% of a fibrinogen monolayer.

The hydrophilic (mica) and the hydrophobic (C16) surfaces are intended to serve as references for strong fibrinogen binding. Both surfaces show an attractive interaction with the fibrinogen-modified probe upon approach and strong adhesion upon retraction, indicating that the proteins establish contact to both probe and sample surfaces. Note the difference in the extent of the attractive interaction of fibrinogen between the two surfaces. Clearly, the attractive force upon approach, the pull-off forces and the

adhesion hysteresis (the area between the approaching and retracting curves) were all greatest for the fibrinogen–C16 system, which is in good agreement with results reported in the literature.[30]

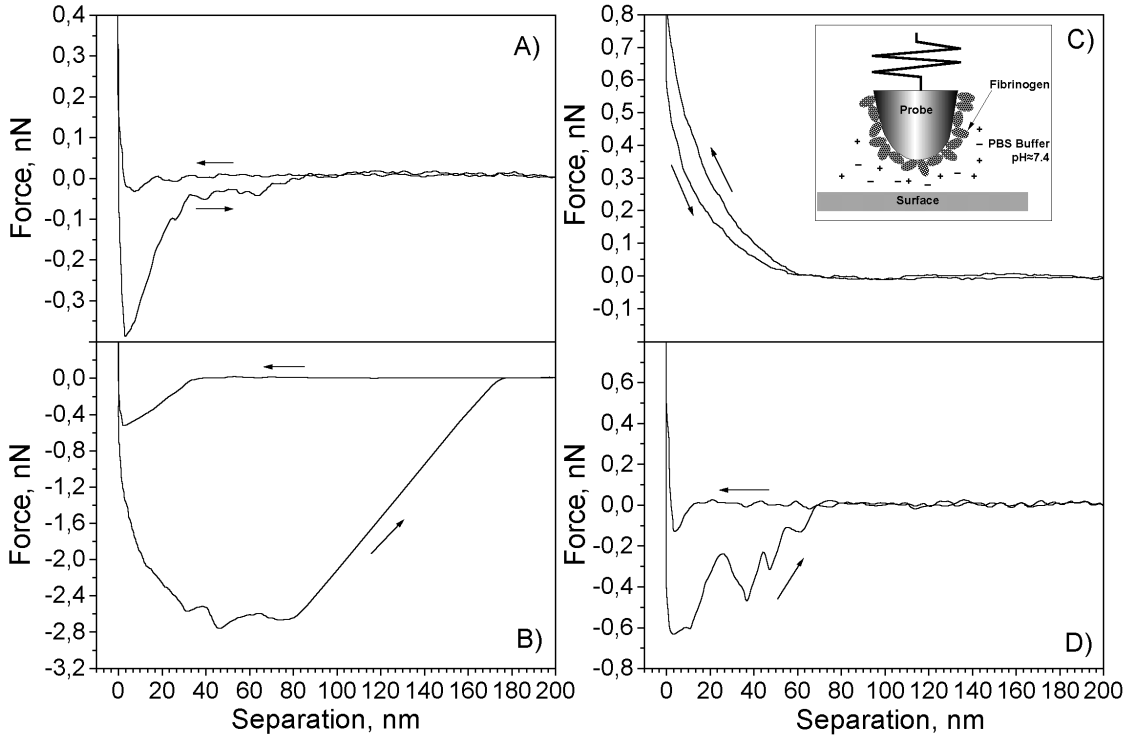

Figure 5.7 *Representative force-versus-separation curves obtained with fibrinogen-modified Si_3N_4 probe (k=0.03N/m) in PBS solution on: a) freshly-cleaved mica surface; b) hexadecanethiol SAM on gold; c) EG3-OMe SAM on gold; d) EG3-OMe on silver showing attractive interaction and multiple pull-offs (representative of the 20% of the force-distance data taken).*

As can be seen in Figure 5.7C, there are no attractive forces between a fibrinogen-modified probe and an EG3-OMe monolayer on gold. 256 force curves consecutively recorded in pure PBS and fibrinogen solution gave no evidence of attractive or adhesive forces. This was reproduced on several samples. However, there is a reproducible loading-unloading hysteresis, which did not change when pure buffer was replaced by fibrinogen solution. Similar observations have been reported by Sheth and Leckband by means of a surface forces apparatus.[32] These authors, however, measured an attractive interaction after *pressing* streptavidin onto PEG. The very small attractive forces found in their experiment might also be present here, but the effect is too small to be unambiguously detected. The presence of a hysteresis in the repulsive part of the force curve measured with a fibrinogen coated Si_3N_4 probe for EG3-OMe on gold (Fig. 5.7C) indicates the presence of energy-dissipating processes, which can be attributed to viscoelastic conformational changes in the protein layer induced by the loading

pressure. Although pressure-induced changes in protein conformation during loading and unloading might lead to aggregation of protein in the contact area, giving rise to long-range repulsive forces,[33] successive measurements at a single surface location showed no changes in the interaction. This also confirms that the protein layer recovers upon the retraction of the probe and that no plastic deformation is induced.

For the EG3-OMe monolayer on silver, we observed multiple pull-off events indicating adhesion of the fibrinogen-coated probe, in agreement with the FTIR protein-adsorption measurements (Fig. 5.7D).

While the measurements with the fibrinogen-coated probe revealed dramatic differences in the resistance to protein adsorption of the EG3-OMe monolayers on gold and silver, the experiments only confirmed the previously reported FTIR study,[9] and did not increase understanding of the physical phenomenon responsible for the distinct behaviour of the same molecules on different substrates. To gain further insight into the nature of the distinctly different protein resistance behaviour of the two monolayers, we employed probes with better-defined surface compositions to "mimic" the non-specific interaction of the fibrinogen macromolecule with monolayers of EG3-OMe. Since proteins contain both hydrophobic and charged domains,[25] we used hydrophobic (C16) and oxygen-plasma-treated Si_3N_4 probes, which acquire a net negative charge at biologically relevant pH values. In order to obtain charged SFM probes we used 'sharpened' Si_3N_4 Microlevers™ (Park Scientific Instruments, Sunnyvale, CA) with a nominal radius of curvature of 20nm, and treated them for 45-60 seconds in a RF-plasma cleaner (Harrick Scientific Corp., Ossining, NY), operated at 40W with a water-enriched oxygen feed to ensure both removal of contaminants and hydroxylation of the probe-tip surface. The plasma-treated tips were stored either in deionised water or in PBS buffer solution.

The largest dimension of a fibrinogen molecule in the native state is on the order of 470Å.[25,34] The size of the charged αC-domains of this protein and of its hydrophobic D-domains is quite comparable to the contact area between the SFM probes and the surface.[26]

5.7 SFM Measurements with Hydrophilic Probes

Measurements with oxygen-plasma-treated probes were performed in air, deionised water and in the same PBS buffer as used in the protein adsorption experiments. Force-versus-distance curves in air with an oxygen-plasma-treated probe (k=0.03N/m) revealed no significant differences between the EG3-OMe SAMs on gold and silver (Fig. 5.8). A large adhesion hysteresis primarily due to capillary forces[35] was found for both surfaces. Pull-off forces were determined to be 11.7±1.4nN for the SAM on gold and 10.6±0.3nN on silver.

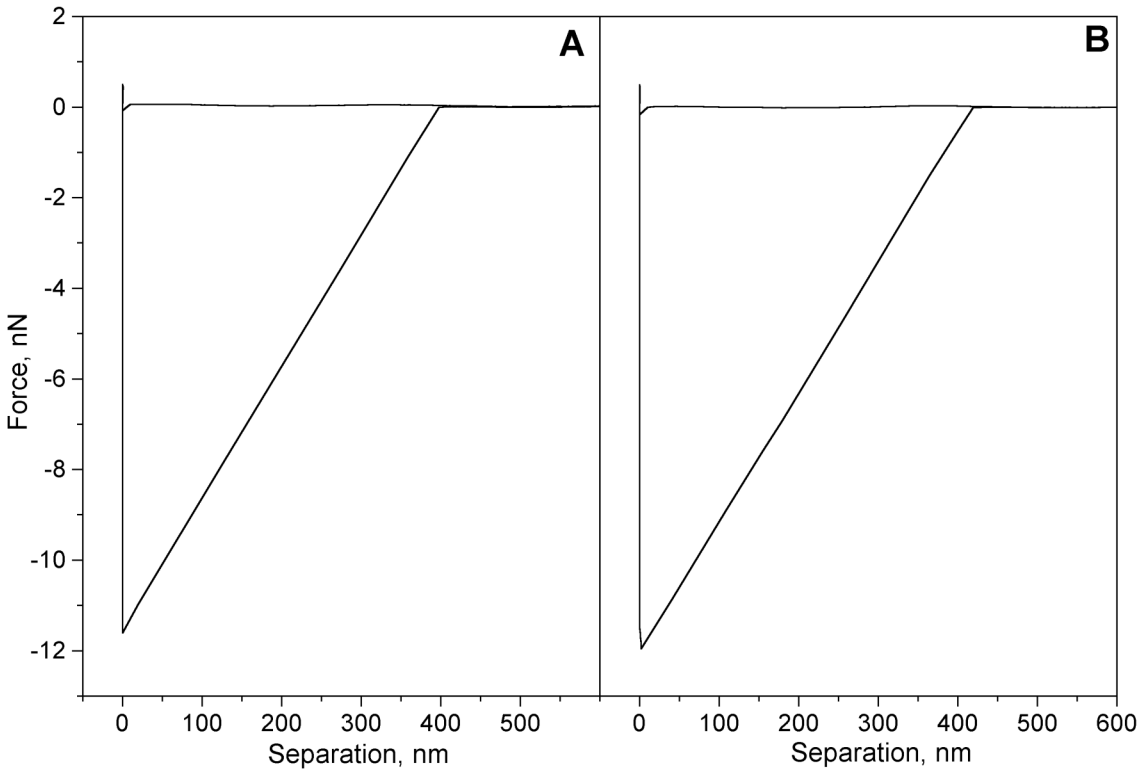

Figure 5.8 *Representative force-versus-separation curves obtained with oxygen-plasma-treated Si_3N_4 probe (k=0.03N/m) in air on the surfaces of EG3-OMe on a) gold and b) silver.*

The broader distribution of the pull-off forces from the EG3-OMe on gold might be due to the variations of the elastic modulus of the SAM on gold, which would, in turn, depend on the degree of crystalline order in the monolayer. The similarity of the pull-off forces on gold and silver in air measured with a hydrophilic, largely hydroxylised probe, is consistent with the similar water contact angles measured for the two monolayers.[9] Similar water-contact angles correspond to similar surface interfacial energies with

water and, therefore, to similar values of the work of adhesion which, in turn, is reflected in the pull-off forces.

Force-versus-distance measurements were also performed with an oxygen-plasma-treated Si_3N_4 probe (k=0.01N/m) in deionised (D.I.) water (18.2MΩ·cm) and PBS buffer (Fig. 5.9). We previously found[36] that probes treated with water-rich oxygen plasma have an isoelectric point at pH≈3, which implies that at higher pH values the probes acquire a negative surface charge due to deprotonation of hydroxyl groups. Our measurements of the EG3-OMe SAMs on gold and silver in D.I. water with a negatively charged probe showed a long-range repulsion followed by a short-range attraction, similar to a DLVO-type interaction.[37] The repulsive force was found to be stronger for the SAM on gold, while the pull-off forces were greater for that on silver. Measurements in PBS buffer did not reveal any significant differences between the two surfaces.

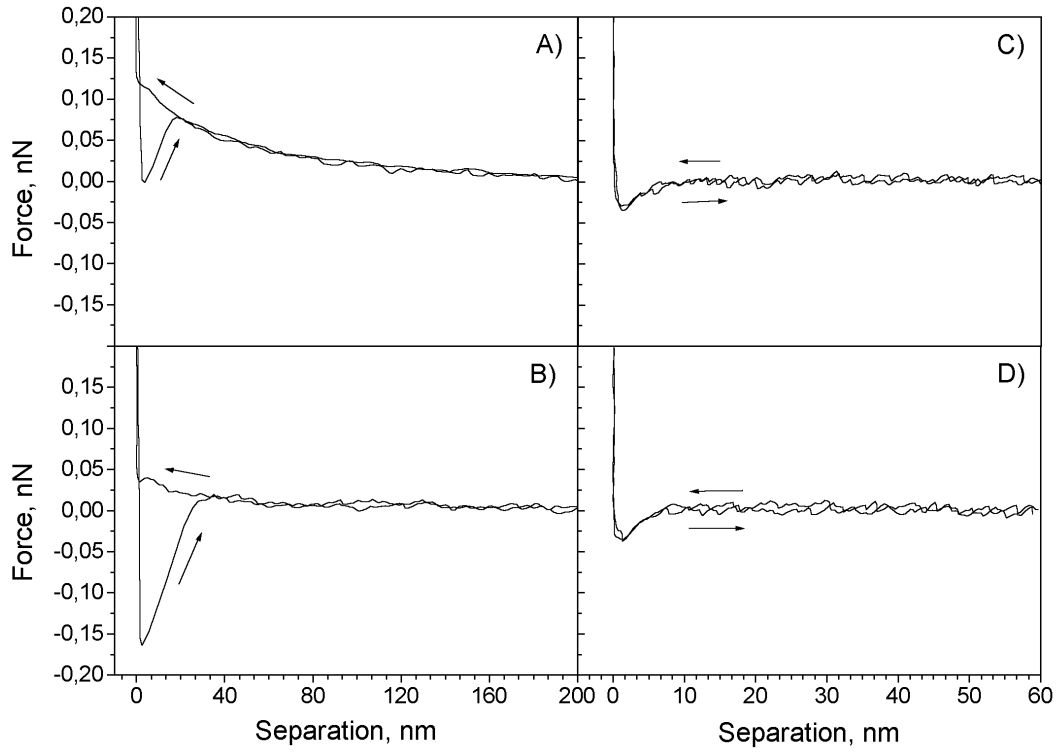

Figure 5.9. *Representative force-versus-separation curves obtained with oxygen-plasma-treated Si_3N_4 probe (k=0.02N/m) measured on: a) EG3-OMe on gold in deionised water; b) EG3-OMe on silver in deionised water; c) EG3-OMe on gold in PBS solution; d) EG3-OMe on silver in PBS solution.*

As expected, the ion concentration had a significant effect on the observed interaction: for both surfaces very weak attractive forces are observed in the PBS experiment, with a significantly smaller range of interaction compared to measurements in DI water.

Measurements with hydrophilic probes were also performed in perfluorinated decalin (PFD). This non-polar medium of low refractive index (n=1.317) is described in detail in the Chapter 4.4. The use of PFD greatly improved signal-to-noise of SFM force-distance measurements, facilitating the differentiation between polymer surfaces. The measurements conducted in PFD with the hydrophilic probe revealed significant differences in the values of the pull-on and pull-off forces as seen in Figure 5.10.

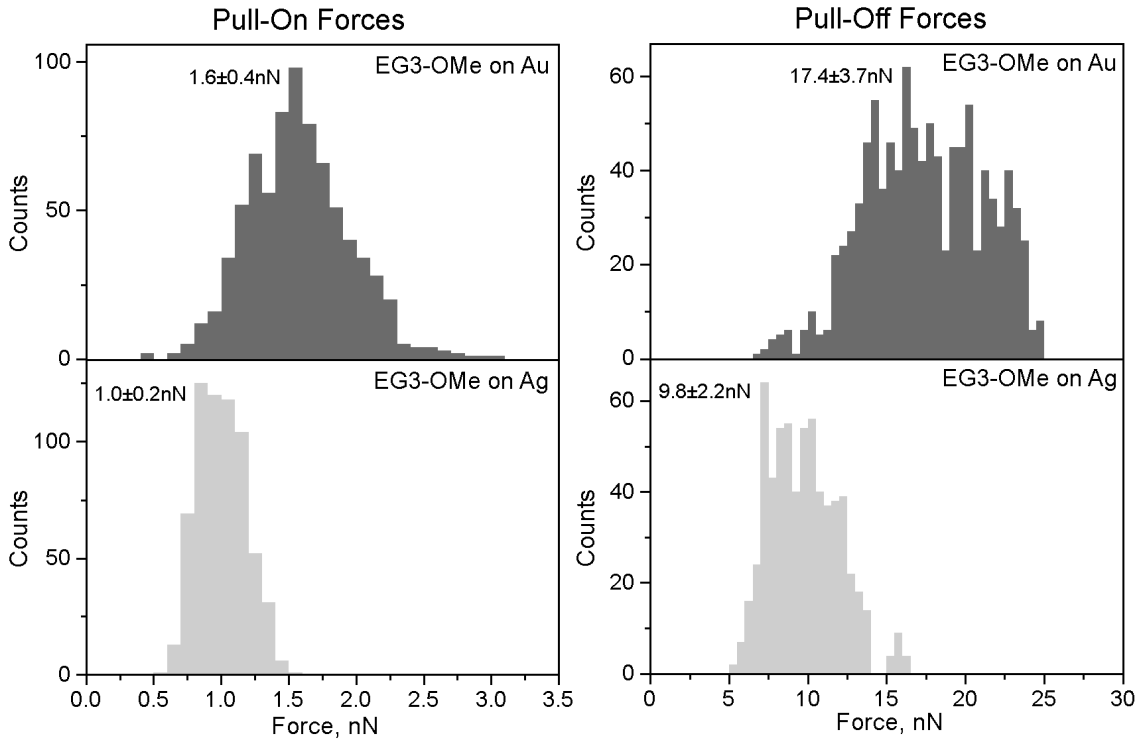

Figure 5.10 *Histograms of the pull-on and pull-off forces measured with oxygen-plasma-treated Si_3N_4 probe (k=0.1N/m) in perfluorodecalin on EG3-OMe SAMs on gold and silver.*

The following values of pull-on and pull-off forces were obtained: for the EG3-OMe monolayer on gold the average pull-on force was determined to be 1.6±0.4nN and the average pull-off force to be 17.4±3.7nN; for the EG3-OMe on silver the average pull-on force was found to be 1.0±0.2nN, and the average pull-off force of 9.8±2.2nN. This data shows that larger forces and also larger adhesion hysteresis were determined for the EG3-OMe SAM on gold. Given the non-polar, inert nature of the medium, the

differences observed should be attributed solely to the extend of the interaction between the probe and the two surfaces. Therefore, mechanical properties of the two films, i.e. elastic behaviour, could not be ignored. If contaminant water molecules remain bound to the OEG tails of EG3-OMe on gold, then the surface should exhibit more liquid-like properties compared to the EG3-OMe on silver. This translates into lower elastic modulus, larger contact area, and larger pull-off force upon the jump from contact of the SPM probe. On the other hand, if the mechanical properties of the two SAMs are similar, the helical conformation of the OEG tails on gold generates a stronger dipole field compared to that of the all-trans, tightly packed SAM on silver (the molecule is terminated by a non-polar methyl group), suggesting stronger Van der Waals interaction for the EG3-OMe on gold. A presence of the hydroxyl groups on the surface of the probe (which is treated in water-enriched oxygen plasma) generates a possibility of forming hydrogen-bonds with the helical OEG tails of the EG3-OMe on gold that would also lead to an increase in the pull-off forces. However, since there is no independent way of measuring refractive index and static dielectric constant of only the OEG tails of the SAMs on the two substrates, these conclusions are only speculative.

5.8 SFM Measurements With Hydrophobic Probes

The most interesting results were obtained with hydrophobic probes. “Hydrophobic” probes (referred to below as C16-probes) were prepared by vapour-phase deposition of hexadecanethiol (Aldrich Chemical Co., Inc., Milwaukee, WI) onto gold-coated Si_3N_4 probes (Digital Instruments, Inc., Santa Barbara, CA) with a nominal radius of curvature of 30nm. Both sides of the plasma-cleaned probes were coated with a 5-nm chromium layer followed by 50nm of gold. After gold deposition, the probes were placed in a metal desiccator containing 200mL of hexadecanethiol, the desiccator was then evacuated to ~0.1mbar and kept under vacuum overnight. To ensure the quality of SAMs, a piece of a silicon wafer was gold-coated and functionalised together with the probes and analysed by ellipsometry, static contact angle and XPS. The analyses did not reveal any notable differences between the SAMs of hexadecanethiol prepared via vapour-phase deposition and those prepared by immersion into 5mM solution in ethanol and therefore we assume a similar quality of the films on the Au coated Si_3N_4 tips used in our force measurements.

Measurements in pure water with C16-probes revealed a long-range repulsion for the EG3-OMe monolayer on gold and a long-range attraction for that on silver (Fig 5.11). When D.I. water was replaced by PBS solution, the extent of the repulsive interaction diminished on gold, but did not change sign. For silver, however, only very small differences were found between PBS buffer and pure water (Fig. 5.11). The experiments were repeated many times with different samples of EG3-OMe and several batches of C16-probes to confirm their correlation with the FTIR protein-adsorption measurements. We also investigated two other 1-undecanethiols, either with a hydroxyl terminated hexa(ethylene glycol) (EG6-OH) or a methoxy terminated tri(ethylene glycol) (EG3-OMe) end group and a $-CH_2OCH_3$ side chain at the C-12 atom (EG[3,1]-OMe). Force-distance measurements on monolayers of either thiol on gold or silver exhibited repulsive interaction with the C16-probes. These monolayers were also found to be resistant to fibrinogen adsorption in the FTIR experiments. An interesting correlation was established for all investigated films–whenever a *repulsive* force was observed upon approach of a *hydrophobic* probe in PBS solution, that surface *resisted* fibrinogen adsorption as determined by the FTIR measurements.

The repulsive curves measured upon approach to EG3-OMe on gold showed some variability with respect to the range of interaction. Some of them were purely repulsive, while occasionally a jump-to-contact at distances of ~5nm before contact appeared. Whenever a jump-to-contact occurred, this was accompanied by a hysteresis in the loading-unloading cycle, while no hysteresis was found in the purely repulsive curves. This variability of the SFM data in terms of the *range* of the forces and the presence of an adhesion hysteresis might be attributed to the structural inhomogeneity of the monolayers, i.e. the presence of different phases with dissimilar mechanical properties in the EG3-OMe layer.

Differences in force-distance measurements with a C16-probe and an EG3-OMe SAM on gold in D.I. water and PBS solution suggested a strong dependence of the range of the repulsive force upon the ionic strength of the solution; the same measurements for the monolayer on silver showed a long-range attractive interaction with very little apparent dependence on the ionic strength. These results imply that, due to different conformations of the EG3-OMe molecules on gold and silver, the observed interactions may well be of a distinct physical nature, i.e. electrostatic for EG3-OMe on gold and

hydrophobic for that on silver. To further elucidate this hypothesis, we performed force-distance measurements with a C16-probe on the two monolayers in aqueous solutions of KNO_3 of various ionic strengths (Fig. 5.12), and, once again, detected repulsive forces for the EG3-OMe on gold that displayed a strong dependence upon the ionic strength of the solution, and attractive long-range forces for EG3-OMe on silver that were less influenced by the presence and concentration of ions.

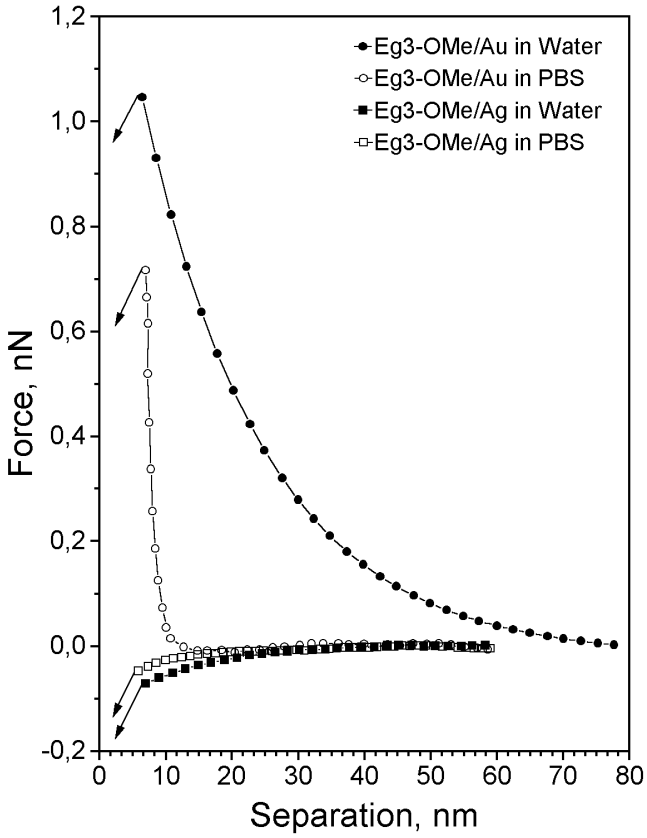

Figure 5.11 *Advancing force-versus-separation curves measured with hydrophobic C16-probe (k=0.12N/m) in deionised water and PBS solution on the SAMs of EG3-OMe on gold and silver.*

According to previous theoretical work on these systems,[10] strong interaction of water molecules with the helical conformer of the EG3-OMe SAM on gold is a necessary condition for protein resistance, because oligo(ethylene glycol) *per se* is not intrinsically protein resistant. Water cannot associate with the all-trans structure of the EG3-OMe SAM on silver, and hence this system exhibits protein adsorption behaviour that is characteristic for a slightly hydrophobic surface. To demonstrate unambiguously that the solvent plays a crucial role in explaining the difference in the adsorption characteristic of the helical and all-trans conformers, force-distance measurements with a hydrophobic probe were performed in perfluorodecalin.

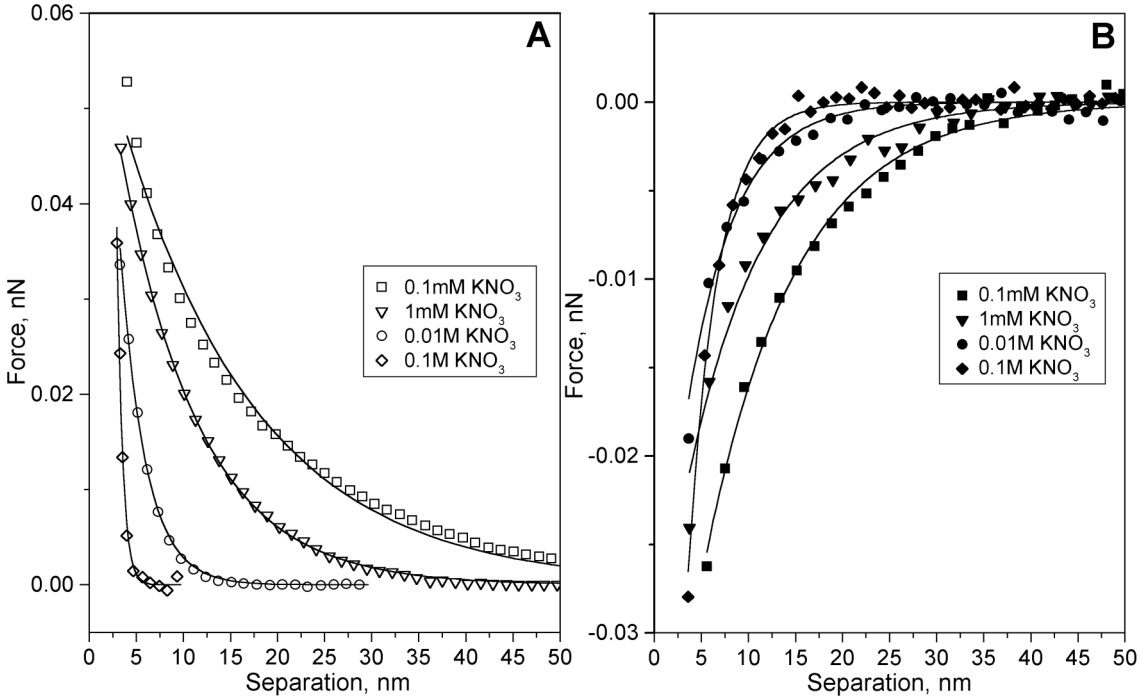

Figure 5.12 *Advancing force-versus-separation curves measured with hydrophobic C16-probe (k=0.06N/m) in aqueous solutions of KNO_3 on the SAMs of EG3-OMe on a) gold and b) silver.*

In agreement with the theoretical arguments, we did not observe any long-range forces in perfluorodecalin on the two SAMs (Fig. 5.13). Instead, we found attractive interactions on both surfaces.

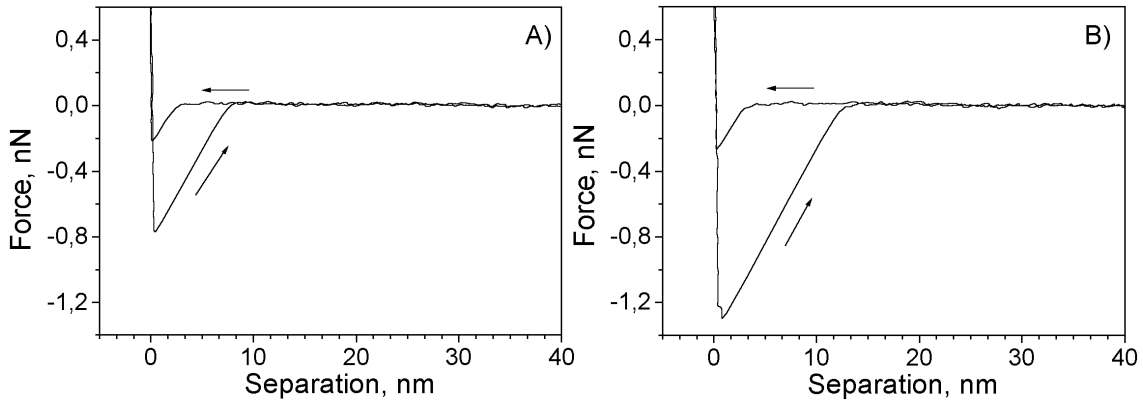

Figure 5.13 *Representative force-versus-separation curves measured with C16-probe (k=0.12N/m) in perfluorodecalin on EG3-OMe on a) gold and b) silver.*

5.9 Electrostatic Versus Hydrophobic Interaction

The SFM experiments on the SAMs of EG3-OMe on gold and silver measured with hydrophobic C16-probe suggested that, due to different conformation of the OEG tails,

the interactions of the two surfaces with the same probe under identical medium conditions are of distinct physical nature. The strong ionic-strength dependence of the repulsive force measured on the EG3-OMe on gold suggests a significant electrostatic contribution, while the attractive long range force for the EG3-OMe on silver, which exhibited little ionic-strength dependence, is indicative of the "hydrophobic" interaction.

The charging of a surface in an aqueous environment, or in another high dielectric constant solvent, occurs through two distinct mechanisms: either, by the ionisation or dissociation of surface groups, for example, deprotonation of the surface carboxyl group, or by a specific adsorption of ions.[38] Whatever the charging mechanism, the final surface charge is balanced by an equal but oppositely charged region of counterions, some of which are transiently bound to the surface within the so-called Stern or Helmholz layer, while others form an atmosphere of ions in rapid thermal motion close to the surface, known as the diffuse electrical double layer.[37] Contrary to intuition, the origin of the repulsive force between two similarly charged surfaces in a solvent (or a charged and an uncharged surface) containing counterions and electrolyte ions is of entropic (osmotic) origin due to the repulsive osmotic pressure between the counterions. On bringing two such surfaces together, the counterions are forced back onto the surfaces against their preferred equilibrium state (osmotic repulsion), giving rise to a net repulsive force.

The interaction between charged bodies in electrolyte solutions can be described by the DLVO-theory, which takes into account both electrostatic and Van der Waals forces.[39,40] For low surface potentials (ψ<25mV) the electrostatic force per unit area between the two flat surfaces bearing charge densities σ_1 and σ_2 can be described by the following equation:[41,42,43]

$$F_{el} = \frac{2}{\varepsilon\varepsilon_0}\left[\left(\sigma_1^2 + \sigma_2^2\right)e^{-2\kappa D} + \sigma_1\sigma_2 e^{-\kappa D}\right] \qquad (5.2)$$

For larger separations, electrostatic force between a sphere of radius R and a flat surface becomes:[43,44]

$$F_{el} = \frac{4\pi R\sigma_1\sigma_2}{\varepsilon\varepsilon_0\kappa}e^{-\kappa D} \qquad (5.3)$$

where $1/\kappa$ is the so-called Debye length and D is the separation between the two bodies. The Debye length, being a solution property, can be calculated from the following equation:[37]

$$\kappa = \left(\sum_i \frac{\rho_{\infty i} e^2 z_i^2}{\varepsilon \varepsilon_0 k_B T} \right)^{1/2} \text{m}^{-1} \qquad (5.4)$$

where $\rho_{\infty i}$ is the bulk ionic concentration, z_i is the ionic charge, k_B is Boltzmann's constant, e is the electronic charge and T is the absolute temperature.

One important implication of the equation (5.1) is that the overall electrostatic interaction is not eliminated when one of the surface charge densities is set to zero, e.g. $\sigma_1 \neq 0$ and $\sigma_2 = 0$. It is therefore not necessary for the both surfaces to carry charges.

Long-range repulsive forces followed by short-range attraction were measured for the EG3-OMe monolayers on gold and silver substrates in D.I. water with a negatively-charged oxygen-plasma-treated Si_3N_4 probe (Fig. 5.9). When comparing the force curves in D.I. water and PBS buffer it becomes clear that the ion concentration has a pronounced effect on the tip/substrate interaction. The two substrates differ only in the strength of the repulsive force. This difference may be explained if we now assume that, due to conformational differences, the EG3-OMe monolayer on gold carries an effective surface charge, while that on silver does not. There will still be a repulsive electrostatic interaction on silver (see Eq. 5.2, with $\sigma_2 = 0$) but it will be weaker than that for gold where $\sigma_1 \neq 0$ and $\sigma_2 \neq 0$. Upon introduction of the PBS solution, the range of the electrostatic force is, as expected, dramatically reduced. The screening of the electrostatic repulsion is due to the high ionic strength of the PBS solution (we calculated the Debye length of the PBS solution to be $1/\kappa = 0.76$nm at room temperature compared to ~1μm for D.I. water) and only the attractive Van der Waals forces are clearly observed (Fig. 5.9). In addition, the type of interaction changed from repulsive in pure water to very weakly attractive in PBS buffer, the range was found to be much shorter in the case of high ion concentrations, and almost no hysteresis was found for measurements performed in PBS buffer, although the hysteresis might also scale with the Debye length and hence be too small to be detectable here.

The issue is of surface charges on the EG3-OMe monolayer on gold is very important. There are no surface groups present that can dissociate in aqueous environment. ToF-SIMS measurements of the EG3-OMe SAMs on gold immersed overnight into 0.1M solutions of NaCl and KNO_3, and PBS buffer did not reveal any specific (preferential) ion adsorption despite the extreme sensitivity of this technique to alkali metals. Similar ToF-SIMS measurements were performed on hexadecanethiol (C16) on gold to detect whether this surface acquires a specific surface charge, but the measurements also failed to reveal any preferential ion adsorption. SFM force-distance measurements were performed on a symmetric system of C16-coated probe and surface in D.I. water and PBS buffer.

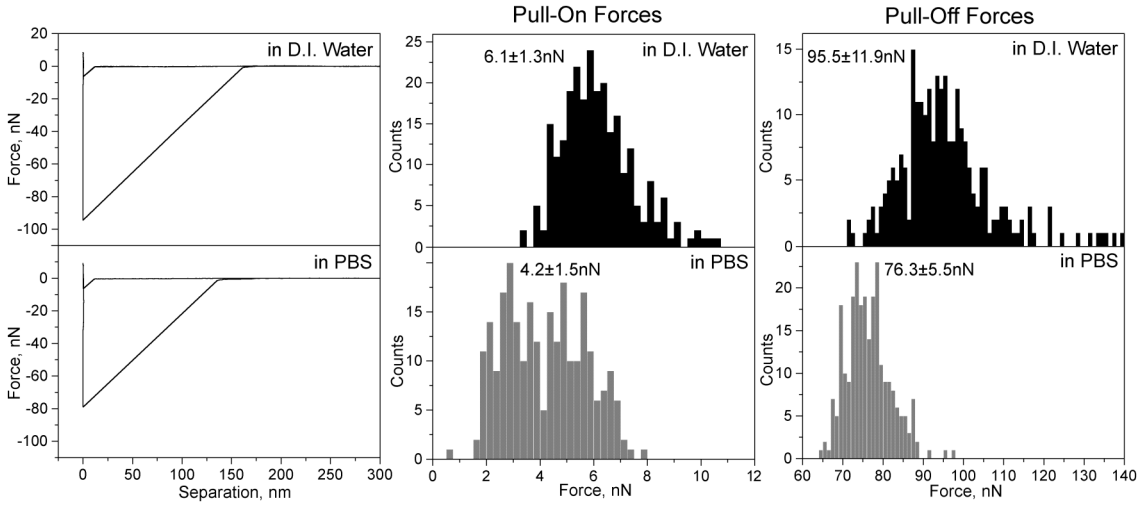

Figure 5.14 *Representative force-distance curves and histograms of the pull-on and pull-off forces measured in D. I. water and PBS buffer between C16-functionalised surface and C16-probe (k=0.12N/m).*

The results are shown in Fig. 5.14 and demonstrate that there are no long-range repulsive forces detected, as it would be expected for a symmetric case of two identical charged surfaces. Therefore, the long-range repulsive interaction observed between the C16-probe and the EG3-OMe SAM on gold, that scales with the ionic strength of the solution, if it is electrostatic in nature, has to originate from the surface charges of the OEG tails of the EG3-OMe monolayer on gold.

It has been shown first theoretically[45,46,47] and later experimentally[48,49] that for soft interfaces, such as polar regions of lipid layers that are permeable to electrolyte, the electric potential in the solution is determined not only by surface charges, but also by the surface dipoles. Thus a surface with nonzero dipole moment perpendicular to the

surface will appear to have an effective charge, σ_{eff}, that depends on the dipole density, ν, and thickness of the "soft" polar region, l; in a Gouy-Chapman form an effective charge is defined as:

$$\sigma_{eff} = \left[\sigma \cosh(\kappa l) + \nu\kappa \sinh(\kappa l)\right] e^{-\kappa l} \qquad (5.5)$$

where σ is an actual surface charge density and 1/κ is Debye length. Therefore, if there are no surface charges (or the net surface charge is zero, σ=0) but there is a dipole field, a surface would bear an effective nonzero charge, which would give rise to an electrostatic interaction. The OEG tails of EG3-OMe on gold can easily accommodate water molecules and seem to be present in both helical and amorphous states; such a "soft", permeable interface with polar tails is very similar to that of a lipid layer. Therefore, the expression for the effective surface charge in Eq. 5.5 appears to be applicable to the EG3-OMe monolayer on gold.

Study of the ionic concentration effect on the range of forces measured between the EG3-OMe SAMs and C16-probes (Fig. 5.12) provided further evidence that the overall interaction with the monolayer on gold had a significant electrostatic component. Data for EG3-OMe on gold shown in Fig. 5.12 was fitted with an electrostatic force law for a case where the second surface (in our case, that of the C16-probe) does not carry a surface charge (see Eq. 5.3). Measurements of the symmetric system C16-probe/C16-surface did not show any repulsive interaction in water or salt solutions, indicating that there were no charges present on these surfaces. The interaction was found to be strongly attractive and occurred at separations of about 10nm. Note that traces of ions (in particular, HCO_3^- from dissolved CO_2) present in the water may reduce the Debye length of dilute solutions significantly.

Although for the case of charge on one side only, Eq. 5.3 reduces to $F_{el} \propto e^{-2\kappa D}$, we found that for most measurements and higher ionic strengths the experimental data was best fitted with $F_{el} \propto e^{-\kappa D}$. We performed measurements using a C16-probe and a bare SiO_x-surface in aqueous solutions of KNO_3—also a "charge-on-one-side-only" system—and also observed in this case that the data was best fitted with the $e^{-\kappa D}$ coefficient. We believe that this is an image force effect, which comes into play for counterions in water that are surrounded by surfaces of higher dielectric constant.[37]

Results of the fits to the data obtained for the EG3-OMe SAMs on gold and silver with C16-probe in aqueous KNO_3 solutions are shown in Table 5.1. The radius of the probe used was checked by scanning over the ridges of a $SrTiO_3$ single crystal[50] and was found to be ~110nm. Dipole moments per molecule were calculated from dipole density, ν, assuming l=1nm in Eq. 5.5 and a packing density of 21.3Å^2/molecule.[9] Data for EG3-OMe on silver was fitted with empirical formula[51] of the form $F_h \propto \exp(-\lambda D)$ to demonstrate that, unlike the situation on gold, the constant $1/\lambda$ only weakly correlates with the calculated Debye length of the solution. Apparently, while the molecular conformers of OEG on the gold surface generate sufficiently strong dipolar fields to cause a screenable electrostatic interaction with the C16-probe, the interaction on silver is dominated by non-electrostatic forces.

KNO_3 Conc., M	$1/\kappa$ Calculated, nm	EG3-OMe on Gold		EG3-OMe on Silver $1/\lambda$, nm
		$1/\kappa$ fitted, nm	Dipole Moment/molec., D	
10^{-4}	30.7	14.5	4.6	9.6
10^{-3}	9.7	9.3	2.5	8.3
10^{-2}	3.1	2.7	2.2	5.1
10^{-1}	1.0	0.7	1.4	3.1

Table 5.1 *Fitting results of the data shown in Fig. 5.12.*

The EG3-OMe monolayer on silver consists of molecules that are tightly packed and expose their hydrophobic methyl groups at the film/water interphase. The observed long-range attractive forces between the hydrophobic C16 probe and the EG3-OMe SAM on silver in water and PBS solution (Fig. 5.11) points to the presence of a hydrophobic interaction.[51,52] Indeed, these force curves are well reproduced by exponential fits with decay lengths of 11nm in pure water and 6nm in PBS buffer (Fig. 5.11). These are typical decay lengths for hydrophobic forces.[52] Further evidence of hydrophobic interaction is presented in Fig. 5.12, where the long-range attractive force between EG3-OMe on silver and hydrophobic C16-probe is measured; the interaction depends only slightly on the ionic strength of the solution as seen in Table 5.1.

The interaction between hydrophobic moieties in an aqueous environment plays an important role in the fundamental forces that govern the self-assembly of organized

structures such as micelles, lipid bilayers, surface films, protein–amphiphile complexes, and biological membranes.[53,54] As a consequence, understanding the nature of the hydrophobic force is the subject of much experimental,[51,55,56] and theoretical interest.[57,58] Direct force measurements have revealed that the hydrophobic force is long-range. For example, attraction at distances as great as 50nm is commonly measured.[51,59,60] A number of theories have been proposed to explain the wide range of experimental findings observed. These theories may be classified as belonging to one of the following groups, with some overlap occurring between them: 1) an interaction of electrostatic nature which arises from fluctuations or patches of polarization in water or on the surface,[59] 2) the formation of vapor cavities and/or bubbles that bridge between two surfaces, and 3) the influence of structure induced in the water or formed on the surface.[52] Despite these theoretical efforts, the current situation regarding the forces that act between hydrophobic surfaces in an aqueous environment is far from clear:[61] the molecular origin of hydrophobic forces is not well understood[61] and the extent of the interaction is often questioned.[62] A good illustration of this problem has been demonstrated in this Chapter for a symmetric case of hexadecanethiol on both probe and surface measured in water and PBS buffer (Fig. 5.14). Clearly, both surface are hydrophobic (static water contact angle measured on hexadecanthiol on gold is ~110°) but there is no evidence of long-range attractive forces upon approach of the probe toward the surface; similar results in water have been reported earlier.[63] The hydrophobic force is indicated by the extremely large value of the pull-off forces (95.5±11.9nN) and therefore large adhesion hysteresis. The absence of the long-range attractive force and the presence of a large adhesion hysteresis suggests that the interaction is due to the explanations 2 and 3 described above. On the other hand, the force-distance measurements with a C16-probe on the EG3-OMe SAM on silver exhibit a long-range attractive force upon approach, with moderate adhesion hysteresis. These results are similar to those obtained using partially and fully covered surfaces of octadecyltrichlorosilanes (OTS), where an attractive force was measured in the range of 2-30nm[51] and where the authors suggest that the hydrophobic interaction is electrostatic in nature. Despite all these difficulties, our measurements show that the long-range attractive interaction between EG3-OMe on silver and a C16-probe, and the adhesion hysteresis for the symmetric C16/C16 system are only slightly influenced by the ionic strength of the aqueous salt solutions (presumably, due to a decrease in the dielectric constant and/or osmotic pressure effect). Since the electrostatic interaction scales with

the Debye length (Eqs.5.2, 5.3), which, in turn, is a function of ionic strength (Eq. 5.4), the hydrophobic interaction cannot be described by classical electrostatic theory, and the electrostatic nature of the hydrophobic interaction remains unclear.

A repulsive force observed between EG3-OMe on gold and C16-probe in PBS buffer (Fig 5.11) and in 0.1M KNO_3 (Fig. 5.12) might contain an additional component to the overall repulsive interaction. Since the helical or amorphous structure of the OEG tails of the SAM on gold allows a strong interaction of water molecules via hydrogen bonding with oxygen atoms of the OEG, there might be an additional repulsive contribution of hydration or steric-protrusion forces, which decay roughly exponentially with a distance of 0.2-0.4nm.[52,62] This short-range, exponentially decaying force observed in PBS solution looks similar to data obtained for lipid bilayers in pure water with SFM[64] and the surface forces apparatus[65] (SFA), where it is assigned to steric/hydration forces.[37,64,65]

The data recorded for EG3-OMe on Au and Ag under perfluorodecalin (Fig. 5.13) illustrate the fact that the difference in the interfacial force does not only depend on the molecular conformation, but also on the solvent, and is significant only in an aqueous environment. Hence, in order to understand resistance to protein adsorption of biological or organic surfaces, it is important that the complete system, i.e. film and solvent, be considered.

To provide a further proof that, due to distinct conformation of the OEG tails of the EG3-OMe monolayers on gold and silver, the interaction is of electrostatic origin for the SAM on gold and hydrophobic for that on silver, SFM force-distance measurements were performed for a symmetric case of EG3-OMe on both gold- or silver-coated surfaces and gold- or silver-coated probes. The results of the measurements are shown in Fig. 5.15. For the symmetric case, we once again observed a long-range repulsive force that scales with the Debye length of the solution for the EG3-OMe on gold. The repulsive interaction, however, ceases in 0.1M KNO_3. For the EG3-OMe on silver, the interaction is long-range and attractive and does not scale significantly with the ionic strength of the solution. Fitting results of the data in Fig. 5.15 are shown in Table 5.2.

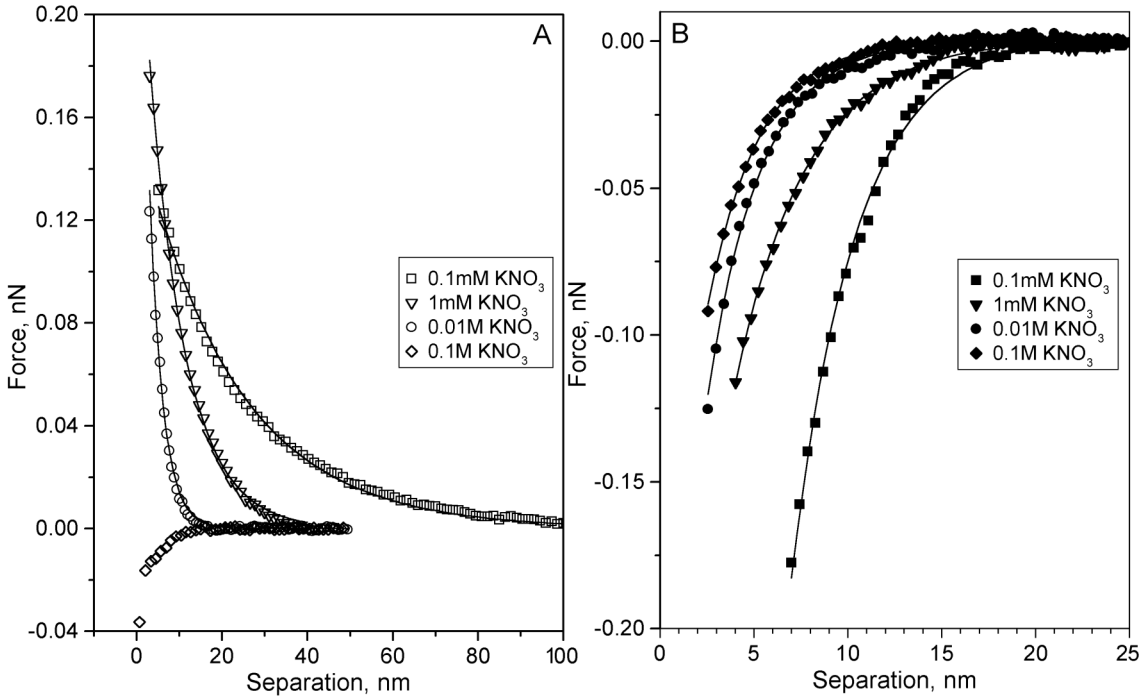

Figure 5.15 *Advancing force-versus-separation curves measured in aqueous solutions of KNO3 for a) EG3-OMe on both gold-coated surface and gold-coated probe (k=0.12N/m) and b) EG3-OMe on both silver-coated surface and silver-coated probe (k=0.12N/m).*

This data clearly demonstrates once again the distinct physical nature of the forces that originate from the differences in the conformational state of the OEG tails.

Experimental data supporting the electrostatic interaction that originates from the dipole field of soft permeable interfaces (Eq. 5.5) is very scarce. It is, therefore, of great interest to study this effect for OEG-terminated SAMs of various lengths. The SFM measurements with a hydrophobic C16-probe were performed on SAMs of undecanethiolates terminated with $-(OCH_2CH_2)_6$-OH, (EG6-OH), and $-(OCH_2CH_2)_9$-OH, (EG9-OH).

KNO_3 Conc., M	1/κ Calculated, nm	EG3-OMe–Au/EG3-OMe–Au		EG3-OMe–Ag/ EG3-OMe–Ag 1/λ, nm
		1/κ fitted, nm	Dipole Moment/molec., D	
10^{-4}	30.7	22.4	3.85	3.76
10^{-3}	9.7	8.5	3.73	3.26
10^{-2}	3.1	3.1	3.35	2.77
10^{-1}	1.0	–	–	2.68

Table 5.2 *Fitting results of the data shown in Fig. 5.15.*

The results of these measurements are shown in Fig. 5.16 and also demonstrate an electrostatic force-law behaviour.

Data for EG6-OH and EG9-OH on gold shown in Fig. 5.16 were fitted with an electrostatic force law for a case where the second surface (in our case, that of the C16-probe) does not carry a surface charge (see Eq. 5.2). The radius of the probe used was checked by scanning over the ridges of a $SrTiO_3$ single crystal[50] and was found to be ~146nm. Dipole moments per molecule were calculated from dipole density, ν, assuming interface thickness, l, in Eq. 5.5 to be 3nm for EG6-OH and 6nm for EG9-OH, and packing density of 21.3Å^2/molecule.[9] Results of the fits are shown in Table 5.3.

KNO_3 Conc., M	1/κ Calculated, nm	EG6-OH–Au		EG9-OH–Au	
		1/κ fitted, nm	Dipole Moment/molec., D	1/κ fitted, nm	Dipole Moment/molec., D
10^{-4}	30.7	15.4	2.62	16.6	1.97
10^{-3}	9.7	4.8	1.96	9.5	1.26
10^{-2}	3.1	3.1	0.71	3.7	0.54
10^{-1}	1.0	0.8	0.44	–	–

Table 5.3 *Fitting results of the data shown in Fig. 5.16.*

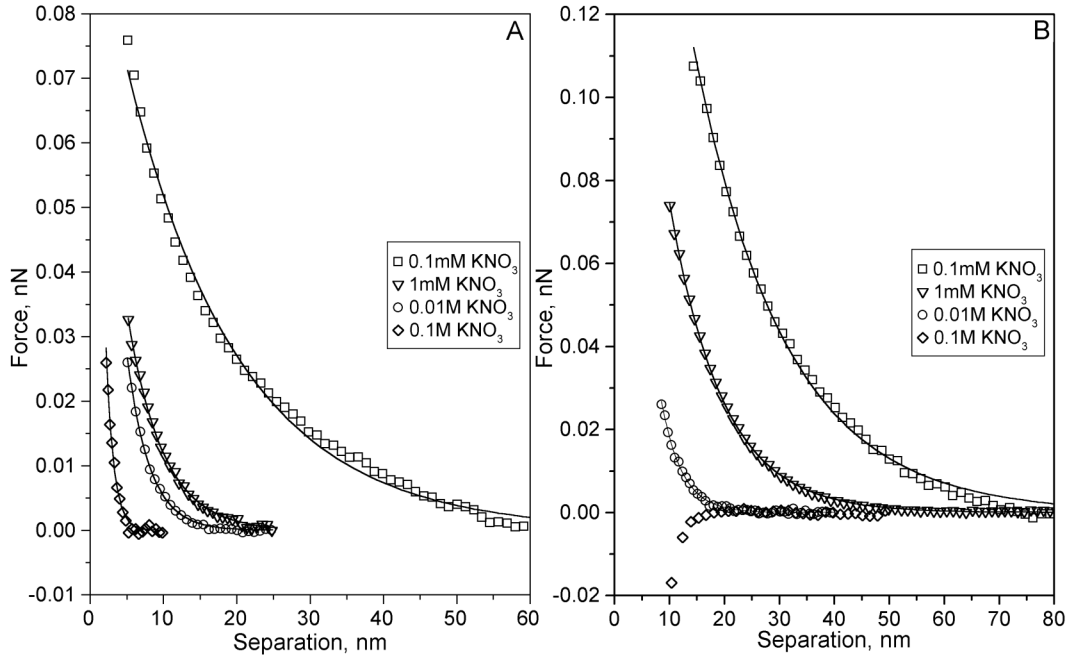

Figure 5.16 *Advancing force-distance curves measured with C16-probe (k=0.05N/m) in aqueous solutions of KNO3 on a) EG6-OH on gold and b) EG9-OH on gold.*

Data in Table 5.3 indicates that, once again, for a case of only one surface bearing an effective charge density the data at higher ionic strength (0.01M and 0.1M KNO_3 for EG6-OH, and 1mM-0.01M KON3 for EG9-OH) is best fitted with $F_{el} \propto exp(-\kappa D)$, which represents an electrostatic force law for the case when both surfaces carry effective charge densities. The data also shows a decrease in the dipole moment per molecule with the increase in the size of the OEG tail. With the increase in the size of the OEG tail there is also a decrease in the conformational order; the OEG tails are in the less confined environment and the total dipole moment of the OEG tail, which is a sum vector of the dipole moments of individual ethylene glycol groups is reduced. Unfortunately, these OEG-terminated thiols are extremely difficult to synthesize and we could not check at what degree of polymerization the OEG-tails no longer possess a conformational order, i.e. the interaction becomes steric and no longer electrostatic. However, we did perform SFM measurements on the brushes of PEG-thiolates of M_w=2K g/mol and M_w=5K g/mol (PEG2000 and PEG5000).

5.10 SFM Measurements of PEG-thiolates

Unlike OEG monolayers, surface-grafted PEGs are used extensively to improve the biocompatibility of foreign materials for both in vivo and ex vivo applications.[66,67,68] The prevalent use of PEG is largely due to its low toxicity and low immunogenicity. In addition, due to its resistance to protein adsorption, it is widely used as a stabilizing surface coating in a biological environment.[68,69,70,71] Grafted PEG chains also have important technological applications in the areas of colloidal stabilization,[72] adhesion[73] and lubrication.[74] At sufficiently high coverage, surface-anchored polymer chains stretch away from the surface forming a polymer brush.[75] It has been shown by Alexander and de Gennes in their pioneering work on polymer brushes[76,77] that the behaviour of end-grafted chains is qualitatively different from that of free chains. For a polymer brush in a good solvent, for instance, the layer thickness, L, is expected to vary linearly with the degree of polymerization, N, while the radius, R, of a free chain in a dilute solution varies as $R \propto N^{0.6}$. Much experimental work has been performed on end-grafted polymers with surface forces apparatus[37] (SFA) and scanning force microscopy.[78,79,80] A recent review on the subject of polymer brushes is available in ref. 81.

Our interest in studying the behaviour of end-grafted PEG chains was sparked by the results obtained on OEG-terminated monolayers, which exhibited long-range interactions, and the measurements with the SFA on the polymer brushes in confined environment that revealed repulsive steric interactions over a range of greater than 10 times the radius of gyration.[82,83] SFM force-distance measurements were performed on synthesized SH-PEG2000 and commercially available SH-PEG5000 (Shearwater Polymer, Inc., Huntsville, USA), self-assembled on gold substrates. The PEG-coated surfaces were prepared by immersion of gold-coated Si wafers in 1mM ethanol solutions of the respective PEG thiols for at least 48 hours to ensure high surface grafting density. The static water contact angle on both surfaces was determined to be 28±1°, which is in excellent agreement with the data reported for the PEO polymer surface.[84] Ellipsometric measurements of the PEG5000 surface revealed a dry film thickness, L_D, of 3.2nm. From this data, the volume fraction, ϕ_0, can be extracted from the following equation:[85]

$$L_D = lN^{0.5}\phi_0^{7/8} \tag{5.6}$$

where l=1.32nm is the length of PEG monomer length and N is a degree of polymerization. Using Eq. 5.6 the volume fraction ϕ_0=0.184 was calculated; the unperturbed radius of gyration for PEG5000 is R_g≈5.7nm. SFM force-distance measurements were performed on a symmetric system of PEG5000-thiolates on gold-coated surface and gold-coated probe in aqueous 0.1M KNO_3, which represents good solvent conditions. A representative force-versus-separation curve with a fit is shown in Fig. 5.17. The data was fitted with a force-law for steric repulsion interaction:[37]

$$F(D) = \frac{200RL}{s^3}k_BTe^{-\pi D/L} \tag{5.7}$$

where L is the film thickness, s is the mean distance between attachment points, D is the separation, T is the absolute temperature, and k_B is Boltzmann's constant. The probe radius was measured over a $SrTiO_3$ single crystal[50] and was found to be ~121nm. From the fit, the film thickness was determined to be L=5.2nm (close to the calculated value of R_g), the mean distance between attachment points s=9.8nm, and the volume fraction of ϕ_0=0.192.

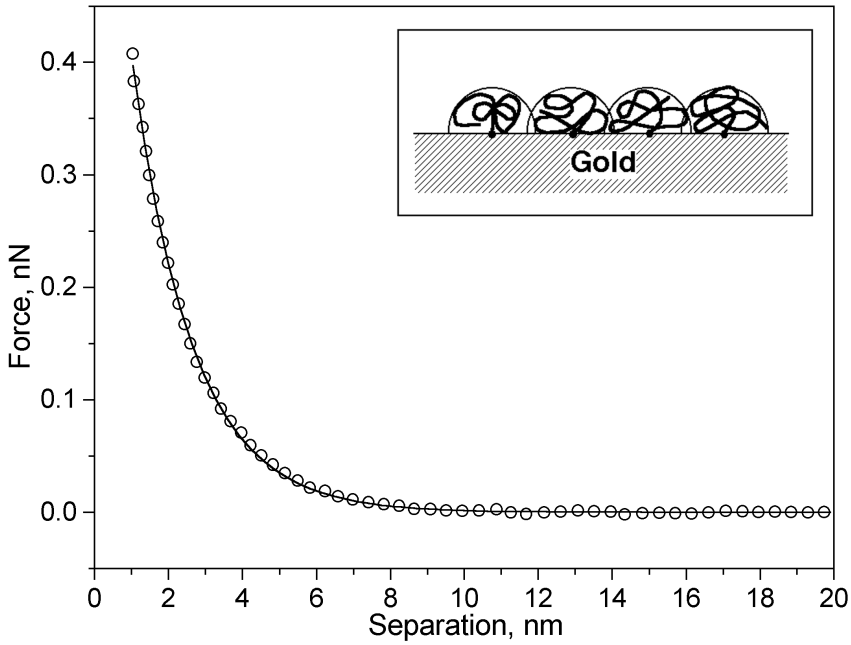

Figure 5.17 *Advancing force-versus-separation curve measured in 0.1M KNO3 for a symmetric system of PEG5000 on gold-coated surface and gold-coated probe (k=0.38N/m).*

It must be noted that for such an SFM measurement, where there is no apparent jump-to-contact, the separation between the PEG-grafted surfaces cannot be measured with high precision. But, nevertheless, the data obtained from ellipsometric and SFM measurements are in good agreement and demonstrate a surprisingly high surface coverage of PEG5000-thiolates on gold with the distance between anchoring points being less than the R_g (see insert in Fig. 5.17).

Another important consequence of the data shown in Fig. 5.17 is that the steric repulsion interaction simply scales with the layer thickness. Measurements in aqueous solutions of KNO_3 of lower concentrations did not reveal any noticeable differences and, unlike the symmetric case of EG3-OMe on gold (Fig. 5.15A), no long-range forces were found. SFM measurements in PBS solution with fibrinogen-modified probes on the surfaces of PEG2000 and PEG5000 showed no sign of an attractive interaction, the data was found to be identical to that reported for protein resistant EG3-OMe on gold (Fig. 5.7C). Measurements were also performed on the surfaces of PEG2000 and PEG5000 in aqueous solutions of KNO_3 of various ionic strength with a hydrophobic C16-probe (Fig. 5.18).

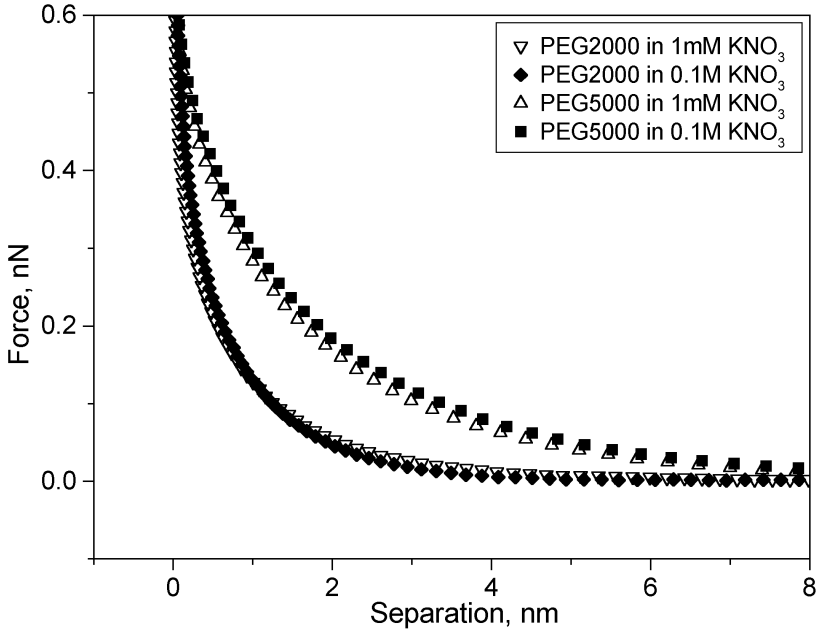

Figure 5.18 *Advancing force-versus-separation curves for PEG2000 and PEG5000 thiolates on gold measured in aqueous solutions of KNO3 with C16-probe (k=0.1N/m).*

Once again, the interaction scaled with the thickness of the PEG layer and no significant effect of ionic strength was detected. In fact, the interaction in 0.1M KNO_3 was slightly more repulsive due to an improvement in the solvent quality. From this data, it was determined that the layer thickness scales as $L \propto N^{0.88}$, an almost linear relationship as had been shown by de Gennes.[77]

5.11 Conclusions

By means of a scanning force microscope with well-defined, functionalised tips, we were able to elucidate the contributions that are relevant to protein adsorption of fibrinogen on SAMs of EG3-OMe on gold and silver.

When using a hydrophobic tip to mimic hydrophobic regions of the protein, interactions of opposite sign were observed on the EG3-OMe–Au and EG3-OMe–Ag systems in aqueous media. While the attractive force observed on the silver system appeared to be hydrophobic in nature, the long-range repulsive force measured on the gold system displayed a strong ionic strength dependence, implying an important electrostatic component. The difference in sign of the forces can be correlated with the distinct molecular conformations of the OEG tails and the resulting difference in their dipolar fields. This effect dominates the interaction between the OEG-derivatised SAM and the

SPM probe in the case of the helical and amorphous conformers on gold but is too small to contribute significantly to the total interaction in the case of the planar, “all trans” conformers on silver.

The lack of long-range interactions for the polymer brush demonstrates that the repulsive interactions found for the short-chain oligomers is unique and not related to the steric repulsion effect responsible for the protein resistance for the end-grafted polymers.

5.12 Post Scriptum: Frictional Properties of Grafted PEGs

Friction measurements of the end-grafted polymer layers under good solvent conditions revealed a dramatic decrease in the friction force compared to that of the unmodified surfaces.[86,87] For end-grafted polystyrene in toluene the friction force reduced to the noise level of the measuring device (SFA) for contact pressure of 1MPa. The effect is interpreted in terms of a limited mutual interpenetration of the brushes in the good solvent, even under moderate compressions, and a fluid interfacial layer where most of the shear occurs. At sufficiently high shear rates, a sharp increase of normal repulsion between the surfaces occurs, which is interpreted in terms of chain stretching, resulting in enhanced osmotic repulsion due to reduced screening of segmental interaction.

It must be noted that these results were obtained with the surface forces apparatus (SFA), for which the normal and lateral forces are measured between two curved cylinders of nominal radius 1cm.[37] On the scale of a polymer brush, these surfaces can be treated as parallel and, for such confined environment, hydrodynamic effects become increasingly important. The liquid needs to flow out of the contact area through the polymer network, and the repulsive forces are now due to the viscous drag of the liquid as it is forced past the polymer segments. The situation might be very different for an SFM friction measurement, where the probe tip may be treated as a single asperity. The probe tip effective radius is on the order of 20-150nm. Therefore, the surfaces are not confining and hydrodynamic effects might be less significant. Also, due to the small tip radius, the pressure in the contact area is several orders of magnitude higher than that of the SFA. It was, therefore, of great interest to perform SFM friction measurements on the PEG5000 bearing surfaces.

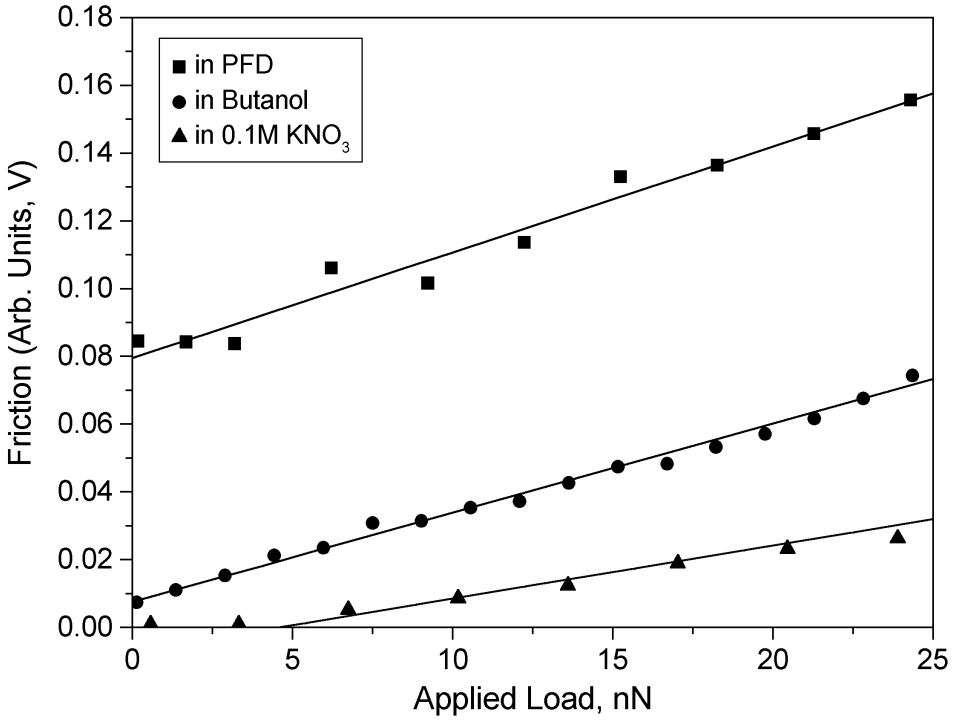

Figure 5.19 *Friction measurements of the PEG5000 grafted surface and probe (k=0.58N/m) in PFD, butanol, and 0.1M KNO_3.*

We measured friction forces as a function of applied load for a PEG5000-thiolate on a gold-coated surface and gold-coated probe in solvents of different qualities: perfluorodecalin (non-solvent), butanol (poor solvent), and 0.1M KNO_3 (good solvent). The results are shown in Fig. 5.19.

Although the friction data is shown in arbitrary units (Volts), it clearly demonstrates a significant reduction in friction force for the PEG-bearing surfaces in the good solvent conditions. The friction force is undetectable until an applied load of ~5nN. The probe tip radius was determined to be R=125nm, so that the mean pressure across the contact circle can be roughly estimated as reaching, at least, 200MPa. Since all data was taken with the same probe, the slopes of the fits, representing friction coefficient, can be compared. While the friction coefficients were found similar for PEG5000 in PFD and butanol, that for the PEG5000 in 0.1M KNO_3 was reduced by 41%. Surprisingly, these results correlate very well even at much higher contact pressures with the dramatic reduction in friction force measured with the SFA.[86] They demonstrate that even for a non-confined geometry, where hydrodynamic effects are less significant, the solvated state of the PEG chains provides a dramatic reduction in the friction force.

References

1. Ulman, A. *Chem. Rev.* **1996**, *96*, 1533.
2. Ulman, A. *An Introduction to Ultrathin Organic Films: From Langmuir-Blodgett to Self-Assembly*; Academic Press: Boston, 1991.
3. Harris, J. M. *Poly(Ethylene Glycol) Chemistry*; Plenum: New York, 1992.
4. Jeon, S. I.; Andrade, J. D. *J. Coll. Interf. Sci.* **1991**, *142*, 159.
5. Taunton, H. J.; Toprakcioglu, C.; Fetters, L. J.; Klein, J. *Nature* **1988**, *332*, 712.
6. de Gennes, P. G. *Ann. Chim*. **1987**, *77*, 389.
7. Gölander, C. G.; Herron, J. N.; Lim, K.; Claesson, P.; Stenius, P.; Andrade, J. D. In *Poly(ethylene glycol) Chemistry: Biotechnical and Biomedical Applications*; Harris, J. M., Ed.; Plenum Press: New York, 1992; 221.
8. Prime, K. L.; Whitesides, G. M. *J. Am. Chem. Soc.* **1993**, *115*, 10714.
9. Harder, P.; Grunze, M.; Dahint, R.; Whitesides, G. M.; Laibinis, P. E. *J. Phys. Chem. B* **1998**, *102*, 426.
10. Pertsin, A. J.; Grunze, M.; Garbuzova, I. A. *J. Phys. Chem. B* **1998**, *102*, 4918.
11. Pertsin, A. J.; Grunze, M. *Langmuir* **1994**, *10*, 3668.
12. Wang, R. L. C.; Kreuzer, H. J.; Grunze, M. *J. Phys. Chem. B* **1997**, *101*, 9767.
13. Vogler, E. A. *Adv. Coll. Interf. Sci.* **1998**, *74*, 69.
14. Florin, E. L.; Moy, V. T.; Gaub, H. E. *Science* **1994**, *264*, 415.
15. Ludwig, M.; Moy, V. T.; Rief, M.; Florin, E. L.; Gaub, H. E. *Microscopy, Microanalysis, Microstructure* **1994**, *5*, 321.
16. Lee, G. U.; Kidwell, D. A.; Colton, R. J. *Langmuir* **1994**, *10*, 354.
17. Florin, E. L.; Rief, M.; Lehmann, H.; Ludwig, M.; Dornmair, C.; Moy, V. T.; Gaub, H. E. *Biosens. Bioelectr.* **1995**, *10*, 895.
18. Allen, S.; Chen, 5. Y.; Davies, J.; Davies, M. C.; Dawkes, A. C.; Edwards, J. C.; Roberts, C. J.; Sefton, J.; Tendler, S. J. B.; Williams, P. M. *Biochem.* **1997**, *36*, 7457.
19. Chowdhury, P. B.; Luckham, P. F. *Coll. Surf. A* **1998**, *143*, 53.
20. Bowen, W. R.; Hilal, N.; Lovitt, R. W.; Wright, C. J. *J. Coll. Interf. Sci.* **1998**, *197*, 348.
21. Rief, M.; Oesterhelt, F.; Heymann, B.; Gaub, H. E. *Science* **1997**, *275*, 1295.
22. Lee, G. U.; Chrisey, L. A.; Colton, R. J. *Science* **1994**, *266*, 771.
23. Moy, V. T.; Florin, E. L.; Gaub, H. E. *Coll. Surf. A* **1994**, *93*, 343.

24. Chen, 5.; Davies, M. C.; Roberts, C. J.; Tendler, S. J. B.; Williams, P. M.; Davies, J.; Dawkes, A. C.; Edwards, J. C. *Langmuir* **1997**, *13*, 4106.
25. Horbett, T. A.; Brash, J. L. *Proteins at interfaces II: Fundamentals and Applications*; ACS: Washington, DC, 1995; Vol. ACS Symposium Series No. 602, 11.
26. Feng, L.; Andrade, J. D. in *Proteins at interfaces II:Fundamentals and Applications*; Horbett, T. A. and Brash, J. L., Ed.; ACS: Washington, DC, 1995; Vol. ACS Symposium Series No. 602, Chapter 5.
27. Dubois, L. H.; Zegarski, B. R.; Nuzzo, R. G. *J. Chem. Phys*. **1993**, *98*, 678.
28. Dhirani, A.; Hines, M. A.; Fisher, A. J.; Ismail, O.; Guyot-Sionnest, P. *Langmuir* **1995**, *11*, 2609.
29. Nygren, H.; Stenberg, M.; Karlsson, C. *J. Biomed. Mater. Res*. **1992**, *26*, 77.
30. Ta, T. C.; Sykes, M. T.; McDermott, M. T. *Langmuir* **1998**, *14*, 2435.
31. Kiaei, D.; Hoffman, A. S.; Horbett, T. A.; Lew, K. R. *Biomaterials* **1995**, *29*, 729.
32. Sheth, S. R.; Leckband, D. *Proc. Natl. Acad. Sci.* **1997**, *94*, 8399.
33. Claesson, P. M.; Blomberg, E.; Froberg, J. C.; Nylander, T.; Arnebrant, T. *Adv. Coll. Interf. Sci.* **1995**, *57*, 161.
34. *Handbook of Biological Physics*; Erlandsson, R.; Olsson, L. ; Bongrand, P., Claesson, P. M. and Curtis, A. S. G., Ed.; Springer: Berlin, 1994, Chapter 4.
35. Grigg, D. A.; Russel, P. E.; Griffith, J. E. *J. Vac. Sci. Technol. A* **1992**, *10*, 680.
36. Feldman, K.; Tervoort, T.; Smith, P.; Spencer, N. D. *Langmuir* **1998**, *14*, 372.
37. Israelachvili, J. *Intermolecular and Surface Forces*; 2nd ed.; Academic Press, Inc.: San Diego, CA, 1992.
38. Lyklema, J. In *Surface and Interfacial Aspects of Biomedical Polymers*; Andrade, J. D., Ed.; Plenum Press: New York, 1985, Vol. 1, 293.
39. Derjagin, B. V.; Landau, L. *Acta Physicochim. URSS* **1941**, *14*, 633.
40. Verwey, E. G. W.; Overbeck, J. J. G. *Theory of the Stability of Lyophobic Colloids*; Elsevier: Amsterdam, 1948.
41. Ducker, W. A.; Senden, T. J.; Pashley, R. M. *Nature* **1991**, *353*, 239.
42. Parsegian, V. A.; Gingell, D. *Biophys. J.* **1972**, *12*, 1192.
43. Butt, H.-J. *Biophys. J.* **1991**, *60*, 777.
44. Butt, H.-J.; Jaschke, M.; Ducker, W. *Bioelectrochem. Bioenerg.* **1995**, *38*, 191.
45. Bell, G. M.; Levine, P. L. *J. Coll. Interf. Sci*. **1977**, *60*, 177.
46. Bell, G. M.; Levine, P. L. *J. Coll. Interf. Sci.* **1980**, *74*, 530.

47. Belaya, M.; Levadny, V.; Pink, D. A. *Langmuir* **1994**, *10*, 2010.
48. Levadny, V. G.; Belaya, M. L.; Pink, D. A.; Jericho, M. H. *Biophys. J.* **1996**, *70*, 1745.
49. Xu, W.; Blackford, B. L.; Cordes, J. G.; Jericho, M. H.; Pink, D. A.; Levadny, V. G.; Beveridge, T. *Biophys. J.* **1997**, *72*, 1404.
50. Sheiko, S. S.; Möller, M.; Reuvekamp, E. M. C. M.; Zandbergen, H. W. *Phys. Rev. B* **1993**, *48*, 5675.
51. Yoon, R. H.; Flinn, D. H.; Rabinovich, Y. I. *J. Coll. Interf. Sci.* **1997**, *185*, 363.
52. Israelachvili, J.; Wennerström, H. *Nature* **1996**, *379*, 219.
53. Hühnerfuss, H. J. *J. Coll. Interf. Sci*. **1989**, *128*, 237.
54. Mehrian, T.; de Keizer, A.; Korteweg, A. J.; Lyklema, J. *Colloids Surf*. **1993**, *A71*, 255.
55. Claesson, P. M.; Herder, P. C.; Blom, C. E.; Ninham, B. W. *J. Coll. Interf. Sci*. **1987**, *118*, 68.
56. Rabinovich, Ya. I.; Yoon, R.-H. *Langmuir* **1994**, *10*, 1903.
57. Tsao, Y.-H.; Evans, D. F.; Wennerström, H. *Langmuir* **1993**, *9*, 779.
58. Podgornik, R.; Parsegian, V. A. *Chem. Phys*. **1991**, *154*, 477.
59. Tsao, Y.-H.; Evans, D. F.; Wennerström, H. *Science* **1993**, *262*, 547.
60. Christenson, H. K. In *Modern Approaches to Wetability: Theory and Applications*; Schrader, M. E., Loeb, G., Eds.; Plenum Press: New York, 1992.
61. Wood, J.; Sharma, R. *Langmuir* **1995**, *11*, 4797.
62. *Handbook of Biological Physics* Claesson, P. M., Bongrand, P., Claesson, P. M., Curtis, A. S. G., Eds.; Springer: Berlin, 1994, Chapter 2.
63. Sinniah, S. K.; Steel, A. B.; Miller, C. J; Reutt-Robey, J. E. *J. Am. Chem. Soc.* **1996,** *118*, 8925.
64. Dufrêne, Y. F.; Barger, W. R.; Green, J. B. D.; Lee, G. U. *Langmuir* **1997**, *13*, 4779.
65. Marra, J.; Israelachvili, J. *Biochem.* **1985**, *24*, 4608.
66. *Poly(ethylene glycol) Chemistry: Biotechnological and Biomedical Applications*; Harris, J. M., Ed.; Plenum Press: New York, 1992.
67. Barenberg, S. A. *MRS Bull*. **1991**, *16*, 26.
68. Elbert, L.; Hubbell, J. A. *Annu. Rev. Mater. Sci.* **1996**, *26*, 365.
69. Papahadjopoulos, D.; Allen, T.; Gabizon, A.; Mayhew, E.; Matthay, K.; Huang, S.; Lee, K.; Woodle, M.; Lasic, D.; Redemann, C.; Martin, F. *Proc. Natl. Acad. Sci. USA* **1991**, *88*, 11460.

70. Amiji, M.; Park, K. *J. Biomater. Sci. Polym.* **1993**, *4*, 217.
71. Llanos, G.; Sefton, M. V. *J. Biomed. Mater. Sci*. **1993**, *27*, 1383.
72. Napper, D. H. *Polymeric Stabilization of Colloidal Dispersions*; Academic Press: London, 1983.
73. Brown, H. R. *MRS Bulletin* **1996**, *21*, 24.
74. Klein, J. *Annu. Rev. Mater. Sci.* **1996**, *26*, 581.
75. de Gennes, P. G. *Adv. Coll. Interf. Sci*. **1987**, *27*, 189.
76. Alexander, S. *J. Phys. Paris* **1977**, *38*, 977.
77. de Gennes, P. G. *Macromol.* **1980**, *13*, 1069.
78. Lea, A. S.; Andrade, J. D.; Hlady, V. *Coll. and Surf. A* **1994**, *93*, 349.
79. Koutsos, V.; van der Vegte, E. W.; Pelletier, E.; Stamouli, A.; Hadziioannou, G. *Macromol.* **1997**, *30*, 4719.
80. Roters, A.; Schimmel, M.; Rühe, J.; Johannsmann, D. *Langmuir* **1998**, 14, 3999.
81. *Advances in Polymer Science: Polymers in Confined Environment*; Granick, S., Ed.; Springer: Berlin, 1999, Vol. 138.
82. Klein, J. In *Studies in Polymer Science*; Nagasawa, M., Ed.; Elsevier: Amsterdam, 1988, Vol. 2, 333.
83. Patel, S. S.; Tirrel, M. *Annu. Rev. Phys. Chem*. **1989**, *40*, 597.
84. Wu, S. *Polymer Interface and Adhesion*; Dekker: New York, 1982.
85. Léger, L.; Raphaël, E.; Hervet, H. *Adv. Polym. Sci.* **1999**, *138*, 185.
86. Klein, J.; Kumacheva, E.; Mahalu, D.; Perahia, D.; Fetters, L. J. *Nature* **1994**, *370*, 634.
87. Klein, J. *Annu. Rev. Mater. Sci*. **1996**, *26*, 581.
88. Prime, K. L.; Whitesides, G. W. *J. Am. Chem. Soc.* **1991**, *113*, 12.
89. Ducker, W. A.; Senden, T. J.; Pashley, R. M. *Nature* **1991**, *353*, 239.

Chapter 6

Conclusions and Outlook

While scanning probe microscopy tools have found numerous applications in polymer science,[1,2,3,4] high-resolution imaging with chemical sensitivity is one area that still represents a substantial analytical and methodological challenge. While many modes of SPM can provide spectacular contrast of heterogeneous polymer surfaces, the contrast mechanism, however, depends not only on the chemical composition, but also on imaging conditions and, most importantly, on viscoelastic properties, which dictate energy dissipation and relaxation processes, adhesional behaviour, and plastic deformation, to name a few. Viscoelastic properties, in turn, are affected by molecular weight, polydispersity, degree of crystallinity, the polymer glass transition temperature, thermal history, etc. All these parameters need to be taken into consideration in order to obtain meaningful results. Scanning force microscopy (SFM) of polymeric thin films with chemical sensitivity is presented in this dissertation. Although the feasibility of achieving chemically specific contrast for polymer blends is demonstrated, it is also shown that the polymer systems have to be carefully chosen and tuned in order for the image contrast to be purely chemically specific. Although SFM is a useful method for *distinguishing* between components, the *identification* of surface species in heterogeneous polymer systems with this tool is possible only when the physical and chemical properties of these components are known, so that the contrast mechanism can first be predicted and then verified by SFM measurements.

Despite these difficulties, the "chemical force microscopy" study of polymeric thin films showed significant sensitivity to chemical composition. For non-polar polymers, it was found that the measured interactions could be well described by the Lifshitz theory of Van der Waals interactions, which provides an estimation of the Hamaker constant

based on the bulk dielectric properties (static dielectric constant and refractive index). The values of the pull-off forces obtained for the non-polar polymer series scaled remarkably well with the refractive indices of these materials. For a series of amorphous polymeric films of increasing chemical functionality, differences in the adhesional forces translated into reversal of contrast when the polymer blends were imaged in friction mode with probes of different surface chemistry, thus facilitating chemically specific SFM imaging and identification of the blend components.

A study of spin-cast polymeric thin films presented in this thesis demonstrated the outstanding ability of scanning probe microscopy to visualise with high spatial resolution morphologies of delicate polymer surfaces, such as those of biocompatible, biodegradable polyesterurethanes. It showed that despite the apparent simplicity of the method (placing a drop of polymer solution on a rotating substrate), the spin-casting process is extremely complex, leading to very elaborate morphologies of polymer films of various structures and roughness. Surface roughness is of great importance in the field of biomaterials, in particular, since it greatly influences the adsorption of surface-active proteins and the adhesion of cells.[5,6] Analytical techniques, such as surface-plasmon resonance[7] and optical waveguide lightmode spectroscopy[8] (OWLS), provide direct measurements of the adsorption behaviour of cells and proteins but require very thin films (less than 100nm) of the examined surface coating. Spin-casting of biopolymers from a range of solvents of different qualities (or solvent/non-solvent mixtures) can provide both the desired film thicknesses and a wide range of surface roughness values, while preserving the same chemical structure. Such measurements may be of great value for this aspect of biomaterials research.

An SFM study of oligo(ethylene glycol)-terminated (OEG) self-assembled monolayers in comparison with the end-grafted layers of poly(ethylene glycol) (PEG), demonstrated substantial differences in the surface-forces of interaction. While classical steric repulsion behaviour was observed for the PEG films, the conformational state of the OEG-tails of the SAMs on gold and silver dictated a particular type of physical forces sensed by an SFM probe. The forces measured for OEG-terminated thiolates on gold (in the helical state) showed a significant electrostatic component, which translated into a long-range repulsive interaction with functionalised SFM probes. The same molecules on silver (in an “all trans” conformation) induced hydrophobic surface behaviour, and

long-range attractive forces influenced only slightly by the solution ionic strength were measured. It was determined that the electrostatic forces of the OEG-terminated SAM on gold originate from the dipole moments of the electrolyte-permeable OEG-tails. It is important to note at this point, that PEG-modified surfaces exhibit resistance toward protein adsorption and are widely used in biomedical applications. Monolayers of OEG-terminated thiolates on gold were also found to be protein-resistant, while those on silver were not. While this study provided a useful insight into the physical effects of conformational states of the ethylene glycol moieties and their relevance to protein adsorption, the importance of the water molecules bound to the OEG-tails remains unclear. While possible structuring of water molecules around the OEG-tails has been proposed, based on computer simulations,[9] there is no experimental evidence of such an effect. A very sensitive SFM technique has recently been developed, which combines modulation of an SFM cantilever at a nanometre-level amplitude with a dramatic decrease in the probe tip radius by attaching a carbon nanotube to an SFM probe.[10] This instrument is extremely sensitive to the structuring effects of liquid media, and may, therefore, be very helpful in establishing experimental evidence of water structuring of the OEG-tails, if it indeed exists.

An SFM frictional study of the PEG-grafted surfaces revealed a dramatic decrease in friction force when the surfaces bearing PEG brushes were in contact under good solvent conditions. In fact, the friction signal was below detection limit for the loads at which the pressure in the contact area reached almost 200MPa. While a similar result for the PEG brushes was reported earlier,[11] it was obtained with the surface forces apparatus (SFA), for which the polymer layers were in a confined geometry and the measurements were conducted at the contact pressure of 1MPa. These effects of dramatic reduction in friction are of great importance in understanding and improving lubrication properties. In contrast to the case of conservative (equilibrium) interactions between polymer-bearing surfaces, there has been few experimental investigations that have examined directly the issue of dissipative forces between such surfaces. It would be of great significance, therefore, to perform a systematic study of frictional behaviour of PEG and OEG-bearing surfaces with an SFM technique.

References

1. Magonov, N. M.; Whangbo, M.-H. *Surface Analysis with STM and AFM*; VCH Publishers: Weinheim, 1996.
2. *Scanning Probe Microscopy of Polymers*; Ratner, B. D., Tsukruk, V. V., Eds.; ACS Symposium Series, 694; ACS: Washington, D. C., 1998.
3. Sheiko, S. S. in *New Developments in Polymer Analytics II*; Schmidt, M., Ed.; *Adv. Polym. Sci.* **2000**, *151*, 61.
4. Microstructure and Microtribology of Polymer Surfaces; Tsukruk, V. V., Wahl, K. J., Eds.; ACS Symposium Series, 741; ACS: Washington, D. C., 2000.
5. *Proteins at interfaces II: Fundamentals and Applications*; Horbett, T. A., Brash, J. L., Eds.; ACS Symposium Series, 602; ACS: Washington, D. C., 1995.
6. Ramsden, J. J. *Chem. Soc. Rev*. **1995**, *24*, 73.
7. Frazier, R. A.; Matthijs, G.; Davies, M. C.; Roberts, C. J.; Schacht, E.; Tendler, S. J. B. *Biomaterials* **2000**, *21*, 957.
8. Kurrat, R.; Textor, M.; Ramsden. J. J.; Boni, P.; Spencer, N. D. *Rev. Sci. Instr*. **1997**, *68*, 2172.
9. Wang, R. L. C.; Kreuzer, H. J.; Grunze, M.; Pertsin, A. J. *Chem. Phys*. **2000**, *2*, 1721.
10. Jarvis, S. P.; Lantz, M. A.; Durig, U.; Tokumoto, H. *Appl. Surf. Sci*. **1999**, *140*, 309.
11. Klein, J.; Kumacheva, E.; Mahalu, D.; Perahia, D.; Fetters, L. J. *Nature* **1994**, *370*, 634.

Samenvatting

Hoewel toepassingen van polymeren in het algemeen berusten op hun bulkeigenschappen zijn er talloze technologieën waarin (ultra) dunne polymeerfilms worden gebruikt. Voorbeelden zijn weerstanden en diëlectrica in micro-elektronische componenten, orientatielagen voor vloeibaar kristallijne materialen en het gebruik van polymeren als smeermiddel in magnetische informatieopslagelementen. Verder worden dunne films toegepast in licht-emitterende diodes (polymere LED's), niet-lineaire optische componenten en biosensoren. Polymere films zijn uitgegroeid tot bouwstenen voor functionele structuren op steeds kleiner wordende lengteschalen.

Moleculaire, actieve elementen op nanoschaal, gevulde systemen en gestructureerde oppervlakken zijn van toenemend belang in de ontwikkeling van microelektronisch-mechanische systemen (MEMS), micro-elektronica, sensortechnologie en biotechnologie. Desalniettemin blijft het aflezen van chemisch specifieke informatie op nanoschaal een analytische uitdaging. De snelle ontwikkeling van de `scanning probe microscoop´ (SPM) in de laatste tien jaar heeft geresulteerd in een aantal waardevolle hulpmiddelen voor het bestuderen van fysische en chemische oppervlakte-eigenschappen met sub-nanometer resolutie. Scanning probe microscopie met chemisch detectievermogen is met succes gebruikt voor het bestuderen van zelf-organizerende moleculaire systemen. De directe toepassing van deze techniek op polymere films is echter moeilijk aangezien behalve de chemische samenstelling van het oppervlak ook andere (fysische) parameters van belang zijn voor het genereren van beelden met een hoog contrast.

Het belangrijkste doel van dit proefschrift is te onderzoeken of SPM op zinvolle wijze gebruikt kan worden voor de karakterisering van de morfologie, en met name de chemische samenstelling, van dunne polymere films en voor het bestuderen van de fysische interacties met deze oppervlakken. Daartoe zijn met behulp van de `scanning

force microscoop´ (SFM) polymere systemen geanalyseerd qua morfologie en chemische structuur door de aantrekkende kracht te meten tussen een serie van polymere filmoppervlakken en een aantal chemisch goed gedefinieerde `scanning probe tips´. Deze aantrekkingskracht bleek sterk afhankelijk te zijn van de chemische structuur van zowel de tip als het monster en was duidelijk verschillend voor polaire en apolaire probe tips. In geval van apolaire polymeren bleek het mogelijk de adhesiekracht te modelleren met behulp van de Lifshitz theorie voor Van der Waals interacties. De verschillen in adhesie bepaald met verschillende probe tips resulteerde voor een serie van polymere films met toenemende oppervlaktefunctionaliteit in een omkering van het contrast in de hoge-resolutie `lateral force´ wrijvingsopnamen van blends van deze polymeren. Deze omkering van contrast ten gevolge van verschillen in chemische samenstelling is kenmerkend voor de potentie van deze techniek voor de bepaling van de chemische oppervlaktesamenstelling op nanometerschaal. Echter, het SFM contrast voor fase-gescheiden systemen, zoals de gebruikte polymere blends, hangt ook sterk af van de mechanische eigenschappen van de afzonderlijke polymere componenten. Daarom kan alleen voor mengsels waarvan de componenten ongeveer dezelfde (wrijvings) mechanische eigenschappen bezitten specifiek chemisch contrast verkregen worden. Dit is tegelijkertijd een voordeel en een nadeel, aangezien gevoeligheid voor chemische verschillen contrast kan bieden in gevallen waar mechanisch contrast afwezig is. Van cruciaal belang voor de experimentele bepaling van de tip-oppervlak interacties bleek het gebruik van perfluorodekaline als medium. De lage diëlectrische constante van deze vloeistof maakt het mogelijk deze krachten nauwkeurig te meten.

De SFM methodiek, ontwikkeld voor het bestuderen van de polymere films, is eveneens toegepast op het probleem van anti-hechting van proteïnes. De weerstand tegen proteïne-adsorptie van polyetheenglycol-gemodificeerde oppervlakken, zoals gebruikt in vele biomedische toepassingen, wordt goed beschreven door de theorie van sterische hindering. De fysische achtergrond van de hechting van proteïnen op korte oligo(etheenglycol)-getermineerde monolagen is echter nog altijd onduidelijk. Voor het onderzoeken en imiteren van de interactie tussen een plasmaproteïne, fibrinogeen en `self-assembled monolagen´ (SAMs) van methoxytri(etheenglycol)undecaanthiolaat (EG3-OMe) op goud- en zilveroppervlakken, werd gebruik gemaakt van gefunctionaliseerde SFM probes. De EG3-OMe SAMs op goud bleken bestand te zijn

tegen proteïne-adsorptie, terwijl de op zilver geadsorbeerde lagen verschillende hoeveelheden proteïne adsorbeerden. Er werden experimenten uitgevoerd met zowel geladen (ionogene) als hydrofobe tips als model voor de lokale proteïne-structuur. Tijdens de experimenten met de hydrofobe tip aan de EG3-OMe SAMs op goud werd een op lange afstand werkende afstotende interactie waargenomen, die schaalde met de ionsterkte van de oplossing. Bij een zelfde analyse aan SAMs op zilver in plaats van goud, werd een lange-afstands aantrekkende interactie gemeten die slechts in geringe mate van de ionsterkte afhankelijk was. Er is aangetoond dat de verschillen in ruimtelijke conformatie (helix structuur voor EG3-OMe op goud en perfecte trans-struktuur op zilver) doorslaggevend zijn voor de fysische interactie tussen EG3-OMe en de tip in een waterig milieu: elektrostatisch voor de monolaag op goud en hydrofoob voor de monolaag op zilver. Verder werd een bijzonder elektrostatisch gedrag gevonden dat wordt geïnduceerd door het dipoolveld van de zachte, permeabele grenslaag van oligo(etheenglycol)-staarten van de EG3-OMe monolaag op goud en zijn zogenaamde `polymere borstels´ (polymer brushes) bestaande uit poly(etheenglycol)thiolaat onderzocht. Het bereik van de afstotende interactie zoals bepaald met SFM probes bleek afhankelijk te zijn van de laagdikte en was in goede overeenkomst met berekeningen op basis van sterische hindering.

In dit proefschrift is aangetoond dat het gebruik van geordende monolagen van korte organische moleculen, zoals thiolaten, uitermate nuttig kan zijn voor het verkrijgen van een beter begrip van de processen die zich afspelen op polymeeroppervlakken zoals adhesie, wrijving, benatting, smering, biologische activiteit en weerstand tegen proteïnehechting. Het is echter van vitaal belang dat SFM experimenten ook aan de werkelijke polymeeroppervlakken wordt uitgevoerd om de relevantie van SAMs als modeloppervlakken te verifiëren.

List of Publications

1. Stutzman, N.; Tervoort, T. A.; Bastiaansen, C. W. M.; Feldman, K.; Smith, P. *Adv. Mater*. **2000**, *12(8)*, 557-562.
   "Solid-State Replication of Relief Structures in Semicrystalline Polymers"
2. Textor, M.; Hofer, R.; Rossi, A.; Feldman, K.; Hähner, G.; Spencer, N. D. *Langmuir* **2000**, *16(7)*, 3257-3271.
   "Structural Chemistry of Self-Assembled Monolayers of Octadecylphosphoric Acid on Tantalum Oxide Surfaces"
3. Feldman, K.; Hähner, G.; Spencer, N. D. In *Microstructure and Microtribology of Polymer Surfaces*; Tsukruk, V. V., Wahl, K. J. Eds.; *ACS Symposium Series 741, 1999*, Chapter 16.
   "Surface Nanochemical Studies of Polymers and Other Organic Surfaces by Scanning Force Microscopy"
4. Feldman, K.; Hähner, G.; Spencer, N. D.; Harder, P.; Grunze, M. *J. Am. Chem. Soc*. **1999**, *121(43)*, 10134-10141.
   "Probing Resistance to Protein Adsorption of Oligo(ethylene glycol)-Terminated Self-Assembled Monolayers by Scanning Force Microscopy"
5. Feldman, K.; Tervoort, T. A.; Smith, P.; Spencer, N. D. *Langmuir* **1998**, *14*, 372-378.
   "Toward Force Spectroscopy of Polymer Surfaces"
6. Feldman, K.; Fritz, M. C.; Hähner, G.; Marti, A.; Spencer, N. D. *Tribology International* **1998**, *31(1-3)*, 99-105.
   "Surface Forces, Surface Chemistry, and Tribology"
7. Barger, W.; Koleske, D. D.; Feldman, K.; Krüger, D.; Colton, R. J. *Polym. Preprints ACS* **1996**, *37(2)*, 606-607.
8. Kwon, C.; Xi, X. X.; Bhattachatya, S.; Doughty, C.; Venkatesan, T.; Zhang, H.; Lynn, J. W.; Peng, J. L.; Li, Z. Y.; Spencer, N. D.; Feldman, K. *Appl. Phys. Lett.* **1993**, *62(11)*, 1289-1291.
   "High Critical Current Densities in Ultrathin $YBa_2Cu_3O_7$-Delta Films Sandwidched Between (PRXY1-X)$Ba_2Cu_3O_7$-Delta Layers"

Acknowledgements

First of all, I want to thank the person who made many important things in my life possible. He hired me 9 years ago as a technician in the surface-analytical group of W.R. Grace & Co. in Columbia, Maryland, USA; after realising what a terrible mistake he had made, he left for Switzerland to become a professor at Swiss Federal Institute of Technology (ETH). The company could no longer function with me working there and with him not, and was soon sold piece by piece. However, life in Switzerland was too quiet and boring and so to spice it up he invited me to work with him at ETH. This person is Prof. Dr. Nicholas D. Spencer and my deepest gratitude goes to him for his friction-and-wear-free confidence and patience, continuous support of my work, as well as kind help in personal and professional matters.

I am especially indebted to Dr. Theo Tervoort, Prof. Dr. Paul Smith and Dr. Kees Bastiaansen for teaching me the ABCs of polymer science, providing valuable suggestions, and inspiring most of the polymer work presented in this dissertation. Without their knowledge, motivation and support most of this work would not have been possible.

I am particularly grateful to Prof. Dr. Piet J. Lemstra for his courageous decision to provide me with an opportunity to defend this dissertation at the Technische Universiteit Eindhoven.

My thanks go to PD Dr. Georg Hähner for his scientific input, support, encouragement and supervision of the study of the self-assembled monolayers presented in this dissertation.

I would like to thank my co-workers, many of whom have become dearest friends, for their help, support, understanding and for always being there for me: Dr. Michaela Fritz, Christian Dicke, Martin Widmer, Alessandro Napoli, Dr. Marcus Morstein, Michael Zäch, Dr. Manfred Heuberger, Natalie Stutzmann, Jeroen Visjager and all the members of the Laboratory for Surface Science and Technology at ETH.

Last but not least, I want to thank my wonderful friends Valentina and Dr. Yuri Podladchikov for their unconditional friendship, understanding, patience and support in all aspects of my personal and professional life.

Curriculum Vitae

The author of this thesis was born in Moscow, Russia, on August 30th, 1968. He started his studies at Moscow's Mendeleev Institute of Chemical Technology, in the department of Physical Chemistry in 1985, but in 1987 had to interrupt his education for a two-year mandatory military service in the Soviet Army. In 1989, he returned to the Mendeleev Institute, but soon after that, in 1990, he emigrated to the United States. From 1992 until 1995 he worked as a technician in the Analytical Research Department of the W.R. Grace&Co. Research Division in Columbia, Maryland, while continuing his education in the Department of Chemical Engineering, University of Maryland, College Park. In May of 1995 he received a degree of Bachelor of Science in Chemical Engineering, and worked until the end of 1995 as a research assistant in the Surface Chemistry Branch of the Naval Research Laboratory, Washington, D.C. From December 1995 until the present time, he has been working as a research assistant in the Laboratory of Surface Science and Technology, Department of Materials of the Swiss Federal Institute of Technology (ETH) in Zurich.